

Master of Science Thesis

A PV Powered BWRO Desalination Installation with Energy Recovery and Hydro-Pneumatic Energy Storage

Implemented and Tested in Urban Jakarta



Rafael G.C. Romero

July 4th, 2013

Delft University of Technology
Faculty of Civil Engineering and Geosciences
Department of Water Management
Section of Sanitary Engineering
Stevinweg 1
2628 CN Delft

www.sanitaryengineering.tudelft.nl

A PV Powered BWRO Desalination Installation with Energy Recovery and Hydro-Pneumatic Energy Storage

Rafael G.C. Romero

A PV Powered BWRO Desalination Installation with Energy Recovery and Hydro-Pneumatic Energy Storage

Implemented and Tested in Urban Jakarta

Rafael Gerardo Carlos Romero

for the degree of:

Master of Science in Sustainable Energy Technology

Date of submission: June 27th 2013

Date of defence: July 4th 2013

Committee:

Prof.Dr.ir. L.C. Rietveld

Delft University of Technology
Sanitary Engineering Section

Dr.ir. S.G.J. Heijman

Delft University of Technology
Sanitary Engineering Section

Prof.Dr. F.M. Mulder

Delft University of Technology
RRR/Fundamental Aspects of Materials and Energy

Sanitary Engineering Section, Department of Water Management
Faculty of Civil Engineering and Geosciences
Delft University of Technology, Delft

“Papa, je bent mijn ster”

Preface

In September of 2010 I started my MSc. Program “Sustainable Energy Technology. I always had a passion for solar driven solutions and for hydraulic energy storage. But after being introduced to solar lighting systems I also quickly developed a passion for “Base of the Pyramid” (BoP) products and solutions.

Having previously attended some gatherings at the Sanitary Engineering Department, I knew there were projects closely related to BoP solutions at this department. During the initial meetings the drinking with the sun and drinking with the wind projects were discussed and I knew immediately I wanted to contribute to this ongoing research in renewable driven desalination solutions. At the time my supervisor had an ongoing project in Bali, and we decided that my research would be a follow up based on the results of the above-mentioned project.

En route tot the successful completion of this MSc. Project, there have been many people who have contributed in one way or another. First of all I would like to thank my supervisors Bas Heijman and Rusnandi Garsadi for supporting and guiding me through this long and at times very tough process. I would also like to thank everyone at PAM Jaya and the ITB for providing me with the necessary support and equipment to perform my research in Jakarta. I would also like to thank Sid Vollebregt and Reinoud Feenstra over at Elemental Water Makers for their ongoing support. A very special thanks goes out to my godfather Robert Voges, without whom I would not have been able to complete this project. Furthermore countless loving friends and university staff supported me along the way, I would like to thank all of you from the bottom of my heart (you know who you are). Lastly and most importantly I would like to thank my mother. Thank you so much for everything you have done throughout my life, I could not have asked for a more loving mother!

Abstract

This MSc. Thesis project was performed at the Sanitary Engineering Department of the TU Delft as part of the Sustainable Energy Technology program. It is one of the unique research projects performed in the field of renewable driven Reverse Osmosis desalination, producing fresh water with only renewable energy sources as driving force.

With the ever-increasing awareness regarding fossil fuel depletion and the global fresh water scarcity, developing innovative renewable powered desalination solutions has claimed its spot amongst the top future development goals. Reverse Osmosis (RO) has proven to be one of the key technologies, showing great potential in combination with renewable energy sources. However, due to the intermittent nature of renewables and the continuous operational requirements of RO membranes, the development of cheap, reliable and environmentally benign energy storage solutions is required.

Previously research has been performed on an innovative Photo Voltaic (PV) driven brackish water RO system with an energy recovery device and pressurized water storage. Inspired by and based on the results obtained during the project mentioned above, a novel concept with hydro-pneumatic energy storage was designed and implemented.

The scope of this project was to implement and test the designed pilot plant, after completion of a comprehensive literature research and detailed sizing & estimation trajectory. The pilot plant equipped with PV modules, a solar pump & controller, an energy recovery device, RO membrane and hydro-pneumatic energy storage was implemented and evaluated in North Jakarta, Indonesia.

The results showed that hydro-pneumatic energy storage is a viable and feasible solution for continuous operation of small-scale renewable powered RO desalination systems. Unfortunately the installed system did not have the required storage capacity for 24/7 water production. However with the acquired experience and knowledge, the system behavior is now better understood and can be more easily predicted.

Table of Contents

Preface	V
Abstract.....	VII
Nomenclature	XXI
Abbreviations.....	XXI
Symbols.....	XXI
1. Introduction.....	1
1.1. Introduction to Research	1
1.2. Research Objective	1
1.3. Thesis Outline.....	1
2. Fresh Water Problem.....	3
2.1. An Introduction to the Looming Water Crisis	3
2.1.1. The Falkenmark Index	3
2.1.2. Analyzing Global Water Scarcity.....	4
2.1.3. Drinking Water and Health Issues	6
3. Location & Climate	7
3.1. Introduction to Jakarta.....	7
3.2. Introduction to Drinking Water & Sanitation in Jakarta	7
3.3. A brief history of Drinking Water in Jakarta.....	7
3.4. Jakarta’s current water network.....	8
3.5. Jakarta’s groundwater quality	9
3.6. Indonesia’s Renewable Energy Sources.....	9
3.6.1. Jakarta’s Wind Climate	11
3.6.2. Jakarta’s Solar Climate.....	12
3.7. Specific Location & Period/Season	13
4. Introduction to Desalination	14
4.1. Reverse Osmosis	16
4.2. Renewable Powered Desalination	20
4.3. Renewable Powered RO Desalination, an Overview	21
4.4. Battery-free Renewable Powered RO Desalination.....	23
4.4.1. Simple battery-free PV-RO System.....	24
4.4.2. Desalination using hydrostatic pressures.....	24
4.4.3. Stand-alone RO desalination system using a pumped storage unit.....	25
5. System Concept	26
5.1. Previous Concept	26
5.2. Current System Concept	26
5.2.1. System Sketch.....	27

5.2.2.	Energy Buffer	27
5.2.3.	Energy Recovery Device	31
6.	Sizing of the System.....	35
6.1.	RO Pumping Requirements.....	35
6.2.	Hydro-pneumatic Vessel.....	36
6.2.1.	Hydro-pneumatic Tank Volume Calculations	36
6.2.2.	Maximum Hydro-pneumatic Pump Power Requirement.....	37
6.3.	Total Power & Energy Demand.....	38
6.4.	Renewable Energy Sources	39
6.4.1.	Wind Energy Calculations	39
6.4.2.	PV Calculations	41
6.5.	Choice of Renewable Energy Source.....	41
6.6.	Additional Investment Costs	42
7.	Experimental Setup	43
7.1.	Test Site.....	43
7.2.	System Components	44
7.2.1.	Raw Water Supply	44
7.2.2.	PV Modules.....	45
7.2.3.	Solar Pump & Controller.....	46
7.2.4.	Pre-Filters & RO Membranes.....	46
7.2.5.	ERPI.....	48
7.2.6.	Hydro-Pneumatic Storage Vessel	48
7.2.7.	Tubing.....	49
7.3.	Instrumentation	49
7.3.1.	Measurement Instrumentation & Datalogger.....	50
7.3.2.	DasyLab Data acquisition Software	51
8.	System Predictions	54
8.1.	Expected PV Performance.....	54
8.1.1.	Shading Losses.....	54
8.1.2.	PV Panel Temperature.....	54
8.2.	Solar Pump & Controller	55
8.2.1.	Cable Losses.....	55
8.2.2.	Hydraulic Losses	55
8.2.3.	Solar Pump & Controller Performance According to Manufacturer	57
8.3.	Membrane & Energy Recovery Device	57
8.4.	Hydro-Pneumatic Energy Storage.....	58
9.	Measurement Results.....	59
9.1.	Initial Test Period – Measurements Without Energy Storage	59
9.1.1.	Sensor Issues & Calibration	59
9.1.2.	Daily Solar Pumped flow and Solar Radiation	60

9.1.3.	Desalination Part	62
9.1.4.	Permeate Flux (Surface Load).....	66
9.1.5.	System Start-up & Shut-off.....	67
9.1.6.	Summary of the Results.....	69
9.2.	Second Test Period – Measurements Including Energy Storage	70
9.2.1.	Sensor Issues & Calibration	70
9.2.2.	Solar Pumped flow and Irradiance	71
9.2.3.	Desalination Part	72
9.2.4.	Permeate Flux (Surface Load).....	76
9.2.5.	Energy Storage.....	77
9.2.6.	System Start-up & Shut-off.....	79
9.2.7.	Summary of the Results.....	80
9.3.	Comparison of the system Parameters.....	80
9.3.1.	Comparison of the Key Performance Values.....	80
9.3.2.	Miscellaneous Noteworthy Comparisons.....	81
10.	Discussion.....	85
10.1.	Measured Solar Irradiation and Expected Solar Irradiation	85
10.2.	PV and Solar Pump Performance.....	85
10.2.1.	PV Module Performance	85
10.2.2.	Solar Pump & Controller Performance.....	86
10.3.	Desalination Part	87
10.3.1.	RO Membrane Performance	87
10.3.2.	ERPI Performance.....	88
10.4.	Hydro-Pneumatic Storage Pressure Performance.....	89
10.4.1.	Interaction Between Water and Air Inside the Pressure Vessel	89
10.4.2.	Buffering Capacity	90
10.4.3.	Permeate Flux (Surface Load)	91
11.	System Evaluation	95
11.1.	System Without Energy Storage.....	95
11.1.1.	Economical Evaluation	95
11.1.2.	Specific Energy Content.....	97
11.2.	System with Hydro-pneumatic Energy Storage.....	97
11.2.1.	Economical Evaluation	97
11.2.2.	Specific Energy Content.....	100
11.3.	System with Scaled-up Hydro-pneumatic Energy Storage.....	100
11.3.1.	Economical Evaluation	100
11.3.2.	Specific Energy Content.....	101
11.4.	Summary of System Evaluation	102
12.	Conclusions & Recommendations	103
12.1.	Conclusions.....	103

12.2. Recommendations.....	104
12.2.1. Possible System Improvements	104
12.2.2. Wind Energy as additional Energy Buffer.....	105
12.2.3. Developing a Model	105
12.2.4. Scale-up Possibilities	105
12.2.5. Seawater Desalination.....	105
References	106
Appendices.....	110
Appendix A – Groundwater Samples throughout Jakarta	110
Appendix B – Average Data.....	111
December 2012.....	111
April 2013.....	111
Hydraulic Pump Power @ 500 [W/m ²]	112
Appendix C – Cost Calculations.....	114

List of Figures

Figure 2.1: Projected water scarcity in 2030, based on the Falkenmark indicator. (Figure taken from: (Rijsberman, 2006)).....	5
Figure 2.2: Worldwide desalination capacity growth. (Taken from (Lattemann, Kennedy, Schippers, & Amy, 2010)).....	5
Figure 3.1: The division of Jakarta’s water distribution, as described above. (Image taken from (Kurniasih, 2008)).....	8
Figure 3.2: Distribution of the energy sources used in Indonesia. (Data taken from (<i>Renewable Energy Potential</i> , 2006)).	10
Figure 3.3: An overview of Energy Potentials in Indonesia. (Taken from (Susandi, 2008)).....	10
Figure 3.4: Windmap of Java and surroundings. (Data taken from (SSE, 2013), image from (Vollebregt & Feenstra, 2012)).....	11
Figure 3.5: Average monthly wind speeds. (Data taken from (SSE, 2013)).....	11
Figure 3.6: Average daily insolation for Jakarta. (Data taken from (SSE, 2013) and (Rumbayan et al., 2012)).....	12
Figure 3.7: Precise location of the pilot plant at Muara Karang, North Jakarta.....	13
Figure 4.1: Worldwide feed water used for desalination. (Figure taken from (Mezher, Fath, Abbas, & Khaled, 2011)).....	14
Figure 4.2: Worldwide desalination capacity by process. (Figure taken from (Mezher et al., 2011)).....	16
Figure 4.3: Global desalination capacities by process and water type. (Figure taken from (Lattemann et al., 2010))	16
Figure 4.4: The principle of Osmosis and Reverse Osmosis. (Taken from (van Dijk et al., 2009)).....	17
Figure 4.5: The principle of spiral-wound RO membranes. (Image taken from (van Dijk et al., 2009)).....	17
Figure 4.6: Schematic presentation of a simple RO desalination plant. (Image taken from (El-ghonemy, 2013a)).....	18
Figure 4.7: Left a schematic presentation of a single pass RO setup, and on the right a RO setup with energy recovery device. (Images taken from (Alghoul et al., 2009)).....	19
Figure 4.8: Possible configuration of renewable energy sources and desalination processes. (From (Eltawil et al., 2009) via (Thye, 2010)).....	20

Figure 4.9: Distribution of renewable powered desalination technologies. (Data from (Eltawil et al., 2009)).	21
Figure 4.10: Comparison between membrane desalination capacity and thermal desalination capacity from 1980 to 2016. (Taken from (Misdan, Lau, & Ismail, 2012)).	21
Figure 4.11: Schematic presentation of a typical PV powered RO desalination unit with battery storage	23
Figure 4.13: Hybrid RO Desalination design, with a PSP. (Taken from (Spyrou & Anagnostopoulos, 2010)).	25
Figure 5.1: System Concept.	27
Figure 5.2: Typical hydro-pneumatic vessel, source: ("Water Safe bc," 2006).	29
Figure 5.3: Schematic view of a typical hydro-pneumatic tank, source:(Pandolph, Unknown)	30
Figure 5.4: Schematic of the working principle of the <i>Clark Pump</i>	32
Figure 5.5: Explanation of the working forces inside the pressure intensifier.	33
Figure 6.1: Schematic depiction of the solar pump	38
Figure 6.2: Power curve & relevant specifications for the donQi Urban 1.5 Venturi Windmill	40
Figure 7.1: Top view of the plant layout at Muara Karang, North Jakarta	43
Figure 7.2: Detailed schematic of the desalination part.	43
Figure 7.3: On the left the well during construction, and on the right the reservoir eventually used.	44
Figure 7.4: PV panels Installed on the roof and their configuration.	45
Figure 7.5: Solar controller and Pump on the right and specifications on the left.	46
Figure 7.7: The white 2540 RO membrane is located in the front of the picture	47
Figure 7.9: Hydro-pneumatic Storage Vessel.	49
Figure 7.10: Sensors & visual indicators integrated into the system	50
Figure 7.11: From top left corner to the bottom right corner: mass balance (MB) over the complete system, MB over T connection, MB over the ERPI, MB over the RO membrane.	52
Figure 8.1: Pump Curves according to the manufacturer.	57
Figure 9.1: Daily solar radiation and daily pumped volume for initial test run.	61
Figure 9.2: Solar Irradiance and pumped flow for 10 & 11 Dec (days 1 & 2 of test run).	61

Figure 9.3: Feed and RO pressures measured during initial test run.	62
Figure 9.4: Feed pressure, RO pressure and feed flow on 10 December 2012.	63
Figure 9.5: Feed pressure, RO pressure and feed flow during a 4-minute period on December 10 th 2012.	63
Figure 9.6: Feed flow, permeate flow and brine discharge flow for 10 December 2012.	64
Figure 9.7: Recovery rates achieved during initial test-run.	64
Figure 9.8: Feed and Permeate TDS on the top, and feed water temperature on the bottom.	65
Figure 9.9: Permeate TDS and feed temperature for December 10 th 20120.	66
Figure 9.10: Flux during test period 1, 10-16 December 2012.	67
Figure 9.11: Flux on December 15 th 2012.	67
Figure 9.12: Feed flow, permeate flow and feed pressure during shut-down on December 10 th 2012. ...	68
Figure 9.13: A closer look at the permeate TDS, Irradiance measured and feed pressure during shutdown.	68
Figure 9.14: Daily solar radiation and pumped volume for second test period.	71
Figure 9.15: Solar irradiance and pumped flow for 17 & 18 April (Days 1 and 2 of test period).	72
Figure 9.16: Feed- and RO pressure measured during the second test period.	73
Figure 9.17: Feed pressure, RO pressure and solar pumped flow on April 19 th	73
Figure 9.18: Feed- and RO pressure and feed flow during a 5 minute period on April 19 th	74
Figure 9.19: System flows on April 19 th	74
Figure 9.20: Recovery Rates achieved during second test period.	75
Figure 9.21: Feed- and permeate TDs at the top and feed water temperature at the bottom.	75
Figure 9.22: Permeate TDS and feed temperature on April 19 th	76
Figure 9.23: Flux for test period 2 (system including energy storage).	76
Figure 9.24: Flux on 19 April 2013	77
Figure 9.25: Storage pressures and volumes measured.	77
Figure 9.26: Storage pressure, volume and flow on April 19 th	78

Figure 9.27: System start-up for April 19 th	79
Figure 9.28: Permeate TDS during start-up on April 19th.	79
Figure 9.29: Flows for period 1 on the left and flows for period 2 on the right.	81
Figure 9.30: Recovery Rates for period 1 on the left and period 2 on the right.....	82
Figure 9.31: Feed pressure and permeate TDS for period 1 and period 2 (left and right respectively).....	83
Figure 9.32: Permeate fluxes for two arbitrary days during test period 1 and test period 2 (left and right respectively).....	83
Figure 10.1: Total system efficiency, Hydraulic Power and Theoretical Power plotted versus the Solar Irradiance.	86
Figure 10.2: ERPI Friction Losses.....	88
Figure 10.3: Illustrating the systems buffering capacity.....	91
Figure 10.4: Sample plots to show the influence of initial pressure increase.....	93
Figure 11.1: Cost Distribution of the installed system.....	99

List of Tables

Table 2.1: List of Countries in Africa and Asia with renewable water sources below the threshold of 1700 [m ³ /capita/year] by the year 2030. The bold names are countries that have entered the list after the year 2000. (Taken from: (Rijsberman, 2006)).....	4
Table 3.1: Yearly average wind speeds.....	12
Table 3.2: Mean daily insolation and the standard deviation	12
Table 4.1: Table showing water classification	14
Table 4.2: Characteristics of the different desalination categories. (Information taken from (Gude et al., 2010; Mezher et al., 2011)).....	15
Table 4.3: Energy requirements and GHG emissions for different desalination processes (Gude et al., 2010).	18
Table 4.4: Examples of RES-RO systems. (Taken from (Vollebregt & Feenstra, 2012)).....	22
Table 5.1: Summarized results of (Vollebregt & Feenstra, 2012).	26
Table 5.2: Advantage and Disadvantages of Hydro-pneumatic Energy Storage.....	29
Table 5.3: List of components for a typical Hydro-Pneumatic Tank.....	31
Table 5.4: List of ERD's	31
Table 5.5: Surface areas and ERPI Recovery Ratio.....	34
Table 6.1: Membrane specifications @Feed TDS of 5000 [mg/l].	35
Table 6.2: Parameters used for power calculations	36
Table 6.3: Relevant parameters required for hydro-pneumatic power requirements	38
Table 6.4: Relevant information regarding wind energy production and costs.	40
Table 6.5: Sundaya LEC-1200 PV module specifications (Measured at 1000 [W.m ²]).	41
Table 6.6: Relevant information regarding PV energy production and costs.....	41
Table 6.7: Power and Energy Requirements.....	42
Table 6.8:List of required components and their costs	42
Table 7.1: Membrane parameters according to Sirio.....	47

Table 7.2: Hydro-pneumatic Energy Storage Specifications.....	48
Table 7.3: Sensors & Datalogger Specifications.....	51
Table 8.1: PV module efficiency for different times during the day(Vollebregt & Feenstra, 2012).	55
Table 8.2: Relevant parameters for the friction loss calculation, their values and units.	56
Table 9.1: Final Sensor Calibration and Adjustment.....	60
Table 9.2:Min, Max, Average and Standard Deviation values measured during test period 1.....	60
Table 9.3: Performance values of the system measured in the period of December 10th - December 16th.	69
Table 9.4: Final Sensor Calibrations and Adjustments used for test period 2.....	71
Table 9.5: Min, Max, Average and Standard Deviation for test period 2	72
Table 9.6: Pressure Loss inside the Storage Vessel.....	78
Table 9.7: Performance values of the system measured during April 17 th to April 23 rd	80
Table 9.8: Comparison of the key performance values	81
Table 10.1: Average daily radiation according to literature and daily radiation measured.	85
Table 10.2: Expected and measured RO performance	87
Table 10.3: Pressure Loss inside the Storage Vessel.....	89
Table 10.4: Daily starting pressure, average daily flux, average daily solar radiation, and daily runtime for period2.....	92
Table 10.5: Some initial sample calculations to illustrate effect of increasing the starting pressure inside the vessel.	94
Table 11.1: Costs for the System without Storage.....	96
Table 11.2: Economic evaluation, system without energy storage.	96
Table 11.3: Cost of the installed system.	97
Table 11.4: Economic Evaluation Installed System (with storage).	98
Table 11.5: Cost distribution for conventional- and renewable powered RO systems.....	99
Table 11.6: Capital and operational costs for the system with adjusted energy storage capacity.	101
Table 11.7: EAC and total annual costs for the system with adjusted energy storage capacity.	101

Table 11.8: Tabular summary of the economical and SEC evaluation for the configurations evaluated in this report. 102

Table 12.1: Tabular summary of the achieved results..... 103

Nomenclature

Abbreviations

List of Abbreviations

AC	Alternating current
BWRO	Brackish water reverse osmosis
EAC	Equivalent annual cost
EC	Electronic Conductivity
ERD	Energy recovery device
ERPI	Energy recovery pressure intensifier
DC	Direct current
HDPE	High-density polyethylene
MED	Multi-effect distillation
MSF	Multi-stage flash
MVC	Mechanical vapor compression
OPEC	Organization of the Petroleum Exporting Countries
PSP	Pumped storage plant
PV	Photovoltaic
PVC	Polyvinyl chloride
RES	Renewable energy sources
PVRO	Photovoltaic reverse osmosis
RO	Reverse osmosis
SD	Solar distillation
SEC	Specific energy content
TDS	Total dissolved solids
TVC	Thermal vapor compression

Symbols

Glossary of Symbols for Hydraulic Calculations

\dot{m}	Mass flow	[kg/s]
v	Liquid velocity	[m/s]
p	Pressure	[Pa]
ρ	Liquid Density	[kg/m ³]
g	Gravitational acceleration	[m/s ²]
z	Head height	[m]
e_{fr}	Friction Losses	[m ² /s ²]
f	Friction factor	[-]
K	Loss coefficient	[-]
L	Pipe Length	[m]
μ	Liquid viscosity	[m*s ² /kg]
Q	Volumetric flow	[m ³ /s]
A	Pipe cross-sectional area	[m ²]
d	Pipe diameter	[m]
Re	Reynolds number	[-]
W	Power	[kg/m*s ²]=[W]

1. Introduction

1.1. Introduction to Research

While the worldwide focus towards climate change and means of controlling the build-up of greenhouse gases is ever more increasing, a less popular but potentially equally as important crisis is looming. This looming crisis is the crisis with regard to the world water resources. The two issues are not unrelated, as the main factor behind both is the world's rapidly developing economies (Jones, 2010). A solution to the looming water crisis is desalination of water. There are several methods in which desalination can be performed, but one of the most energy efficient and popular technologies to desalinate water is reverse osmosis (RO). Traditionally RO is powered by energy derived by fossil fuels, but RO technology shares many of the advantages which micro energy regenerators such as PV panels' exhibit. This is one of the many reasons why small-scale renewable powered RO desalination is gaining popularity, especially in remote arid/coastal region where fresh water sources are limited.

1.2. Research Objective

The goal in this research is to re-design and re-locate a Photovoltaic (PV) powered brackish water reverse osmosis installation to urban Jakarta and operate this installation continuously for 24 hours a day. The original brackish water reverse osmosis (BWRO) installation was designed with pressurized water storage. After evaluating the possibilities for implementing this concept in Jakarta, gaining commitment proved to be a challenge. There for a different concept will be evaluated, one that is more easily implemented in areas such as Jakarta, the most important criteria is that the concept should be completely free of batteries.

This thesis research for the Sustainable Energy Technology (SET) master was performed at the Sanitary Engineering Department, located at the faculty Civil Engineering at the TU Delft. The project was performed in collaboration with the Institute Teknologi Bandung (ITB) and PAM Jaya (largest water production/distribution company of Jakarta).

A design was developed, consequently the pilot plant was built and evaluated in Jakarta, the data obtained during this period will be evaluated and used to draw conclusions about the system behavior. It is at this stage that the new design can be compared to the design by Vollebregt and Feenstra (2012) and that conclusion can be made about the systems feasibility. As a conclusion to this study recommendations will be made for further research. In the following paragraph the thesis outline will be presented.

1.3. Thesis Outline

Chapter 2 of this thesis will discuss the fresh water crisis and health & safety issues related to drinking water.

Next in chapter 3 an introduction about Jakarta is given, followed by a short introduction on the drinking water distribution network and its current state and also by local climate conditions are introduced.

Chapter 4 presents the results of the literature study on the available desalination techniques, and explores the most popular desalination solutions powered by renewable energy sources.

Next in chapter 5 and 6 the developed concept, the key components and the scaling calculations are presented. In these two chapters the system design is clarified.

Chapter 7 introduces the experimental setup and chapter 8 discusses how the system is expected to behave and perform.

All these chapters build up the information regarding the importance of desalination and the chosen design. Chapter 9 presents the measurement results obtained in Jakarta, for illustrational purposes a series of plots are chosen and presented in this chapter. Consequently these results and plots are discussed and further evaluated in chapter 10.

In chapter 11 the system is evaluated based on the cost of water produced and the specific energy content (SEC). These two key performance values enable the possibility to setup a comparison between the feasibility and quality of the current design compared to that of other systems previously explored.

Chapter 12 is the final chapter of this thesis, here conclusions are drawn based on the results obtained. Finally the knowledge gathered during this project is used to setup a list of possible improvements and recommendations for further research.

2. Fresh Water Problem

2.1. An Introduction to the Looming Water Crisis

As mentioned in the “Introduction”, the world is facing a crisis with regard to the world water resources. This water crisis is often referred to as “water scarcity”, Rijsberman (2006) discussed the definition of water scarcity in his paper. According to Rijsberman (2006), a person can be characterized as water scarce when: An individual does not have access to safe and affordable water to satisfy his or her needs for drinking, washing or their livelihoods. An area is said to be water scarce when a large number of people in that area are water insecure for a significant period of time. The author however also mentions that there is no commonly accepted definition for water scarcity and that whether or not a certain area qualifies as “water scarce” depends on some of the following parameters:

- What fraction of the resource is made available, or could be made available to satisfy those needs
- The temporal and special scales used to defines scarcity
- How people’s needs are defined

What can however be clearly stated, is that currently there are approximately 1.1 billion people without access to safe and affordable water (WHO, 2011) and that approximately 900 million people in rural areas are currently living in “Base of the Pyramid” conditions (i.e. have an income bellow one dollar per day) and lack access to safe drinking water. And what is now commonly an accepted theory is that as long as the world population increases, fresh water resources will continue to decrease. In the following section the Falkenmark Index will be discussed.

2.1.1. The Falkenmark Index

As mentioned previously identifying water scarcity can be quite complex and tends to differ for specific areas, one of the reasons water scarcity is hard to identify is that discussions about water resources are generally conducted around average values. But it is commonly known that water is not evenly distributed across the lands. Also when discussing for example yearly rainfall, average numbers are used but everyone knows that rainfall is distributed over the seasons. And while during rainy seasons a certain area can experience water as a nuisance (during floods), the same area can experience water as a lifesaving resource within the same year during drought (dry season). So due to this complexity of the term “water scarcity”, several tools/indicators have been developed over the years to help identify water scarcity. The most commonly used indicator is the “Falkenmark Indicator”, this indicator is the most popular because it is relatively easy to apply and understand. While other indicators better explain the true nature of water scarcity, they are not widely applied because they require specific data which is often not available and also they tend to be less intuitive (Rijsberman, 2006). The “*Falkenmark indicator*” proposes a threshold of 1700 [m³] of renewable water sources per capita per year, this figure was set based on estimates of water requirements in the households, agricultural, industrial and energy sectors, and environmental needs. When a country’s water supplies cannot sustain this figure it is said to be in *water stress*. When supply falls below 1000 [m³] and 500 [m³], it is said that the country experiences *water scarcity* and *absolute scarcity* respectively. But as with any tool, the Falkenmark indicator has limitations. Its limitations are that:

- It uses annual, national averages which hide important scarcity at smaller scales
- It does not take into account the availability of infrastructure that modifies the availability of water to users
- It does not reflect important variations in the demand among countries due to lifestyle, climate, etc.

So now that the Falkenmark indicator has been introduced, let's use it to analyze the global water scarcity.

2.1.2. Analyzing Global Water Scarcity

Based on the literature read (Jones, 2010; Meerganz von Medeazza, 2004; Rijsberman, 2006), the general conclusion can be made that a large share of the world's population will be affected by water scarcity over the next several decades. Several studies have used the Falkenmark index to illustrate that as the world population increases, proportionally less water will be available per capita. Currently it is already the case that many arid areas, where there is relatively low amount of rainfall but a high population density, suffer the most from water scarcity. This can be seen in Table 2.1 below, where the International Water Management Institute (IWMI) shows a list of countries in Africa and Asia with renewable water sources below the suggested 1700 [m³/capita/year] threshold.

Table 2.1: List of Countries in Africa and Asia with renewable water sources below the threshold of 1700 [m³/capita/year] by the year 2030. The bold names are countries that have entered the list after the year 2000. (Taken from: (Rijsberman, 2006)).

Afghanistan	Egypt	Kenya	Niger	Tanzania
Algeria	Eritrea	Korea Republic	Nigeria	Togo
Burkina Faso	Ethiopia	Lebanon	Pakistan	Tunisia
Burundi	India	Libya	Rwanda	Uganda
Cape Verde	Iran	Malawi	Saudi Arabia	Emirates
Comoros	Israel	Maldives	Somalia	Yemen
Cyprus	Jordan	Morocco	South Africa	Zimbabwe

Other studies have already presented projections of global water scarcity in the near future, one of the examples can be found below. In the figure it can be seen that approximately 62% of the world's population will be experiencing (or almost experiencing) water stress. As mentioned previously, these figures are based on projected population increase in the next several decades. All of the above mentioned arguments show that the current (and future) shortage of potable water sources is alarming and that this issue should not be taken lightly.

In the following paragraphs drinking water & health related issues, and water characterization will be discussed.

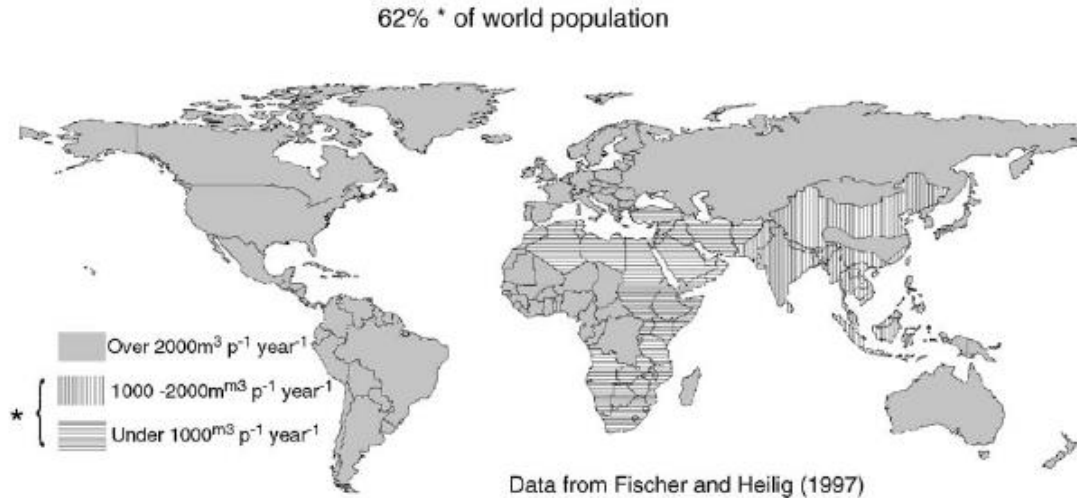


Figure 2.1: Projected water scarcity in 2030, based on the Falkenmark indicator. (Figure taken from: (Rijsberman, 2006)).

The global fresh water scarcity has gradually increased over the years, and an obvious solution seems to be desalination.

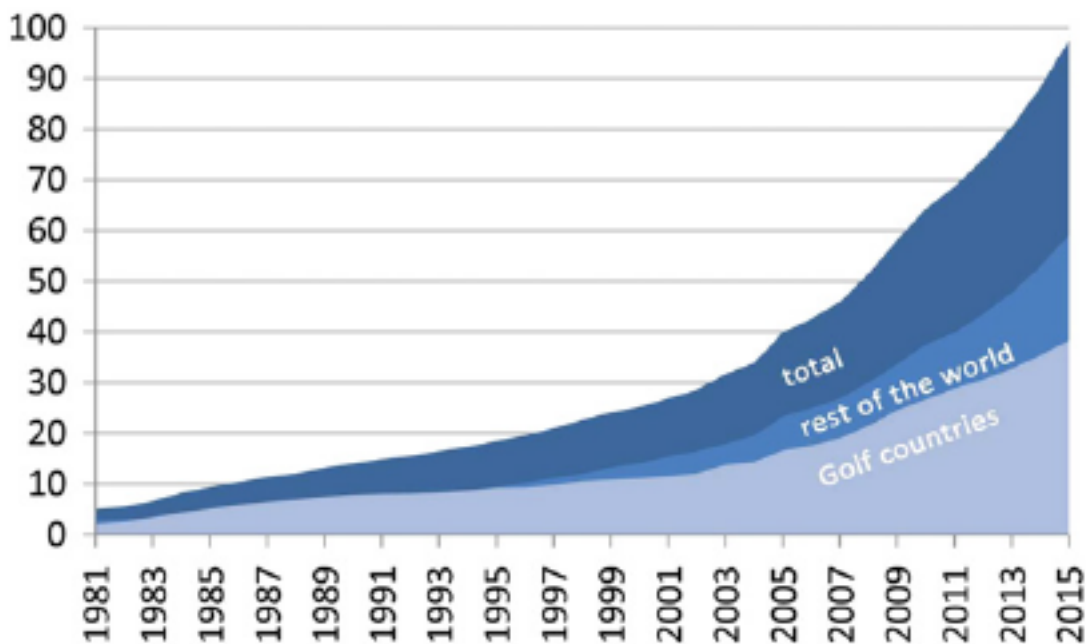


Figure 2.2: Worldwide desalination capacity growth. (Taken from (Lattemann, Kennedy, Schippers, & Amy, 2010)).

Above in Figure 2.2 the growing worldwide desalination capacity from 1981 to 2015 (partly projected) is shown. A very strong growth can be observed, thus making research in this field increasingly interesting. More on desalination will follow in chapter 4.

2.1.3. Drinking Water and Health Issues

Drinking water, often referred to as potable water, can be defined as water delivered to the consumer which can be safely used for drinking, cooking and washing purposes. Generally potable water must satisfy the following requirements:

- It shall contain no disease-producing organisms
- It shall be colorless and clear
- It shall be good-tasting and free from odors
- It shall be non-corrosive
- It shall be free from gases, such as hydrogen sulfide and staining, such as iron and manganese
- It shall be plentiful and low in cost

In order to meet these requirements water is typically taken from an approved source and fed through a properly designed and operated treatment and disinfection scheme. After being properly treated the water is supplied to the consumers through a protected distribution system that ensures sufficient water at sufficient pressure. Another important aspect is the temperature of the water in the distribution system, this mainly to prevent water borne diseases such as for example legionella. Conditions which are favorable to multiplication of legionella and should be avoided are: a water temperature in between 25 [°C] and 40 [°C], a long residence time and the presence of biofilms and sediments (van der Kooij, Veenendaal, & Scheffer, 2005).

3. Location & Climate

3.1. Introduction to Jakarta

Jakarta is the capital and largest city of Indonesia, it is located on the lowlands of the northwest coast of the Java province and covers an area of about 652 km². Jakarta is relatively close to the equator and has a humid tropical climate, the average annual temperature is 27°C and the yearly rainfall is 2000 mm due to the influence of Monsoon (Onodera et al., 2009). Jakarta was established in the fourth century and rapidly became an important trading port for the Kingdom of Sunda. Later on it was colonized and known as Batavia, the facto capital of the Dutch East Indies. Jakarta has a population of approximately 9.6 million and it is listed as a global city in the 2008 Globalization and World Cities Study Group and Network research (Wikipedia, 2012). The city has an approximate population of 11-12 million during the week, this due to commuters who work in the city during the week. It's quite obvious that due to the recent urbanization the water demand in Jakarta has significantly increases. The following paragraphs will briefly discuss drinking water and sanitation in Jakarta and Jakarta's wind & solar climate.

3.2. Introduction to Drinking Water & Sanitation in Jakarta

Inequitable access to (drinking-) water supply and sanitation has been characterized as a critical development challenge for the South (Bakker, Kooy, Shofiani, & Martijn, 2008). After having read several papers, it was concluded that the same could be said for (drinking-) water and sanitation in Jakarta. Several studies (Brennan & Richardson, 1989; McIntosh, 2003) have even characterized Jakarta's water and sanitation sector as one of the weakest in Asia. Jakarta's water supply is said to be highly fragmented and official (generous) estimations indicate that the cities formal water supply system reaches no more than 56% of its inhabitants (Bakker, 2007). In the paper by Bakker et al. (2008) it is also mentioned that especially the urban poor lack access to the Indonesian water supply, these (poorer) Jakarta inhabitants which are not connected to the municipal water supply system rely on a variety of sources, amongst which: shallow and deep groundwater wells, water via municipal supply networks, spring water, rain water, rivers and other distribution methods (bottled water etc. etc.). But most of the above mentioned water sources are often characterized by poor water quality. The city's small sewerage system, which according to Bakker et al. (2008) covers less than 2% of the households, is one of the main causes of the poor quality. Due to the limited coverage the vast majority of wastewater is disposed rivers, canals or poorly operating septic tanks, as a consequence the water quality in the piped network and shallow groundwater is poor and thus of particular concern.

3.3. A brief history of Drinking Water in Jakarta

All of the above mentioned issues regarding Jakarta's water system could largely be accounted to the Dutch Colonial era. Bakker et al. (2008) researched the design of the original colonial network and showed that Jakarta's original water supply was deliberately limited to the "European" urban inhabitants, the non-European villages often referred to as "Kampungs" were barely included in any of the city's water network. They also showed an interesting statistic where in 1929, the European population, comprising only 7% of the population, yet they consumed 78% of the water supplied via the networks. But even in the post-colonial period (the decades following the Independence) water supply in Jakarta continued to be highly differentiated and has been characterized by many similarities

to the colonial patterns mentioned above. This can be partially explained by the notion that since the Independence, the government has often emphasized its focus on converting Jakarta into an international showpiece to symbolize Indonesian unity. Hereby little of the financial means have been spent on improving the city's infrastructure, the little network expansions which have taken place were deliberately limited to upper class residential areas. Now that the history of Jakarta's water network has been introduced, let have a look at the cities current water supply.

3.4. Jakarta's current water network

Before we continue, it is important to remember that the water supply system in Jakarta can be split in to two rough sections. Namely the formal and informal water supply, as highlighted earlier the informal water supply exists of: vendors, private wells etc. etc., and the formal water supply refers to the piped water system. Since roughly the 1990's there is a growing trend towards water privatization in East Asia, and in Jakarta the situation is no different. Since 1998 this approach has been introduced to the formal water supply in Jakarta. After independence and up until 1997 the network was managed PAM Jaya, a government operated water distribution company. Since the privatization PAM Jaya has divided the distribution network in two regions. The regions are separated by the Ciliwung River, and have been managed by the two private companies: Thames Water Overseas and Suez Lyonnaise des Eaux. Both companies were awarded contracts to run the water supply in Jakarta for 25 years. The Western sector is formerly operated by PAM Lyonnaise Jaya (Palyja) and the Eastern sector is operated by PT. Thames PAM Jaya (TPJ).

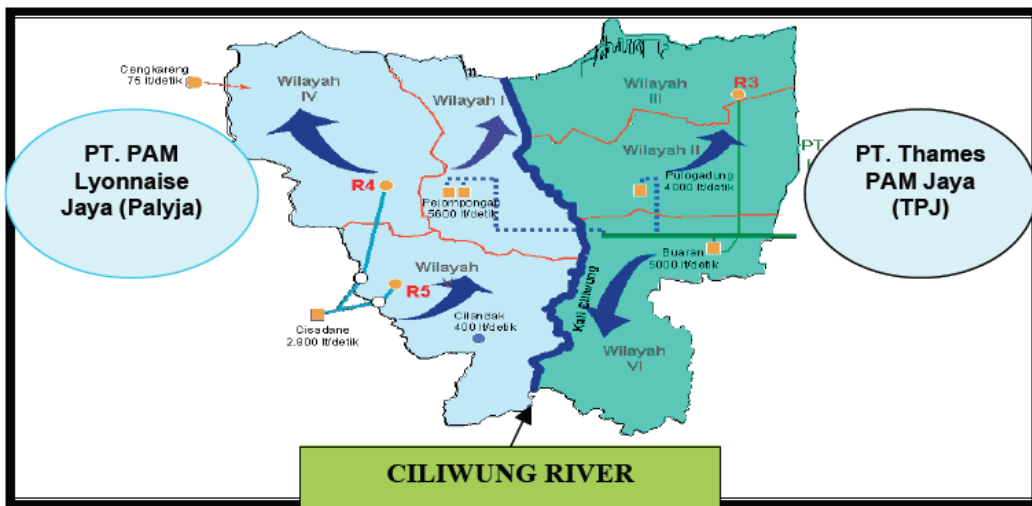


Figure 3.1: The division of Jakarta's water distribution, as described above. (Image taken from (Kurniasih, 2008)).

Due to the scope of this project, the motivations for/and effect of the privatization will not be discussed thoroughly, but the main reason for privatizing the water sector was that it was believed that the private sector as better managerial capacity, better experience & technological capacity, and stronger financial capacity to solve the water supply issues in Jakarta. One of the many read articles (Kurniasih, 2008)discusses however that these assumptions have not been realized and (many) problems still exist

despite of a decade of private water supply. The main issues which Kurniasih (2008) discussed can be found below, for further information it is suggested to study the above mentioned paper.

1. Residents who have access to piped water have been affected by privatization through significant water tariff increases. Meanwhile, water services are poor, and thus the need for alternative safer drinking water has increased.
2. Water service expansion is mainly based on profit considerations, and thus the poorer inhabitants are often excluded from the formal water network.
3. Environmental problems increase as private sector focuses on economic management and profit while often neglecting environmental management.

Partially due to the above mentioned reasons it seemed like the opportune place for implementing the PV powered RO system. But before discussing this system let's discuss Jakarta's groundwater quality, as this will be the source of water in this project.

3.5. Jakarta's groundwater quality

Jakarta has several natural sources of (fresh) water, there is: groundwater, surface water, spring water, and less frequently used river- and rainwater. As it has been mentioned earlier most of these sources are characterized by poor quality. What has not really been mentioned however, are the issues regarding overutilization of the groundwater resources due to the recent urbanization. This overutilization has resulted in dropping natural water levels and subsequent seawater intrusion mainly in North Jakarta, which in turn has led to a deteriorating groundwater quality (higher salt concentrations) in many areas of Jakarta (Steinberg, 2007). It is of utmost importance to acknowledge this over-pumping problem, but it could comprise of an entire research on itself. But as it has been said earlier about the possible effects of the privatization of the water supply, this problem needs to be acknowledged but will not be further researched in this section or report. What will be discussed now however is the quality of the groundwater in Jakarta. What has become clear after having read multiple papers it is become clear that the groundwater quality is very specific for every individual location/well in Jakarta. A specific example of this was found the paper by Delinom et al. (2009), where they presented a table with groundwater samples collected over 41 boreholes across the whole of Jakarta (please see Appendix A). What can be seen in this table was that the pH of the water ranged from 4.04 to 8.01 and greatly varying total hardness's of the water (THH), and a groundwater TDS ranging between 1000-9000 [mg/l]. What these values indicate (mainly the latter) is that during this project there will be dealt with brackish water. It is hard to provide a more narrow range of groundwater quality, as this will strongly depend on the exact well used, but what can however be more accurately predicted is the available solar irradiation and wind speeds in Jakarta, this is what will be discussed in the following paragraph.

3.6. Indonesia's Renewable Energy Sources

As the only Southeast Asian member of the OPEC, Indonesia has significant fossil fuel reserves. Thus it's no surprise that despite the countries RES, approximately 65% of its primary energy production is based on fossil fuel sources such as: coal, oil and natural gas. This is illustrated in the figure below, which was taken from (*Renewable Energy Potential*, 2006).

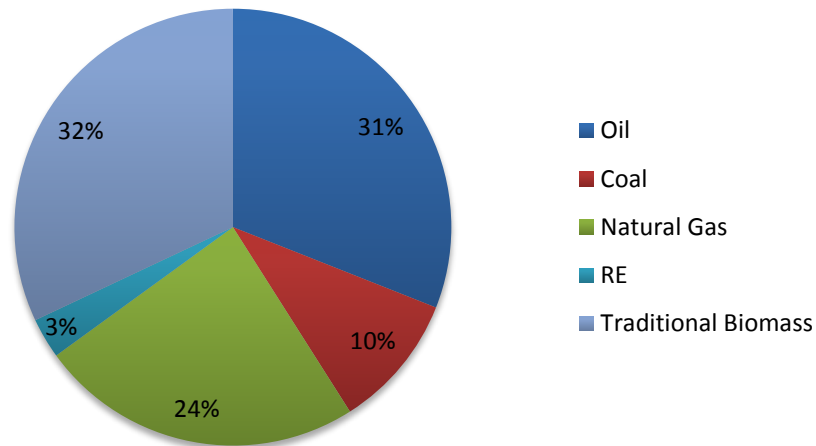


Figure 3.2: Distribution of the energy sources used in Indonesia. (Data taken from (*Renewable Energy Potential, 2006*)).

The figure also shows that at the time of the report, RES contributed to roughly 3% of the countries total energy production. What Figure 3.2 doesn't show however is that it's mostly biomass from the sugar and wood industries, hydropower, and some geothermal energy which contribute to this 3% of RES. One would expect that photovoltaic (PV) and wind energy sources are also abundant in a country, which seems to be so ideally located right along the equator. But despite its favorable location Jakarta still exhibits two clearly identifiable seasons, namely the rainy season, which typically runs from November through June and the remaining 4 months, which form the cities dry season. Figure 3.3 gives an overview of the Energy sources as they are spread along the different regions of Indonesia. If one is familiar with the location of Jakarta, it can be seen that Jakarta itself seems like a promising location for the implementation of mainly solar energy. But more specifics on Jakarta's wind and solar climate can be found in the sections to follow.

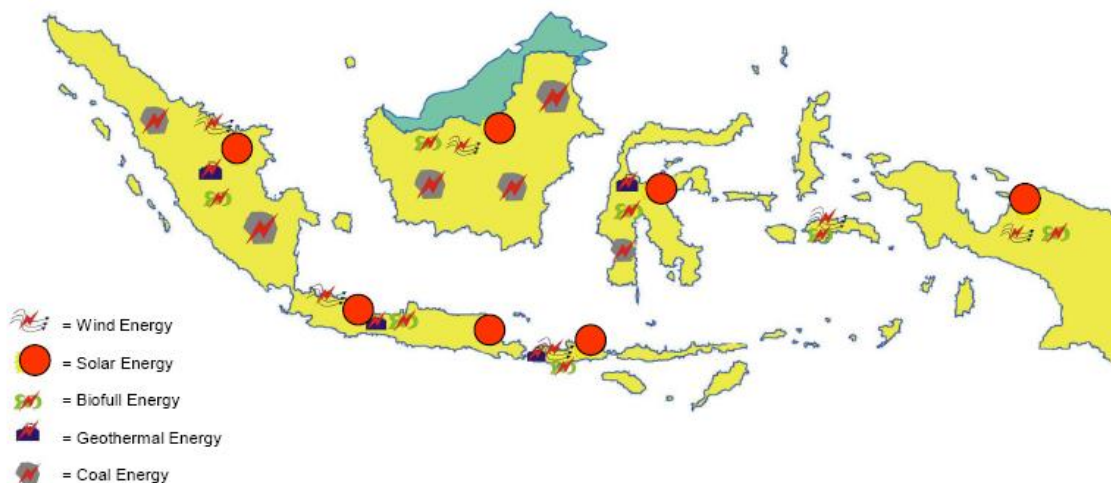


Figure 3.3: An overview of Energy Potentials in Indonesia. (Taken from (*Susandi, 2008*))

3.6.1. Jakarta's Wind Climate

As mentioned in paragraph 3.6, it is very important to evaluate renewable powered RO systems based on accurate available RE sources. Typically, obtaining such data is no problem. For the case of Indonesia and more specifically Jakarta, this however proved to be a bit more challenging than usual. The wind and solar data obtained in these sections were found in a wide variety of sources. Most of the presented data were taken from scientific papers, university presentations, the Internet or modeling software.

In the case for the wind data, the data was found on SSE (2013). On average the wind speeds found in Indonesia are between 2 – 5,5 [m/s]. This can be seen below in Figure 3.4, where a wind map with the average wind speeds on and around the island of Java is shown.

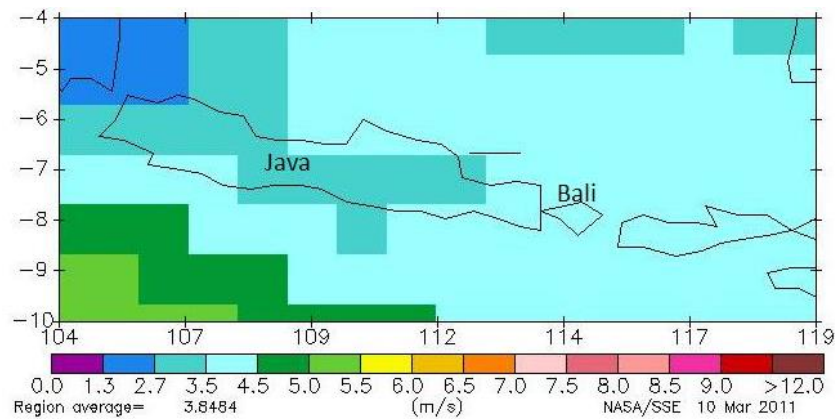


Figure 3.4: Windmap of Java and surroundings. (Data taken from (SSE, 2013), image from (Vollebregt & Feenstra, 2012)).

The figure shows that the average wind speed in the Jakarta region is between 2.7 - 3.5 [m/s]. But in order to determine if wind turbines are a viable option, a more detailed analysis is required. Below graphs with the average monthly wind speeds for Jakarta can be found, these are wind speeds measured at 10 [meters] above sea-level.

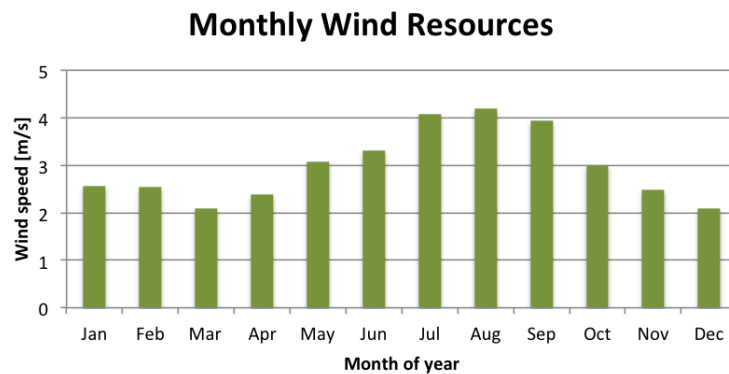


Figure 3.5: Average monthly wind speeds. (Data taken from (SSE, 2013)).

A simple research showed these lower wind speeds make it harder to implement small-scale wind turbines. Since cut-in wind speeds typically start at 3[m/s] for smaller wind turbines, simply looking at the average wind speeds and the Weibull distribution one could say that wind turbines will most likely

not be the ideal energy source for this location. However, wind energy calculations will still be performed in chapter 6.1.

Table 3.1: Yearly average wind speeds.

Mean	Standard Deviation
2.9775	0.721469854

3.6.2. Jakarta's Solar Climate

Simply looking at the results of Vollebregt and Feenstra (2012) who previously experimented in Bali, it could be said that Jakarta's solar is also favorable for the implementation of this project. However a detailed examination of the local solar climate is still required. The solar data presented in this sections were found on (SSE, 2013) and in the paper written by Rumbayan, Abudureyimu, and Nagasaka (2012).

Average Daily Radiation

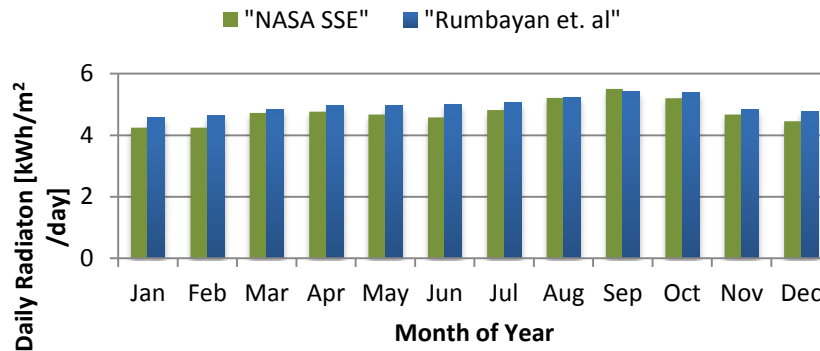


Figure 3.6: Average daily insolation for Jakarta. (Data taken from (SSE, 2013) and (Rumbayan et al., 2012)).

In the figure above the average daily radiation for Jakarta can be found. At a glance the data seems comparable, below in Table 3.2 the daily mean values and their standard deviation can be found.

Table 3.2: Mean daily insolation and the standard deviation

Data Found	Mean insolation [kWh/m2/day]	Standard deviation [kWh/m²/day]
NASA SSE	4.76	0.37
Rumbayan et al.	4.97	0.26
Data used for Calculations		
Rumbayan et al.	4.97	0.26

For further sizing calculations the data found in the paper by Rumbayan et al. (2012) will be used. The reason for this is, because this data was originally obtained using actual measurements on the ground. As opposed to the NASA/SSE data that were generated using a data software package. PV power output calculations will be performed later in chapter 6.

3.7. Specific Location & Period/Season

During the latter stages of this project contacts were established with Pam Jaya, the government-owned water company mentioned earlier in chapter 3.4. Cooperation was established between the TU Delft, the ITB and PAM Jaya, making it possible to perform the research at the ex-water treatment plant of Pam Jaya located at Muara Karang, North Jakarta. The treatment plant was shut down around the year 2000 due to deteriorating groundwater quality in the north. Immediately after the initial contact, it became evident that all parties could benefit from this research. From the point of view of the student, it was the perfect location, being close to the coast meant that the groundwater would most likely meet the “brackish condition” required. For PAM Jaya this research was interesting mainly due to the nature of the water production. All of the company’s originates from southern Jakarta and/or villages located south of Jakarta, this due to the deteriorating ground water quality (salt water intrusion amongst things). Thus making reverse osmosis water desalination an interesting option if PAM Jaya would wish to re-open their water treatment plants in the northern (coastal) areas of Jakarta.

The period in which the research was initially performed was from July through December 2012. Actual measurements however were taken in the month November and December, this due to delays and unforeseen problems encountered during the period in Jakarta. This meant that the actual measurements were taken during the first months of the rainy season. The rainy season in Indonesia runs from the months November through April and the average solar insolation is less (as shown in section 3.6.2). A map with the test location at Muara Karang, North Jakarta can be found below in Figure 3.7.

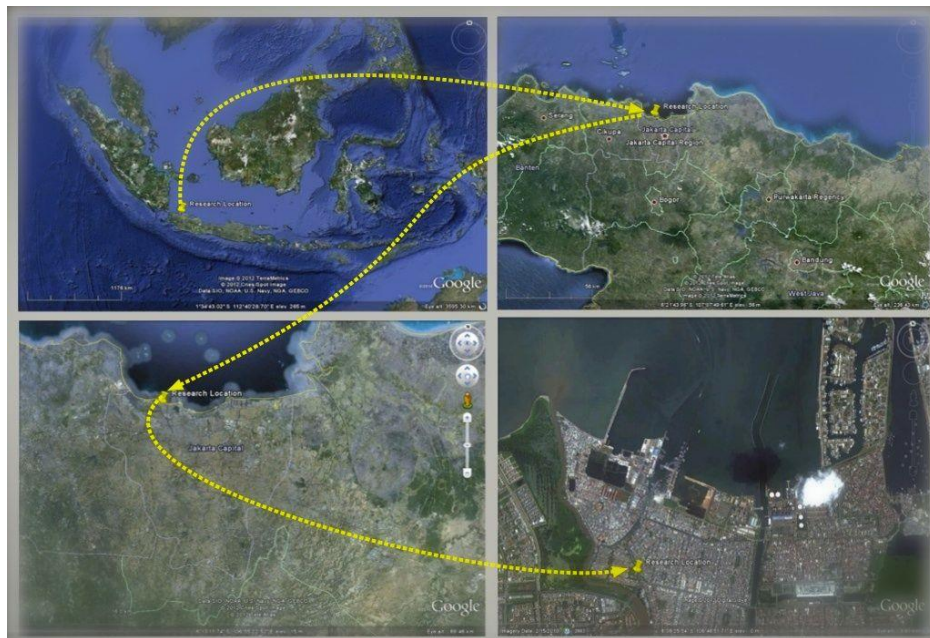


Figure 3.7: Precise location of the pilot plant at Muara Karang, North Jakarta.

A second set of measurements was taken at the pilot plant in the period of March – April 2013. But before discussing the exact plant setup and sizing details, let's take a look at the mainstream desalination techniques available on the market.

4. Introduction to Desalination

Hopefully it is clear by now that accessibility to potable drinking water in Jakarta is rather limited. And while conventional water treatment technologies are adequate to treat water with low amounts of salinity (often measured in total dissolved solids (TDS)), more advanced desalination techniques are required in locations like Jakarta where the groundwater has higher TDS values (Gude, Nirmalakhandan, & Deng, 2010). As it has been said, desalination is the treatment process which removes salts or other dissolved minerals and contaminants such as dissolved metals, radionuclides, bacterial and organic matter from high salinity water to produce fresh water (Alghoul, Poovanaesvaran, Sopian, & Sulaiman, 2009). When discussing (drinking-) water, three different categories of water can be identified: seawater, brackish water and fresh water. There are many different standards, but the most common states that water is considered as seawater when it has a TDS of 15,000 [mg/l] or more, brackish water is considered to have a TDS of 1000-15000 [mg/l], and fresh water/low-salinity has a TDS below 500 [mg/l] (Alghoul et al., 2009; El-Manharawy & Hafez, 2001).

Table 4.1: Table showing water classification

Water Classification	TDS [mg/l]
Sea Water	$\geq 15,000$
Brackish Water	1,000 – 15,000
Fresh Water	≤ 500

Figure 4.1 shows the worldwide feed water type used for desalination processes. It can be seen that Seawater still accounts for the largest source of desalinated water, followed by brackish water. River- and wastewater follow respectively with significantly lower shares.

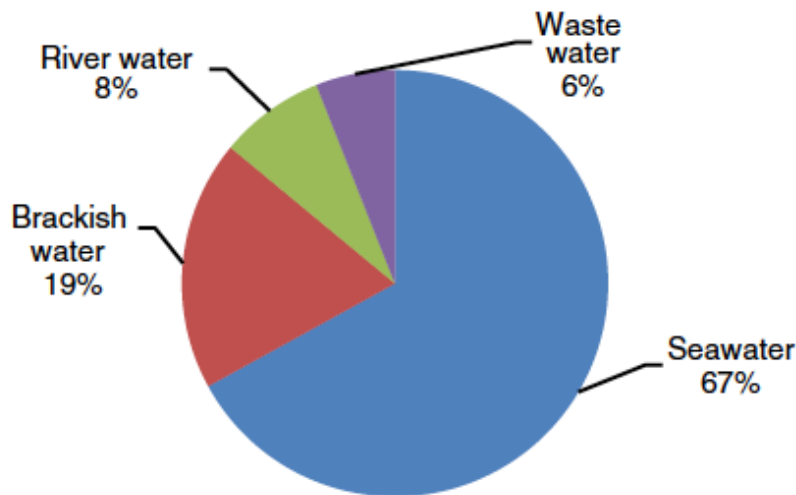


Figure 4.1: Worldwide feed water used for desalination. (Figure taken from (Mezher, Fath, Abbas, & Khaled, 2011)).

Typically, desalination processes are energy intensive and are often powered by energy derived from fossil fuels. As explained by Gude et al. (2010) current desalination techniques can be divided into the three categories:

- Phase Change Processes: These are typically thermal processes that involve heating of the feed to “boiling point” at the operating pressure to produce steam, and condensing the steam to produce fresh water. Typical examples of phase change processes are: solar distillation (SD), multi-effect distillation (MED), multi-stage flash (MSF) and mechanical- & thermal vapor compression (MVC and TVC respectively).
- Non-Phase Change (*also Membrane Separation*) Processes: Here separation of dissolved salts from the feed water is achieved by means of mechanical or chemical/electrical means using a membrane barrier between the feed and the product. Applications of this principle are electro dialysis and the recently popular reverse osmosis (RO) process.
- Hybrid Processes: As the name indicates, these processes involve combinations of phase change and non-phase change processes, an example is RO combined with MSF or MED processes.

Below in Table 4.2 the basic principle of the three different desalination categories can be found, the information was taken from (Gude et al., 2010; Mezher et al., 2011).

Table 4.2: Characteristics of the different desalination categories. (Information taken from (Gude et al., 2010; Mezher et al., 2011))

Characteristic	Phase change process	Non-Phase change process	Hybrid
Nature	Thermal process: MED, MSF, MVC, TVC (evaporation and condensation)	Pressure/concentration gradient driven: RO (membrane separation), ED (electrical separation)	-
Membrane pore size	-	0.1 – 3.5 nm	0.2 – 0.6 µm
Feed temperature	60 – 120 °C	<45 °C	40 – 80 °C
Cold water stream	May be required	-	20 – 25 °C
Driving force for separation	Temperature and concentration gradient	Concentration and pressure gradient	Temperature and concentration gradient
Energy	Thermal and mechanical	Mechanical and/or electrical	Thermal and mechanical
Form of energy	Steam, low-grade heat or waste heat and some mechanical energy for pumping	Requires prime quality mechanical/electrical energy derived from fossil fuels or renewables	Low grade heat sources or renewable energy sources
Product quality	High quality distillate with TDS<20 ppm	Potable water quality TDS<500ppm	High quality distillate with TDS 20 – 500 ppm
Technology Growth Trend	Moderate – High	High	-
Environmental Impact	Brine Discharge at temperatures above ambient temperature, TDS increase of 15-20%	Brine discharge at ambient temperatures, TDS increase of 50-80%	-

According the World Health Organization (WHO), water with a TDS of 600 [mg/l] or less can be considered as good drinking water (WHO, 2011). So looking back at Table 4.2, it can be seen that all of

the desalination techniques mentioned meet the WHO requirements. Below in Figure 4.2 the worldwide desalination capacity by process is shown, it can be seen that RO has a very large share in the overall desalination capacity.

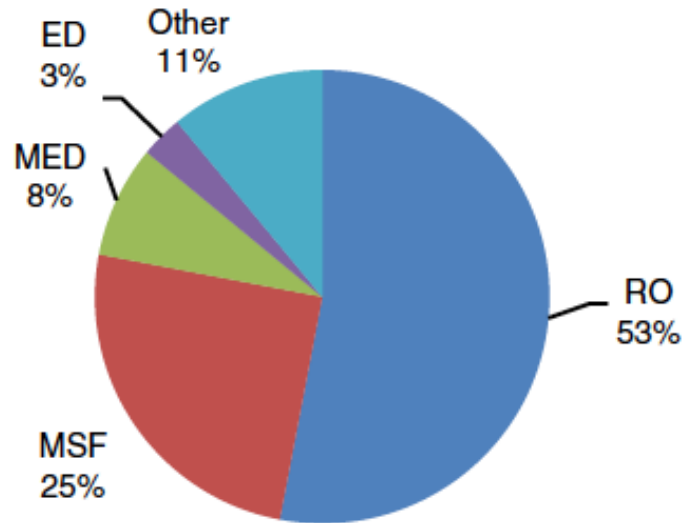


Figure 4.2: Worldwide desalination capacity by process. (Figure taken from (Mezher et al., 2011))

The literature study also lead to the figure below, where the information of Figure 4.1 and Figure 4.2 were combined to show the desalination capacity by feed water source and process type. It can be seen that for brackish- and wastewater, RO has the largest share. While for seawater desalination, MSF still has the largest share.

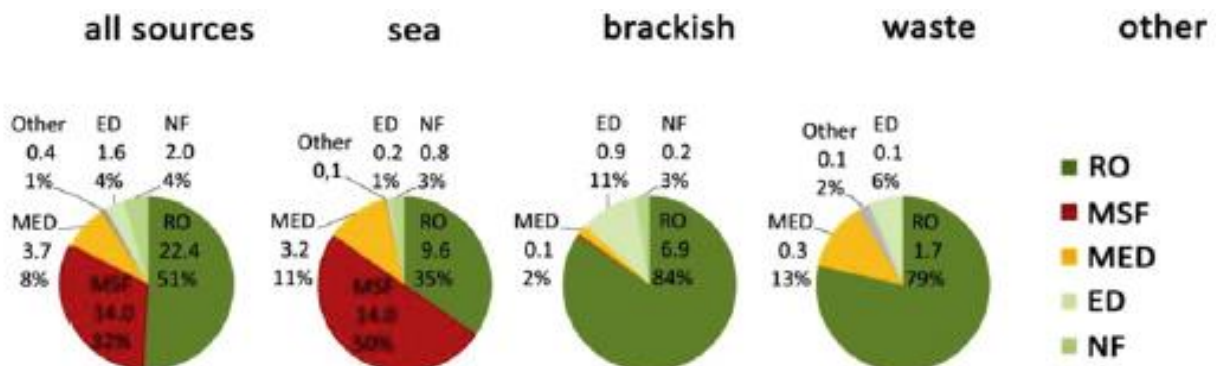


Figure 4.3: Global desalination capacities by process and water type. (Figure taken from (Lattemann et al., 2010))

4.1. Reverse Osmosis

Osmosis is a natural process of flow through a semi-permeable membrane, when the salt concentration on one side is higher than the concentration on the other side water will flow through the membrane from the “lower concentration water” to the side with the higher salts concentration. Nature will try to equalize the concentration difference, however when pressure is applied on the side with the higher salts concentration a new equilibrium will develop. The extra pressure applied will result in a flow of

water through the membrane (while the salts are retained), this phenomenon is called reverse osmosis (van Dijk et al., 2009). Below in Figure 4.4 a schematic of osmosis and reverse osmosis can be seen.

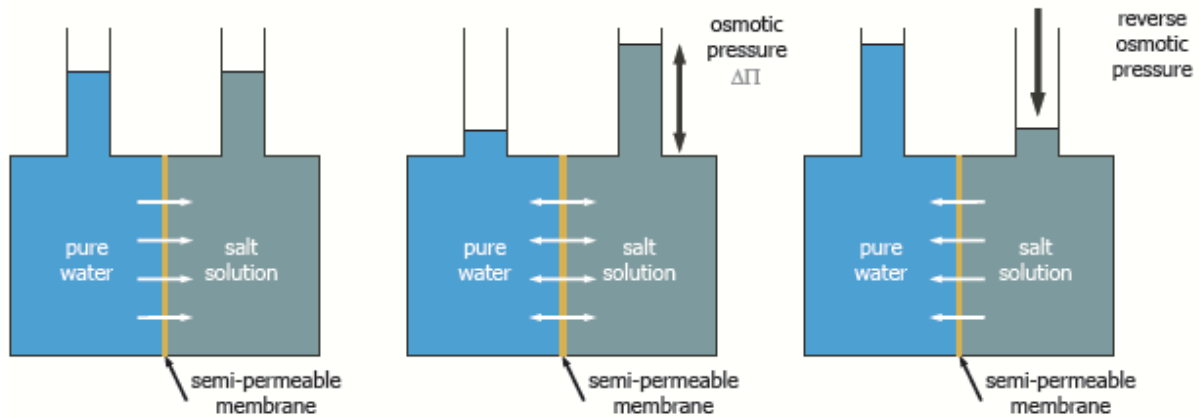


Figure 4.4: The principle of Osmosis and Reverse Osmosis. (Taken from (van Dijk et al., 2009)).

The driving force of this process is the overpressure that is present after subtracting the osmotic pressure from the applied pressure. As (van Dijk et al., 2009) explain, RO membranes are typically have a spiral-wound configuration. Water is fed from one side into the RO module. Spacers (supporting layers between the membrane sheets), distribute the water over the membrane element. An element is defined as a number of membrane sheets twisted around a central permeate collecting tube. The principle described above is illustrated below in Figure 4.5.

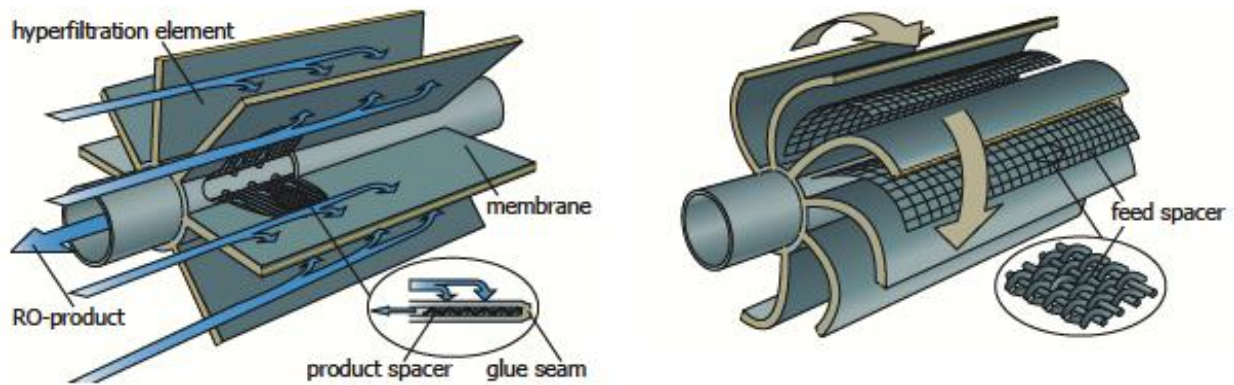


Figure 4.5: The principle of spiral-wound RO membranes. (Image taken from (van Dijk et al., 2009))

The energy consumption of this process is directly related to the salts concentration and the membrane properties, thus desalination of water with higher salts concentration will require more energy. Table 4.3 below shows the energy requirements and green-house-gas emissions (GHG) for several desalination techniques. When comparing the energy requirements and the GHG emissions, it appears that RO outperforms the other techniques. The data was taken from Gude et al. (2010).

Table 4.3: Energy requirements and GHG emissions for different desalination processes (Gude et al., 2010).

Process	Multi-effect solar still (MESS)	Multi-stage distillation (MSF)	Multi-effect distillation (MED)	Mechanical Vapor Compression (MVC)	MED-TVC	RO	ED
Energy Requirements							
Thermal energy [kJ/kg]	1500	250-300	150-220	-	220-240	-	-
Electrical energy [kWh/m ³]	0	3.5-5	1.5-2.5	11-12	1.5-2	5-9	2.6-5.5
GHG emissions [kgCO₂/m³H₂O]							
Total electric equiv. [kWh/m ³]	0	15-25	8-20	11-12	21.5-22	5-9	2.6-5.5
Maximum value	0	24	19.2	11.5	21	8.6	5.3

When discussing RO systems, it is important to distinguish salt-water reverse osmosis (SWRO) systems and brackish water reverse osmosis (BWRO) systems (as discussed earlier). In this project the feed water will be brackish and thus only the BWRO systems will be further elaborated in this report. As it has been indicated earlier in this report, BWRO requires less energy when compared to SWRO. This due to the lower operating pressure require for BWRO. Despite this difference, the general the setup of BWRO and SWRO are quite similar. For a simple RO setup, feed (raw) water is pumped into the system where the membrane separates the raw water (feed flow) into a product (permeate flow) and waste product (concentrate flow). This simple setup can be seen below in Figure 4.6.

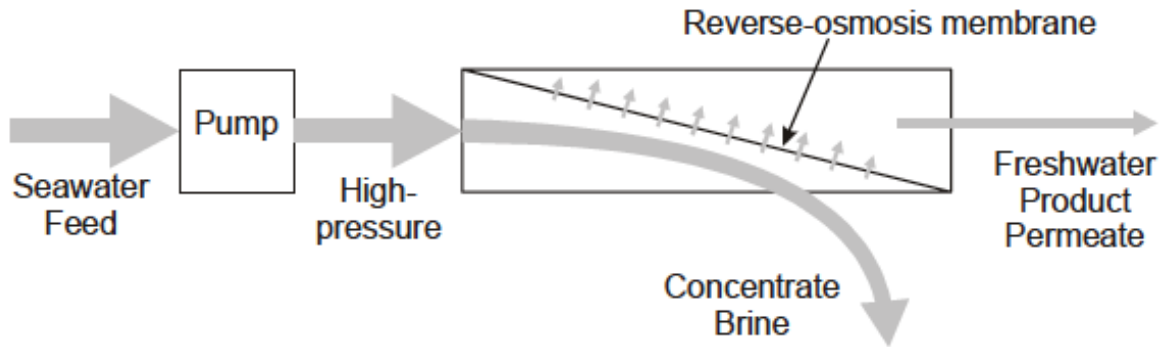


Figure 4.6: Schematic presentation of a simple RO desalination plant. (Image taken from (El-ghonemy, 2013a)).

The main (often electrical) energy required for this process is for pumping the water at relatively high operating pressures. For this reason RO installations typically are a bit more advanced than the above shown configuration. Often a multiple pass setup or a setup with some sort of energy recovery device is used. This way the high-pressure waste stream (concentrate) is re-used, thus making better use of the high amounts of energy required to run this process. A schematic presentation of both systems is shown below in Figure 4.7.

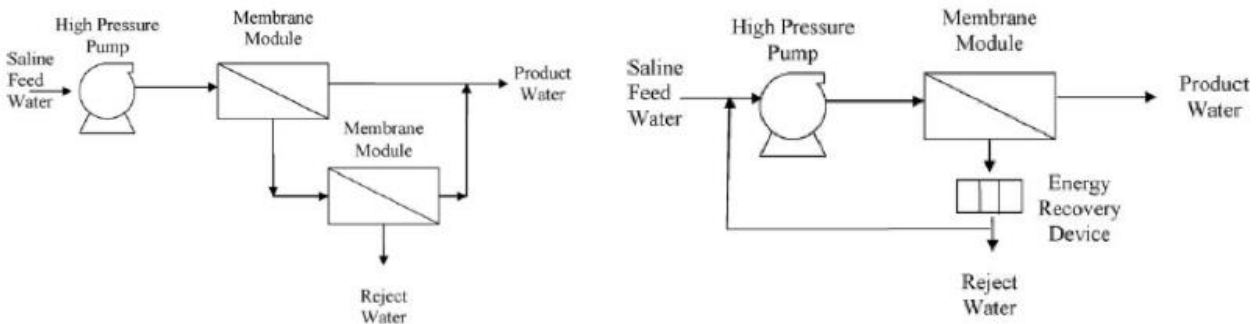


Figure 4.7: Left a schematic presentation of a single pass RO setup, and on the right a RO setup with energy recovery device. (Images taken from (Alghoul et al., 2009)).

As indicated earlier, RO holds several advantages over thermal processes. These advantages are:

- Lower Energy Consumption
- Relative low investment costs
- No cooling required
- Less vulnerable to corrosion and scaling due to lower operating temperatures
- High space/production capacity
- Removal of contaminants other than salts
- Modular design
- Higher recovery ratios possible.

But as any technology there are also disadvantages associated with RO technology, below is a list of disadvantages:

- Membrane replacement costs
- Sensitive to feed water quality changes
- Proper pre-treatment required to elongate membrane life
- Membranes susceptible to bio fouling
- Mechanical failure possible, due to relatively higher operating pressure
- High salts concentration in the waste stream (negative environmental impact when discharged)
- Requires post treatment

All of the data listed above was taken from (Eltawil, Zhengming, & Yuan, 2009; Richards & Schäfer, 2010). Many of the above listed advantages are also mirrored by renewable energy micro generators (such PV and wind turbines), thus combining these two technologies seems like an obvious solution. In the following chapter the combination of renewables and RO technology will be discussed.

4.2. Renewable Powered Desalination

As mentioned earlier in this report, desalination requires large amounts of energy. Typically the energy to fuel these processes is derived from fossil fuels. And since the peak oil theory has also been acknowledged worldwide, incorporating renewables into desalination processes is a popular topic. Recall also that it was mentioned above in chapter 4.1, that renewable micro generators exhibit many of the same advantages as RO technology. Thus the fusion of these two technologies is imminent. One of the main advantages that makes the combination of these technologies such a success is their modularity. Gude et al. (2010) discussed several approaches towards incorporating renewables and desalination. The paper presented a chart of some possible configurations, a similar yet more elaborate chart was also found in the paper by Eltawil et al. (2009), this chart can be found in Figure 4.8.

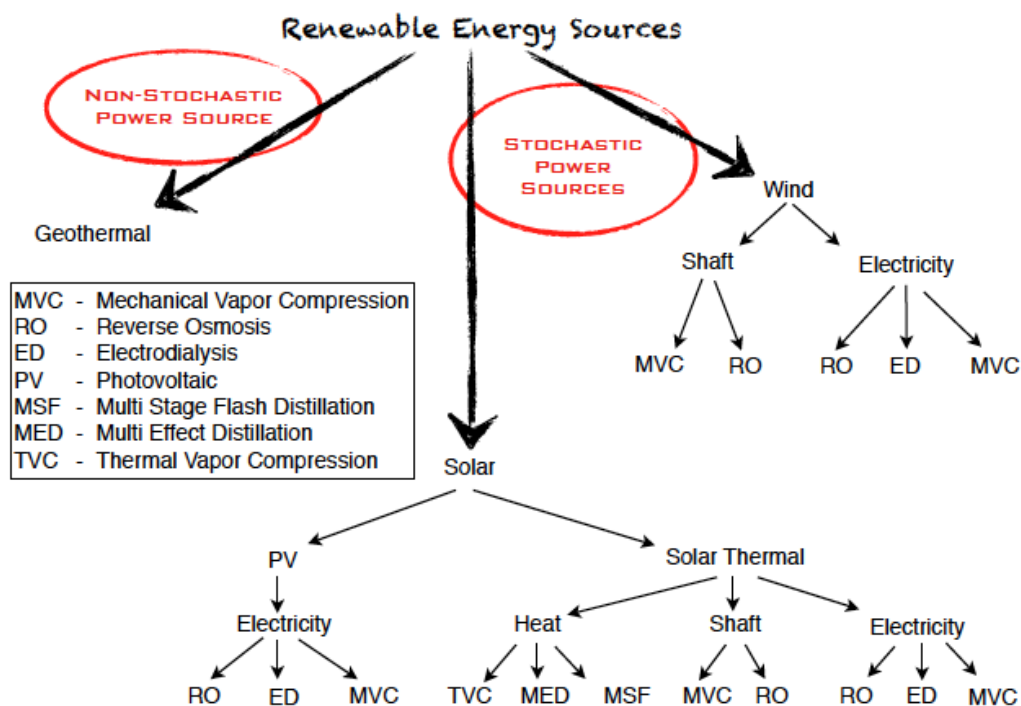


Figure 4.8: Possible configuration of renewable energy sources and desalination processes. (From (Eltawil et al., 2009) via (Thye, 2010)).

The figure shows many possible configurations, however when discussing renewable energy sources for desalination purposes, wind- and solar (PV) energy show the largest potential. The main hurdles that are encountered with the implementation of renewable powered desalination are similar to the hurdles present when introducing new technologies into any market. Namely they are:

- Capital Costs
- Technical issues
- Required regulation
- Training and information

4.3. Renewable Powered RO Desalination, an Overview

Renewable powered desalination projects have enjoyed most of their successes when implemented in small-scale and stand-alone installations. Amongst the installations completed, PV-RO however seems to be the most promising solution. This can be seen in Figure 4.9 and Figure 4.10, where the distribution of renewable powered desalination technologies is shown and a comparison between membrane desalination capacity and thermal desalination capacity can be found.

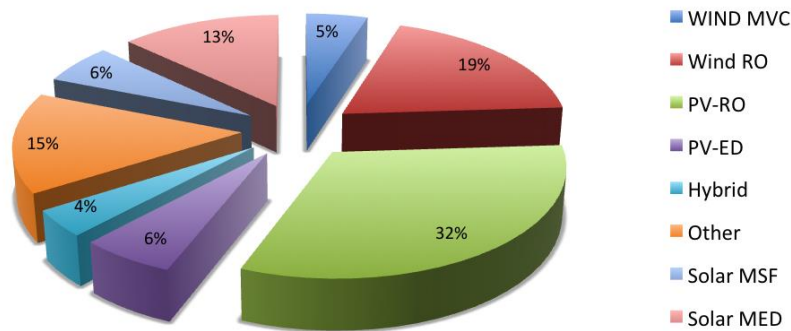


Figure 4.9: Distribution of renewable powered desalination technologies. (Data from (Eltawil et al., 2009)).

The main reasons for the success of the PV-RO combination are: Their modularity and also due to the fact that RO exhibits a relatively low specific energy content (SEC) for seawater and brackish water. Another advantage of the PV-RO combination is that it is possible to make use of the DC output of PV modules in order to directly power a DC pump. Thus elimination the need for DC-AC converters and hence also reducing conversion losses caused by DC-AC conversion (Richards & Schäfer, 2010). However, due the stochastic and intermittent nature of PV modules and other renewable energy sources, some sort of storage system is often required in order to avoid excessive rejection of the produced energy. Also storage is required in order to guarantee operation of the desalination units during unfavorable weather conditions (Spyrou & Anagnostopoulos, 2010).

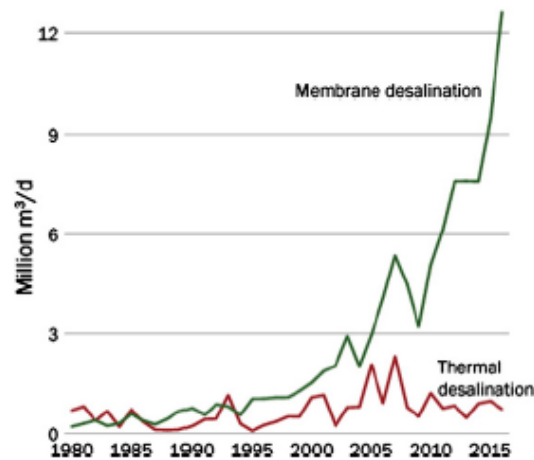


Figure 4.10: Comparison between membrane desalination capacity and thermal desalination capacity from 1980 to 2016. (Taken from (Misdan, Lau, & Ismail, 2012)).

During the literature study, many renewable powered RO desalination installations were found. It would be impossible to discuss all of the concepts found. But in order to get a better insight into the most recent developments in this field, it would be useful to give an overview with some example systems. In their report Vollebregt and Feenstra (2012) presented a table with examples. The table consists of relative recent examples of systems with a wide range of feed water qualities and combinations of with and without batteries.

Table 4.4: Examples of RES-RO systems. (Taken from (Vollebregt & Feenstra, 2012)).

Location	Year	Feed TDS [ppm]	Energy Source	Battery Storage	Production [m ³ /day]	Costs [euro/m ³]	Reference
Greece	2006	30,000	PV	no	0.35	7.8	(Mohamed, Papadakis, Mathioulakis, & Belessiotis, 2008)
Brazil	2000	1,200	PV	yes	6	10.2	(de Carvalho, Riffel, Freire, & Montenegro, 2004)
UK	2001	32,800	PV	no	1.45	2.4	(Thomson, 2003)
USA	2003	1,600	PV	no	1.5	5.2	(Cheah, 2004)
Australia	2008	5,300	PV	no	1.1	3	(Cheah, 2004)
Gran Canaria	2000	35,500	PV	yes	1.24	7.7	(Herold & Neskakis, 2001)
Bahrain	1994	35,000	PV	yes	0.2	2.2	(Al-Qahtani, 1996)
Curacao	2008	sea	WD-M	no	5-10	na	(Heijman, Rabinovitch, Bos, Olthof, & van Dijk, 2009)
Australia	1991	2,000 - 6,000	WD-M	no	0.2	16	(Robinson, Ho, & Mathew, 1992)
Hawaii	2002	3,000	WD-M	no	3.7	na	(Liu, Jae-Woo, Migita, & Gang, 2002)
Colombia	2004	35,000	WD-E	yes	0.4	na	(Moreno & Pinilla, 2005)
UK	2002	40,000	WD-E	no	8.5	na	(Miranda & Infield, 2003)
Jordan	1994	1,500 - 4,000	WD-E	yes	22-33	0.8-1.4	(Habali & Saleh, 1994)
India	2003	sea	WA-OWC	yes	14.4-21.6	na	(Sharmila, Jalihal, Swamy, & Ravindran, 2004)
Greece	2004	sea	PV, WD-E	yes	3.1	23	(Tzen, Theofilloyianakos, & Kologios, 2008)
Greece ^{design}	2003	40,000	PV, WD-E	yes	8.5	5.2	(Mohamed & Papadakis, 2004)

As it can be seen in the table, there are several concepts that do and several that do not make use of batteries. Batteries are often an easy solution, the main advantages of employing a battery bank in such a RO system is to buffer and provide constant energy flow during periods of no (or insufficient) electricity production. But according to the information found in (McKenna, McManus, Cooper, & Thomson, 2013; Thomson, 2003; Thomson & Infield, 2003; Thomson, Miranda, & Infield, 2003) batteries are widely seen as the weakest link in PV-RO desalination plants, because of the pre-mature failure of

batteries. And while the capital costs of batteries are reasonable, the maintenance costs for batteries are very high. Moreover batteries increase the (electrical) losses of the system, while their performances also degrade more rapidly in hot and coastal (salty) climates. Where efficiencies are usually around 85%, in hot and arid climates the battery losses can exceed 25%. Also battery life can be reduced to as little as two years. In order to improve battery life, complex control strategies must be applied and thus Thomson prefers battery free system without any means of energy storage (McKenna et al., 2013; Thomson, 2003; Thomson & Infield, 2003; Thomson et al., 2003). However the author also mentions that continuous operation of RO membranes is preferred, the main advantages of continuous operation of RO system are listed below:

- Maximize operation, thus improving cost-efficiency
- Constant operation produces more constant water quality
- Intermittent and variable flow is said to cause membrane fouling

And while not much information is documented on the effect of intermittent/variable operation of RO installations and the negative influence of hot climates interest in continuously operated (small-scale) battery-free renewable powered RO systems is large. In the sections to follow some of the battery-free designs found during the literature research will be presented.

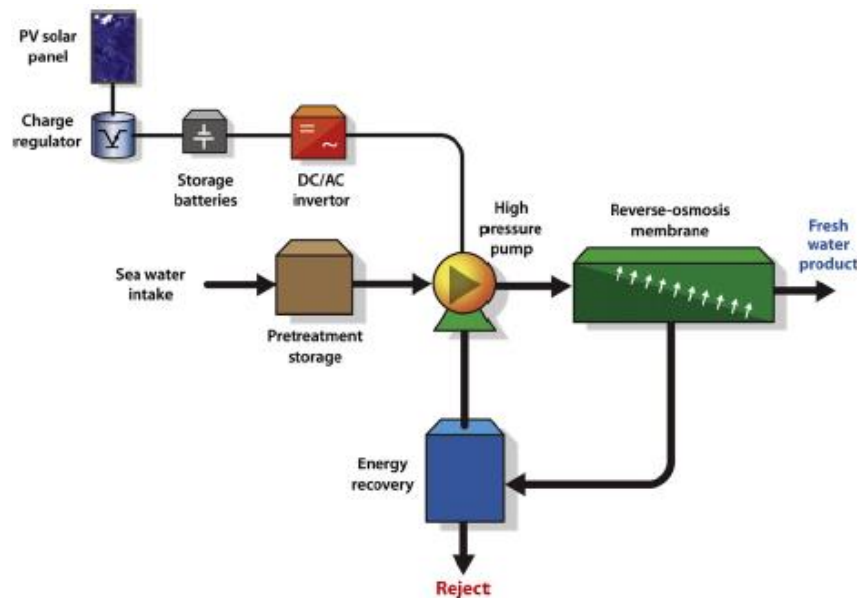


Figure 4.11: Schematic presentation of a typical PV powered RO desalination unit with battery storage

4.4. Battery-free Renewable Powered RO Desalination

In the paragraph above many of the disadvantages of batteries have presented, however the preference for a continuously operating RO desalination plant was also clearly stated. As mentioned in the introduction, this thesis will present an innovative battery-free continuously operating PVRO plant. There aren't many examples of (small-scale) continuously operated renewable powered (RO) desalination installations, however some interesting concepts were found while performing the literature research. In the following sections a couple of these will be discussed, first we will start with a

simple battery-free desalination plant. One that is not operated continuously, but nevertheless is helpful to understand the general setup of a RO desalination installation.

4.4.1. Simple battery-free PV-RO System

One way of operating renewable powered RO system without batteries is by slightly over-sizing the system and storing energy in the form of product water (Richards & Schäfer, 2010), the problem with this approach however is that the water tank must remain free of biological contamination. Another non-documented issue, is the claim that intermittent and variable operation cause the RO membranes to foul more rapidly. However, such (simple) systems have been proven to be successful in the field, and can be found in the papers by (Richards & Schäfer, 2003; Riffel & Carvalho, 2009) amongst others. This (basic) configuration can be slightly altered, in order to increase efficiencies. The main strategies applied are discussed below and can be seen in back Figure 4.7:

- Using multiple pass systems that re-use the waste (concentrate) stream, which is still pressurized.
- Incorporating an energy recovery device (as mentioned by (GKEREDAKI, 2011), more about energy recovery devices can be found in section 5.2.3.

4.4.2. Desalination using hydrostatic pressures

Another possibility found during the literature research was powering a RO system by means of hydrostatic pressure. This concept is not necessarily powered by renewable energy sources, but renewables could easily be incorporated into the design. The main idea of this design is that the RO desalination system uses hydrostatic pressure generated by a column of water with a storage tank, which is placed directly above the RO membrane (Al-Kharabsheh, 2006). Salt water is fed to the membrane, once the membrane is full the valve regulating the water column is opened and the hydrostatic pressure of the column forces to salt water through the membrane (via a piston), this (batch-) process is repeated over and over. And the authors claim that seawater can be desalinated with a SEC of 0.85 [kWh/m³]. This indeed is significantly less, when compared to traditional SEC's for RO seawater desalination. The system described, above can be seen in Figure 4.12.

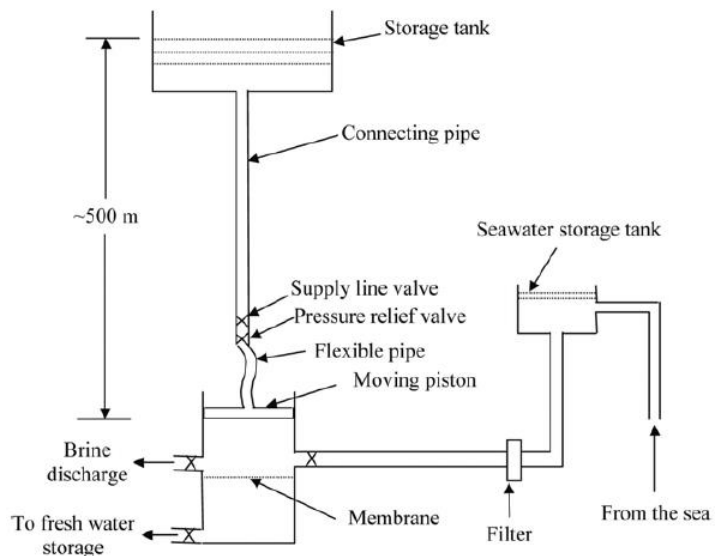


Figure 4.12: Proposed hydrostatic desalination installation. (From (Al-Kharabsheh, 2006)).

4.4.3. Stand-alone RO desalination system using a pumped storage unit

Another alternative for battery-free renewable powered RO systems, is a combination with a pumped storage unit. The design discussed in the paper by Spyrou and Anagnostopoulos (2010) is a hybrid renewable energy powered system which consists of an RO desalination unit, a fresh water storage tank, wind turbines an PV panel, and a pumped storage unit. A pumped storage unit typically consists of pump/turbine, an upper and lower water reservoir, and the required pipelines. When there is excess energy, this energy is used to pump water up into the upper reservoir and when there is a shortage of energy water is released through the turbine and electrical energy is generated. The upper and lower reservoirs serve purely as a pumped storage plant (PSP). The size of the reservoirs is mainly determined by the amount of storage required, and the head height of the storage reservoir. This system was only designed and a model was built, and wasn't tested physically. Spyrou and Anagnostopoulos (2010) claim that their design could produce (desalinated) drinking water, at a price of 1.5 – 3 [€/m³]. A schematic presentation of the design discussed is shown in Figure 4.13. In the following chapter the concept developed will be introduced.

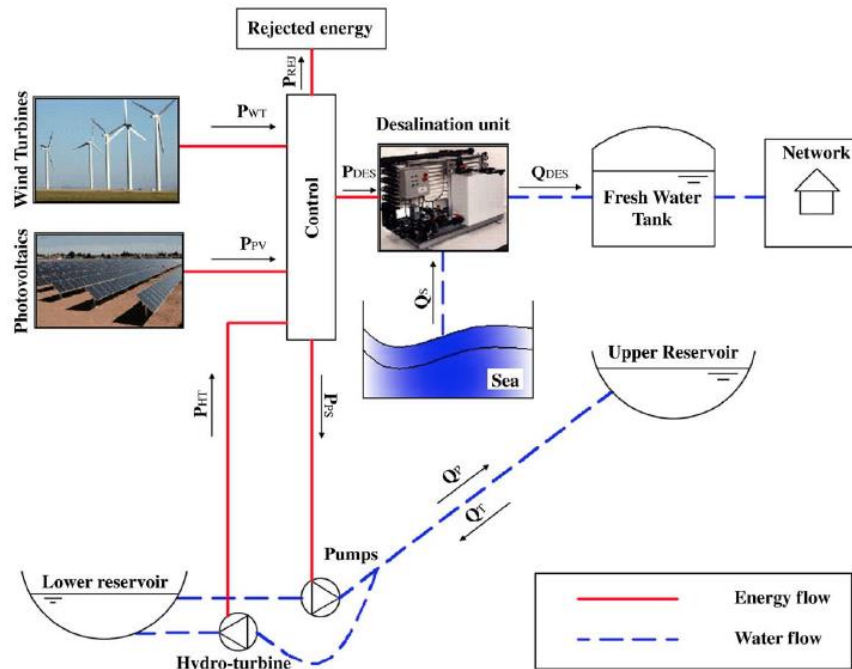


Figure 4.13: Hybrid RO Desalination design, with a PSP. (Taken from (Spyrou & Anagnostopoulos, 2010)).

5. System Concept

Now that the global water scarcity has been introduced and that that potential of (renewable powered) reverse osmosis as a solution has been discussed, it's time to discuss the initial concept of this research.

5.1. Previous Concept

As it has been mentioned earlier, this project is a follow up on previous work performed by (Vollebregt & Feenstra, 2012). In that project the authors designed and implemented a continuously operated battery free PVRO desalination installation. The authors implemented the design in South Bali, Indonesia and the system proved to be a success. The summarized results of this project can be seen below in Table 5.1.

Table 5.1: Summarized results of (Vollebregt & Feenstra, 2012).

Total solar irradiance received	196.1 kWh/m ²
Total permeate water produced	63.16 m ³
Total Solar pumped volume	453.45 m ³
Average solar irradiation per day	6.72 kWh/m ²
Average permeate water produced per day	2176 liter
Average solar pumped volume per day	15.63 m ³
Average conductivity feed water	12.6 mS/cm
Average conductivity permeate water	0.4 mS/cm
Average feed flow rate	10.58 l/min
Average water temperature	28.28 °C
Amount of pre-filters used	27
Amount of ERPI greasing moments	4
Percentage desalination run time (excluding system crash and stop tests)	99.50%

5.2. Current System Concept

The concept introduced in this chapter is based on the design by Vollebregt and Feenstra (2012). In their report the authors discussed several concept, and based on the location opted for the concept with pressurized water storage. During this project the plant will be re-designed and moved to Northern Jakarta. The design parameters applicable to this location are:

- Concept is solely powered by renewables (Wind and/or PV)
- Maximum power input 1200 [Watt] (limited by controller unit)
- Concept is designed to desalinated brackish water with a TDS of approximately 5,000 [mg/l]
- The means of desalination is RO
- The RO is ideally operated continuously
- At least 8 – 12 hours of energy storage required
- Brackish water will be pumped up from a shallow well, with a dynamic groundwater level of maximum 10 [m]
- The maximum flow and pressure of the solar pump exceed the systems requirements. Thus the maximum feed flow is not limited by the solar pump, but by the energy recovery device, storage vessel, and RO membrane

- Maximum production maximum 5 [m³/day] (if Schenker Energy Recovery Device is part of the design)

The equipment already available mainly limits the capacity of the new design. All expansions/upgrades must be checked in order to remain within the operating/safety limits of the previous equipment. The main limiting factors are the capacity of the inverter/controller (1200 [Watt]) and the maximum capacity of the Schenker Energy Recovery Device (210 [l/hr.]). Originality is rather limited, seeing that this is a follow up project. Nevertheless, the concept design and implementation should be challenging enough to meet the requirements of a Master’s Thesis.

5.2.1. System Sketch

The concept for this RES-RO installation is shown in Figure 5.1. It can be seen that PV modules and/or a wind turbine form the possible power inputs for the system. The sketch also indicates that a submersible pump will be placed in a (shallow) well and will pump water into the desalination unit and energy (water) storage unit. Hydro-pneumatic energy storage is a common way of storing water (energy) under pressure. However, typically these vessels are referred to as “surge tanks” and mainly serve as buffer of clean water to avoid the pumps from constantly having to switch on and off. In other words typically their main purpose is to avoid surges in the distribution system.

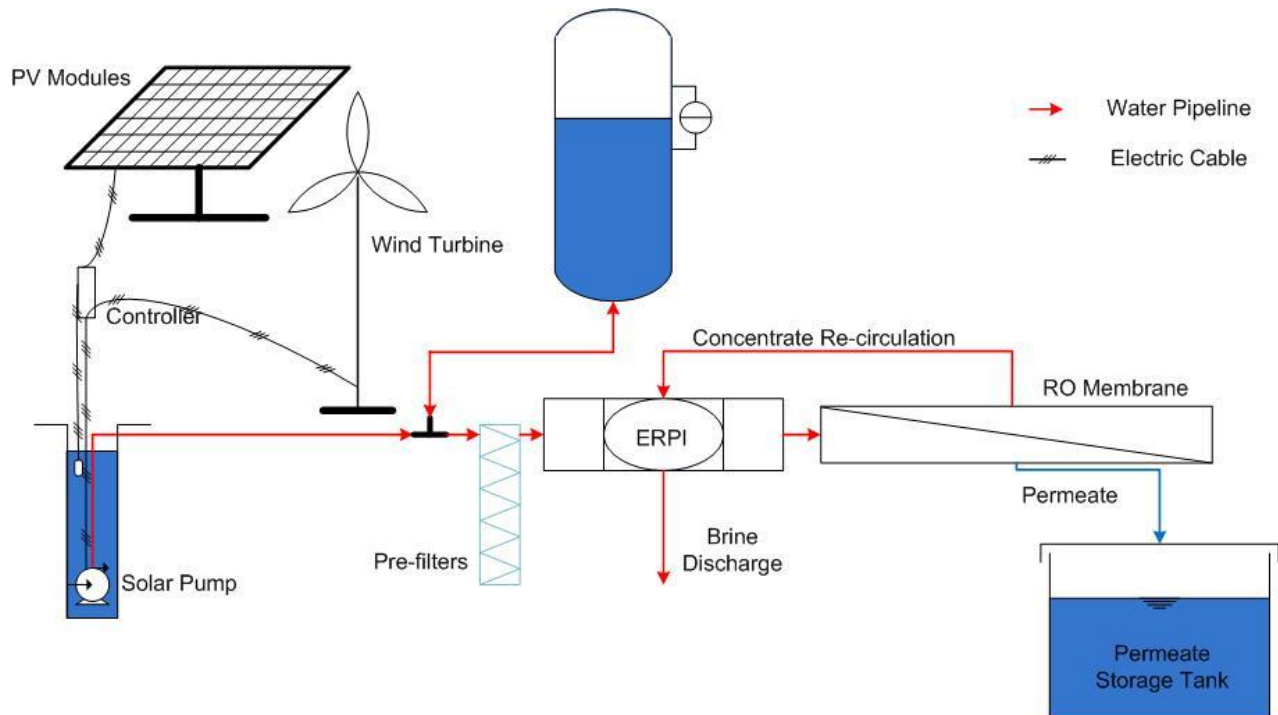


Figure 5.1: System Concept.

5.2.2. Energy Buffer

As mentioned earlier, the two most interesting renewable energy sources for this desalination project are wind energy and PV. Unfortunately these energy sources are of intermittent nature and thus often

require energy storage for periods of little or no power production. Vollebregt and Feenstra (2012) discussed several methods of storing energy in their thesis, the different options can be found below.

- Batteries as energy storage
- Compressed air as energy storage
- Novel pressurized water storage
- Hydro-pneumatic energy storage

The authors thoroughly evaluated the above-mentioned options to cope with lack of renewable energy sources for a 12-hour period. It was found that batteries proved to be a reasonable alternative, but battery life and performance are however negatively affected in hot and arid regions such as Jakarta. Thus maintenance of a battery-based system could be costly. Compressed air and hydro-pneumatic energy storage were found to have lower conversion efficiencies, they required larger volumes and also exhibited higher investment costs. The novel pressurized water storage was found to be the best option as it exhibited only one energy conversion step and thus reduced the losses. Also due to limited energy conversion steps, investment costs were relatively low. During the initial stages of the project it became clear that implementing such a pressurized water storage would be difficult in urban Jakarta, initially incorporating the previous design into a high-rise building seemed feasible. But finding partners who were interested in this concept proved to be difficult. For this reason during this project the alternative concept containing a hydro-pneumatic energy storage will be further evaluated and possibly implemented.

5.2.2.1. Hydro-pneumatic Energy Storage

Hydro-pneumatic energy storage is a way of storing energy (water), by means of pressurized air and water in a pressure vessel (tank). The principle of this type of storage lies in the difference between the densities of air and water. The density of water is approximately 800 times larger than that of air, thus when the two are present in an airtight vessel air is compressible. Hydro-pneumatic tanks are commonly used in small water systems that use wells to supply drinking water. The piping of these water systems offer little to no storage capacity, and require the well pump to be constantly running. Hydro-pneumatic tanks prevent this pump from starting and stopping too often and minimize pressure transients associated with this start-up/of behavior, the tank delivers water in a preset pressure range to the system. Hydro-pneumatic tanks are generally used as (downstream) water storage, but tend to be only used for very short periods of time. A typical setup of a hydro-pneumatic tank can be seen below in Figure 5.2. The principle of hydro-pneumatic energy storage is relatively simple and can be explained as followed:

Water is pumped into the airtight vessel, as this water enters the vessel the volume of air inside is reduced (compressed) and thus the pressure inside the vessel increases up to a pre-defined maximum pressure. When water is released, the volume of water decreases and the air layer above expands causing the pressure inside the vessel to decrease. This above-mentioned cycle will continuously take place within the pre-defined pressure range. Thus in theory this seems like an optimal solution for this

project since excess energy is stored by means of pressurized water which can be directly fed to the RO installation without any conversion.

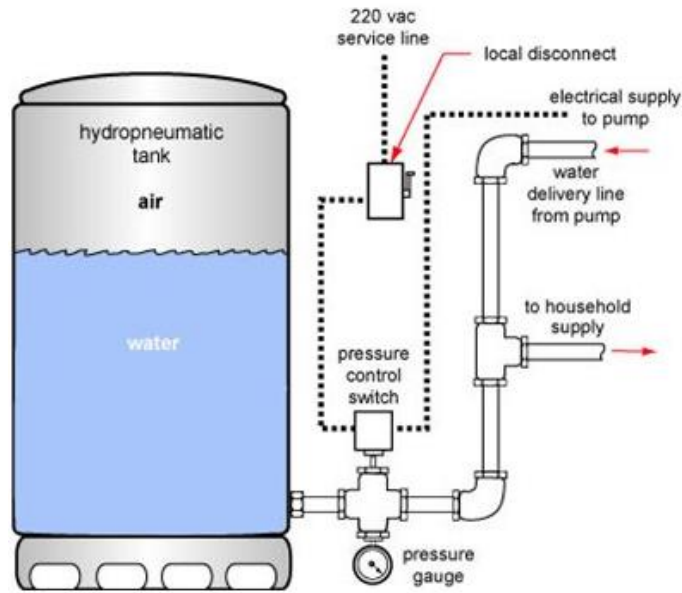


Figure 5.2: Typical hydro-pneumatic vessel, source: ("Water Safe bc," 2006)

However, it is known that air can dissolve into water and thus with traditional hydro-pneumatic tanks an air compressor is required (Pandolph, Unknown). But before going any further let's discuss the advantages and disadvantages and also the different types of hydro-pneumatic tanks.

5.2.2.2. Advantages/Disadvantages of Hydro-pneumatic Tanks

Below a list of main advantages and disadvantages of hydro-pneumatic tanks can be found.

Table 5.2: Advantage sand Disadvantages of Hydro-pneumatic Energy Storage

Advantages	Disadvantages
They are well-known in the water distribution sector	Generally only about 50% of the tank volume is use for actual water storage
In the case of this project, electrical losses are avoided because no extra energy conversion step is required	Not easily scaled up (size and costs)
The system is fairly self-regulatory, no advanced control system is required	Safety, when dealing with pressurized water safety is always an concern
Serves as surge controller, i.e. less pressure surges	Periodic re-charging of air required
If a separator is used, there will be no contact between water and air. I.e. water will be store under anaerobic conditions and no oxidation will take place.	

5.2.2.3. *Types of Hydro-pneumatic tanks*

In general when discussing hydro pneumatic tanks, there are a couple of basic types that need to be mentioned. Depending type and size of the tank, it can be chosen to place the tank vertically or horizontally. But besides this, the main difference between the different types of tanks lies mainly in the separation method of the air and water in the tank. The four main types are mentioned and shortly discussed in the following sections.

- **Traditional hydro-pneumatic tank with an air compressor:** This type of tank does not separate the air and water, and thus an air compressor and volume controller are required in order to prevent the tank from becoming *waterlogged*. This must be done because this phenomenon causes an increase in energy costs, reduces efficiency and can cause equipment failure (*Hydropneumatic Tank Control Systems, 2011*).
- **Tanks with flexible separators:** These tanks provide a complete separation of the air and water, typically the air is contained in an air bladder, but sometimes a separator is fastened around the inside of the tank. Typically this is the best and easiest when discussing energy storage devices, since air and water are completely separate and thus air cannot dissolve into water.
- **Floating Wafer Type:** Typically there is a floating wafer constructed of rigid material, flexible rubber or plastic, which separates the air and water. This wafer however does not ensure a 100% separation of the water and air, but significantly lower the absorption rate of air into water. Therefore less dissolving of air in water is expected, and thus these types of tanks only require occasional recharging with air.

5.2.2.4. *System Components of the Hydro-pneumatic Tank*

Before performing the calculations regarding to sizing of the hydro-pneumatic tank, let's have a look at the components of hydro-pneumatic tanks. Of course depending on the type of tank, it will depend whether there is a bladder bag, diaphragm or wafer. For the moment the components of a typical hydro-pneumatic tank will be discussed. From the presentation of Pandolph (Unknown) the following schematic of a typical hydro-pneumatic tank was found.

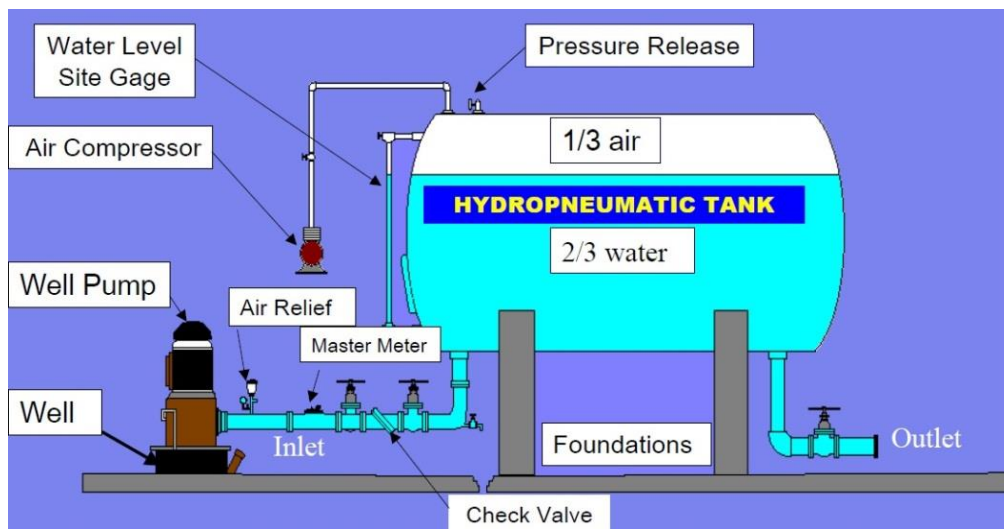


Figure 5.3: Schematic view of a typical hydro-pneumatic tank, source:(Pandolph, Unknown)

Figure 5.3 shows the major components of a hydro-pneumatic tank, the relevant components for this project can be found in Table 5.3 accompanied by a short description.

Table 5.3: List of components for a typical Hydro-Pneumatic Tank

Component	Description
1 Water Source	Typically the water source is a well, in order force water in the tank a pump is required.
2 Tank/Pressure Vessel	The vessel stores water and air under pressure. Note the typical composition of 1/3 air and 2/3 water when the tank is filled to its maximum water level.
3 Tank Foundation	The foundation supports the tank and ensures the tanks stability.
4 Air Volume Controller and Compressor	The air volume controller regulates the air volume in the tanks. It controls the compressor and ensures the tank does not get <i>waterlogged</i> .
5 Pressure Relief Valve	When dealing with pressure vessels safety must always be taken into account. Tanks have a pre-determined maximum operating pressure, the pressure release valve prevent excessively high pressure in the tank.
6 Inlet/Outlet	Allows water to flow in and out of the vessel. Both must be fitted with special valves.
7 Sight Glass	Allows direct observation of “air-to-water ratio”. Generally the ratio should be 1:2 (1/3 air and 2/3 water), but at all times it must remain between 1:3 and 1:1 (i.e. ¼ air to ¾ water and ½ air to ½ water).
8 Pressure Gauges	For monitoring pressure inside the vessel and in the distribution system.
9 Pump Controls	Controls “cut-in” and “cut-out” of the water entering the vessel
10 Water Flow Meter	Measures quantity of water pumped

5.2.3. Energy Recovery Device

Energy recovery (often referred to as brine stream energy recovery) substantially reduces energy demand for RO systems. Energy recovery devices (ERD’s) are commonly applied in large-scale SWRO systems, however in small-scale BWRO systems an energy recovery devices are less common. In small-scale BWRO system an ERD will increase capital costs, but if they are omitted running cost will be significantly higher. However, Thomson (2003) also mentioned that another reason that ERD’s are less commonly used in BWRO is due to the higher recovery ratios and consequently less energy available in the concentrate stream for BWRO systems. There are several types of energy recovery systems available on the market, the most common types of ERD’s are listed below:

Table 5.4: List of ERD's

Recovery Device	Manufacturer	Working Principle
Danfoss SWPE X-Pump	Danfoss Ocean Pacific Technologies	Axial Piston Axial Piston Pump combined with ERD
Spectra Clark Pump	Spectra Water-makers	Positive-displacement reciprocating pressure intensifier
Pelton Wheel	-	Turbine type
Hydraulic Booster	Turbo Fluid Equipment Development Co.	Single-stage radial inflow turbine and a single-stage centrifugal pump
DWEER Exchanger	Work Desal Co. Ltd.	Dual cylinder, each with a free piston

ERI Exchanger Vari RO	Pressure	Energy Recovery Inc.	Twelve co-axial cylinder without pistons
		-	Combination of water hydraulics and oil hydraulics

For the scope of this project it is more relevant to provide a more detailed explanation of the working principle of the *Clark Pump*. For detailed description of the other ERD's please take a look at the reports by (Generaal, 2011; Thomson, 2003).

5.2.3.1. Principle of the Clark Pump

As discussed above, when making use of ERD's the required energy is significantly lowered. In other words, the required pressure for the desalination process is significantly less. One of the most popular solutions in modern RES-RO systems is based on the principle of the *Clark Pump*. In order to better understand this principle, an overview is given in Figure 5.4.

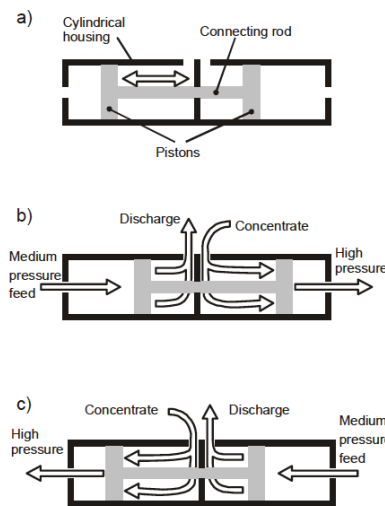


Figure 5.4: Schematic of the working principle of the *Clark Pump*

A rod inside a cylindrical housing connects two pistons, the rod creates a difference in effective area on the two side of each piston. The image in the center of Figure 5.4 shows that medium pressure feed enters the left chamber. Together with the inflow of the concentrate pressure feed the piston assembly is pushed to the left, producing a higher pressure leaving the device via the chamber on the right. This assembly reciprocates inside the cylindrical housing, the reversal of the pistons are facilitated by a novel reversal valve patented by Clark Permar (Thomson, 2003). The process in the reverse direction is shown at the bottom of Figure 5.4. Because of the presence of the two connected pistons, the energy from the medium pressure feed (low/medium pressure pump) and the energy of the concentrate feed (concentrate flow leaving the membrane) are added up and thus producing an output pressure that exceeds that of the concentrate. For this reason such a device is often referred to as a *pressure intensifier*.

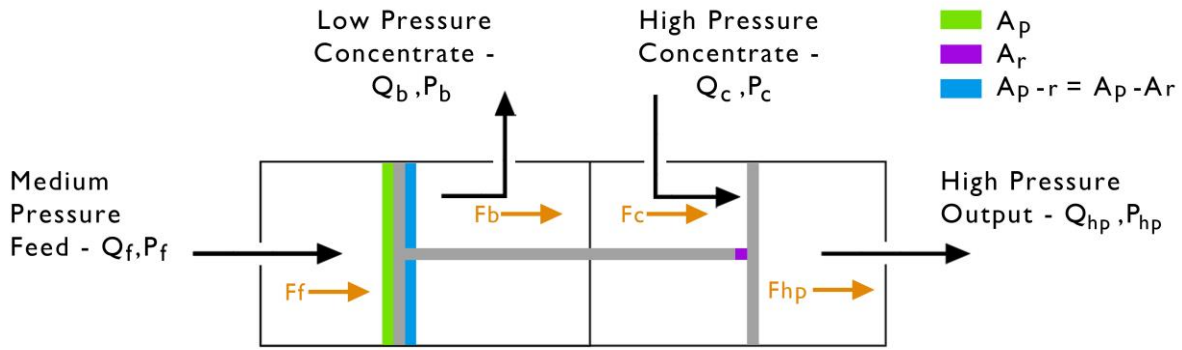


Figure 5.5: Explanation of the working forces inside the pressure intensifier.

From a mechanical point of view it could be said that there are four forces working on the system, these forces are shown in the figure above and are the product of the respective pressure applied on the respective surface area multiplied by the respective surface area itself. If the friction losses are neglected and the brine is assumed to leave the system at the same pressure as the environment, these forces are given by:

$$F_f = A_p * P_f \quad (5.1)$$

$$F_c = A_{p-r} * P_c \quad (5.2)$$

$$F_{hp} = A_p * P_{hp} \quad (5.3)$$

$$F_b = A_{p-r} * P_b \quad (5.4)$$

$$F_b = A_{p-r} * P_b = 0 \quad (5.5)$$

Now by using a basic mass balance and assuming no leakage losses and a constant water density, it could be said that due to the equal piston displacement, the inner- and outer piston surface area's determine the ratio between the volumetric flow:

$$Q_f = Q_{hp} = \left(\frac{A_p}{A_{p-r}} \right) * Q_c \quad (5.6)$$

This partially explains that the recovery ratio is limited (fixed) by the surface ratio between the inner- and outer piston surface area. Now if the assumption is made that there is no acceleration during this process, setting up a force balance provides the following relation.

$$F_f + F_c = F_{hp} \quad (5.7)$$

$$A_p * P_f + A_{p-r} * P_c = A_p * P_{hp} \quad (5.8)$$

$$P_f = P_{hp} - P_c * \left(\frac{A_{p-r}}{A_p} \right) \quad (5.9)$$

The recovery ratio of a RO system with pressure intensifier is given by:

$$R = \frac{Q_p}{Q_f} = \frac{A_r}{A_p} = 1 - \frac{A_{p-r}}{A_p} \quad (5.10)$$

The equations above help to give a better insight into the mechanics of the *pressure intensifier*, however the equations above do not account for losses within the system. Also these ERD's are designed for seawater applications, so determining the actual required pressure will be done using experimental data on the performance of the actual ERD.

5.2.3.2. Schenker Energy Recovery Device

As mentioned, the type of ERD discussed above is often referred to as *pressure intensifiers*. For this reason from now on, the energy recovery device will be called an *energy recovery pressure intensifier* (ERPI). The ERPI used in this project was a Schenker ERPI (Schenker), this ERPI has the same working principle as the Clark pump discussed above. As mentioned in the previous section, the recovery of the system is fixed by surface ratio between inner- and outer piston. Since these surface areas are known, the fixed recovery ratio for this system can be calculated. In the table below are all the relevant data and the calculated fixed surface area.

Table 5.5: Surface areas and ERPI Recovery Ratio

Schenker Energy Recovery Pressure Intensifier	
A_{out}	69.398 [cm ²]
A_{in}	59.219 [cm ²]
Fixed Recovery	14.67%

6. Sizing of the System

6.1. RO Pumping Requirements

In order to make an initial estimation of the pumping requirements for the desalination process some detailed assumptions are required. It should also be noted that pumping requirements for two different flow rates evaluated. The membrane in question is the LOW3-4040 membrane by Oltremare, manufactured by an Italian based company (OLTREMARE, 2013).

Table 6.1: Membrane specifications @Feed TDS of 5000 [mg/l].

Permeate flow [m ³ /day]	5	3.25
Permeate flow [l/min]	3.5	2.25
Feed flow [m ³ /day]	33.55	21.6
Feed flow [l/min]	23.3	15
Membrane Area [m ²]	7.9	7.9
Flux [l/h/m ²]	26.6	17.1
Recovery Ratio [%]	15	15
Relative Feed Pressure [bar]	7.91	6.33
Relative Concentrate Pressure [bar]	7.72	6.23
Pressure pre-ERPI [bar]	6	3.5

In order to determine the required pressure by the ERPI, one could use the relation presented in section 5.2.3.1. However research has been performed by (ElementalWaterMakersB.V., 2012), on the pressure loss in the Schenker ERPI. From personal and confidential correspondence knowledge was obtained that at a feed flow of approximately 23 [l/min], the pressure losses are roughly 4 [bar]. One could say that at this flow the benefits of the ERPI are rather limited. For this reason the system will be designed based on a feed flow of 15 [l/min], this means that the daily production will be approximately 3.25 [m³/day]. Now that the feed flow and required pressure are known, let's proceed to the required power calculations. The required power to drive the RO desalination can be calculated using an energy balance for flow inside tubing, based on the assumption that water is incompressible (Akker & Mudde, 2008).

$$0 = \dot{m} \left[0.5v_1^2 + \frac{p_1}{\rho} + gz_1 - 0.5v_2^2 - \frac{p_2}{\rho} - gz_2 \right] + W - \dot{m} * e_{fr} \quad (6.1)$$

The equation shown above can also be written in a different form, one that is more suitable for this application. The volumetric flow related form is shown below in Eq.(6.2), all the symbols used in these equations are specified in the Nomenclature.

$$W_{pump} = Q * \{ (p_2 - p_1) + .5 * \rho * (v_2^2 - v_1^2) + \rho * g * (z_2 - z_1) + \rho * e_{fr} \} \quad (6.2)$$

Where Q represents the flow rate, p_2 & p_1 the pressure in the system tubing and in the well respectively, v_2 & v_1 the velocity in the tubing system and the velocity of water in the well, ρ the density of the water, g the earth gravitational acceleration, z_2 & z_1 the relative elevation of the tank and the relative elevation

(depth) of the pump and e_{fr} represents the frictional losses in the tubing. In order to simplify the calculations, it is chosen to neglect the friction losses. In reality there will be losses due to friction (bends, distance etc. etc.), but for now the following simplified equation will suffice.

$$W_{pump} = Q * \{(p_2 - p_1) + .5 * \rho * (v_2^2 - v_1^2) + \rho * g * (z_2 - z_1)\} \quad (6.3)$$

In Table 6.2 the values are given for the used parameters. It should be noted that all piping within the desalination part consists of ½" HDPE tubes, with an inner diameter of approximately 16.3 [mm].

Table 6.2: Parameters used for power calculations

Feed flow [m ³ /12 hours]	10.8
Q [m ³ /sec]	2.5000e-04
d [m]	0.0163
v ₁ [m/s]	0
v ₂ [m/s]	1.1980
p ₁ [Pa]	0
P ₂ [Pa]	350000
z ₁ [m]	-10
z ₂ [m]	0

Using the parameters above, it was calculated that **112 [Watt]** of pumping power is required for the desalination. This value does not regard possible friction losses and/or any other losses within the piping system.

6.2. Hydro-pneumatic Vessel

As mentioned earlier hydro-pneumatic tanks are most commonly used in small water systems, where the water demand tends to vary. In this project the hydro-pneumatic tank will be used slightly different, the RO membranes require a constant feed flow and if possible also a constant pressure. Since the aim for this project is to design a simple and self-regulating system, there will be no pressure regulator. Thus water leaving the vessel will not always have a constant flow and pressure, this makes the initial estimations a bit tricky. Also the various sources found discussing sizing of hydro-pneumatic tanks, discuss this issue based on the traditional function of hydro-pneumatic tanks (as booster pump, or surge protector in potable water distribution network). The literature explains that sizing of traditional hydro-pneumatic tanks is based on: variation in pipe system demand, drawdown, pump cycle time, operating pressures and the maximum tank flow rate (*AED Design Requirements: Hydropneumatic Tanks*, 2009; "Hydropneumatic Pressure Systems," 2005; "Pump Cycles Program," 2009).

6.2.1. Hydro-pneumatic Tank Volume Calculations

The volume of the vessel used during this project will be determined mainly based on the feed flow required by the membranes, the pressure (range) required by the ERPI and the amount of energy that needs to be stored. Also the advised air to water ratio will be considered. The minimum design pressure for this system will be set at 2 [bar]. To determine the volume of the tank some assumptions must be made, below is a list of assumptions taken in order to determine the tank volume.

- There is no interaction between water and air inside the tank.
- There is no heat exchange between air and its surroundings and the air temperature remains constant.
- The air inside the tank is pre-pressurized to 2 [bar] (minimum pressure).
- The maximum pressure inside the tank is 6 [bar] (max pump head is 70 [m], well depth is 10 [m]).
- For the time being a tank with a volume of 9.37 [m³] is used for the calculations.

Recall the air-to-water ratio of 1:2 mentioned in Table 5.3 and Figure 5.3, we must check if with these parameters this ratio is met. This calculation can easily be performed using Boyles law, a special case of the ideal gas law (Wikipedia, 2013) which describes the inversely proportional relationship between the pressure and volume of a gas when it is kept a constant temperature. The amount of air inside the pressure vessel can be calculated with the following equation (Moran & Shapiro, 2006).

$$p_1 * V_1 = p_2 * V_2 \quad (6.4)$$

Where p_1 is the minimum pressure ([bar]) in the vessel, V_1 is the initial volume of air ([m³]) in the tank, p_2 is the maximum pressure ([bar]) allowed in the vessel and V_2 is the volume of air ([m³]) when it is compressed. Rewriting Eq. (6.4) yields the following:

$$V_2 = p_1 * V_1 / p_2$$

Since p_1 , V_1 and p_2 are all known this equation can be filled in and the compressed air volume can be found accordingly.

$$V_2 = 2 * 9.37 / 6 = 3.13 \text{ [m}^3\text{]}$$

So if the original volume of air inside the tank was 9.37 [m³], there is now 9.37 – 3.13 = 6.25 [m³] of water stored inside the pressure vessel, this shows that the air-to-water ratio is roughly 1:2 (acceptable according to literature). Now that it is known how much water can be stored inside the vessel, the time " $T_{storage}$ ", during which the RO installation can run when supplied solely on pressurized water from the hydro-pneumatic tank can be calculated. The simple calculation shown below yields a run-time of:

$$T_{storage} = \frac{V}{Q_f} = \frac{6.25 \text{ [m}^3\text{]}}{.9 \text{ [m}^3\text{/h]}} \approx 7 \text{ [hrs]} \quad (6.5)$$

This does not meet the minimum of 8 hours, but as the project proceeded it became clear that obtaining larger hydro-pneumatic tanks would be very challenging.

6.2.2. Maximum Hydro-pneumatic Pump Power Requirement

In order to make an initial estimation of the amount of energy required for filling the hydro-pneumatic tank, Eq. (6.3) can be applied again. Below is a list of assumptions that are required to make an initial estimation of the required power.

- Water in the well has no velocity (v_1)
- P_1 and p_2 are the (water) pressure in the well and inside the tubing system (The water pressure in the tubing depends on the pressure inside the hydro-pneumatic tank)
- The hydro-pneumatic tank is located at height is zero and the solar pump is located at 10 meters (negative) inside the well
- The tubing system is relatively short and thus friction losses are ignored.

These assumption and other parameters required for the calculation can be found in Table 6.3.

Table 6.3: Relevant parameters required for hydro-pneumatic power requirements

Feed flow [$\text{m}^3/12 \text{ hours}$]	10.8
Q [m^3/sec]	2.5000e-04
d [m]	0.0254
v_1 [m/s]	0
v_2 [m/s]	0.4934
p_1 [Pa]	0
P_2 [Pa]	600000
z_1 [m]	-10
z_2 [m]	0

Figure 6.1 shows a schematic of the pump located in the well, on the left side is the inlet and on the right is the exit of the pump (i.e. tubing of the system). Filling the above-mentioned values and assumptions into Eq. (6.3) yields a required maximum power of **175 [W]**. Again this is the power required, without keeping in account any pressure losses within the pipes.

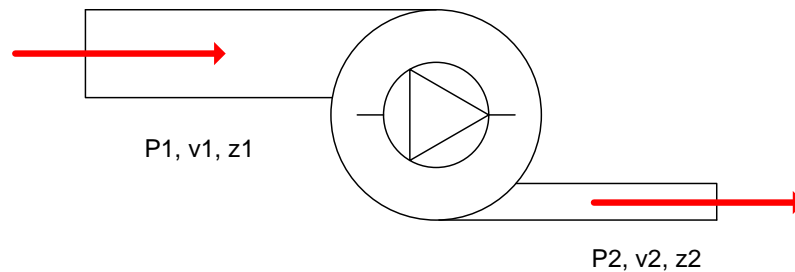


Figure 6.1: Schematic depiction of the solar pump

6.3. Total Power & Energy Demand

The RO power requirements and hydro-pneumatic storage power requirements were performed separately in order to simplify calculations. In reality these processes will occur simultaneously and the minimum required power is estimated simply by adding the calculated values. This yields in a required pumping power of **287 [Watt]**. This value neglects all losses within the piping system, thus a safety factor of 1.2 was applied resulting in a required pumping power of **345 [Watt]**. The power calculated above is based on a 100% efficient pump, in reality the pump will not be 100% efficient and also converter losses and electrical losses will play a role in the overall efficiency. According to the data sheet the *Lorentz PS1200 HR14-2* Solar pump and controller has a maximum total efficiency of 65%. Taking

into account all these losses, efficiencies and safety factors, a total required pumping power of approximately **532 [Watt]** was determined. This means that the installed power must be at least 532 [Watt], however due to the variable nature of RES the installed power will most likely be slightly over scaled. The installed power will also be determined by the daily-required energy.

The daily-required energy for the RO desalination is calculated by multiplying the required power by the solar runtime. Assuming 12-hour power production and thus 12 hours of running the installation on solar power. The total daily-required energy for the RO desalination was calculated as follows:

$$E_{RO} = P * T = .207 [kW] * 12 = \mathbf{2.48 [kWh]}$$

Now recall the emptying time of the hydro-pneumatic storage tank. Assuming the filling and emptying time are equal, the energy required for filling the hydro-pneumatic storage vessel can be calculated as follows:

$$E_{vessel} = P * T = .323 [kW] * 7 = \mathbf{2.26 [kWh]}$$

Adding the two values results in a total of **4.74 [kWh/day]** of energy required. In the following sections the possible renewables energy sources will be evaluated. Where after the choice of renewable energy source and total installed power will be made, also the additional investment costs will be estimated.

6.4. Renewable Energy Sources

As could be seen in the system concept, both PV and wind energy were considered as possible renewable energy sources. There is currently already 739 [W_{peak}] of PV modules available. The calculations performed in the following sections will determine which energy source(s) will be used and also the installed capacity will be determined.

6.4.1. Wind Energy Calculations

Recall that the wind speeds discussed in section 3.6.1, due to the relatively low wind speeds a wind turbine with low cut-in wind speeds would be required. For the sample calculations the *donQi Urban 1.5 Venturi Windmill* will be used, its power curve and other relevant data are shown below.

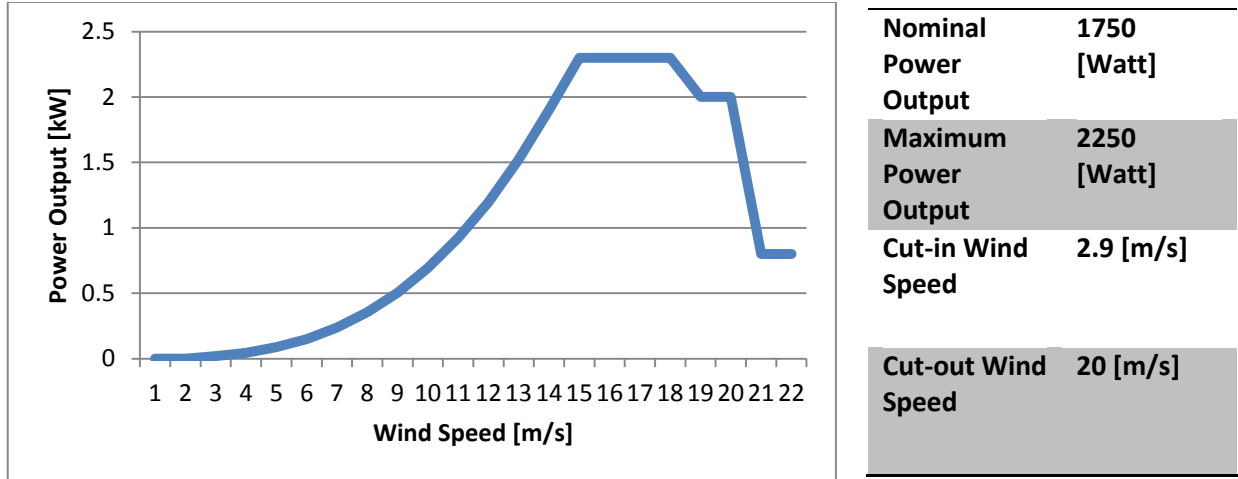


Figure 6.2: Power curve & relevant specifications for the donQi Urban 1.5 Venturi Windmill

To determine the performance of a wind turbine at different locations (and thus at different wind climates) the annual yield can be determined. This annual energy yield is equal to the number of hours per year (T) times the summation of the contribution of each wind speed to the annual energy production. The following equation can be used (Manwell, McGowan, & Rogers, 2009):

$$E = T \int_{V_{ci}}^{V_{co}} P_{el}(V_{wind}) \times f(V_{wind}) dV_{wind} \approx T \sum P(V_{wind}) f(V_{wind}) \Delta V_{wind} \quad (6.6)$$

where E is the annual energy yield; T is the total amount of hours per year; P_{el} is the electric power output and $f(V)$ is the Weibull distribution. This Weibull distribution is given by:

$$f(V) = \frac{k}{a} \left(\frac{V}{a}\right)^{k-1} e^{-\left(\frac{V}{a}\right)^k} \quad (6.7)$$

where k is the shape parameter and a the scale parameter. For this case the following assumptions are made:

- $k = 2$
- $a = V_{avg} / .89$

Because the wind data was measured at a height of 10[meters] and this will approximately be the height at which the wind turbine could be installed, the wind data was used as is for the wind energy calculations. In the table below all relevant parameters and the results of the calculations can be found.

Table 6.4: Relevant information regarding wind energy production and costs.

T	8760 [hrs]
$E_{donQi\ 1.5}$ (per day)	0.813 [kWh/day]
$E_{donQi\ 1.5}$ (per year)	296.9 [[kWh/year]
Windmill Costs	\$5752
Lifetime	15 [years]
Costs per kWh	\$1.29

6.4.2. PV Calculations

Based on the solar data presented in Table 3.2, the average daily power production of a PV module can be estimated. The PV modules used in this project will be the *Sunday LEC-1200* modules, the specification chart is shown in Table 6.5.

Table 6.5: Sundaya LEC-1200 PV module specifications (Measured at 1000 [W.m²]).

Manufacturer	Sundaya
Type	LEC-1200
P _{max} [W]	92.36
V _{mpp} [V]	17.8
I _{mp} [A]	5.18
V _{oc} [V]	22.3
I _{sc} [A]	5.65
Dimensions [mm]	1007*734*36

In order to predict the average daily production of a single PV module the following equation can be used:

$$E_{module} = I_{in} * A_{module} * \eta \quad (6.8)$$

Where E_{module} is the energy produced by the module, I_{in} is the mean solar insolation, A_{module} is the module surface area, and η the efficiency of the PV module. I_{in} is known, it is the mean solar insolation given in Table 3.2. A_{module} is simply calculated using the module dimension given above, while the efficiency can be calculated using the following equation (Zeman, 2010):

$$\eta = P_m / P_{in} \quad (6.9)$$

Where P_m is given in Table 3.2 and P_{in} is equal to 1000 [W/m²] (standard test conditions). The required data and the results of filling in the above-mentioned equations are shown below.

Table 6.6: Relevant information regarding PV energy production and costs.

I _{in}	4.97 [kWh/m ² /day]
A _{module}	0.739 [m ²]
A _{module, effective}	0.533 [m ²]
η _{max}	17.3 [%]
E _{module} (per day)	0.46 [kWh/day]
E _{module} (per year)	168 [kWh/year]
Module costs	\$187.50
Lifetime	25 years
Cost per kWh	\$0.05

6.5. Choice of Renewable Energy Source

First of all, let's give a better overview of the power and energy requirements calculated in section 6.1 & 6.2.

Table 6.7: Power and Energy Requirements

	Power Required [Watt]	Daily Energy Required [kWh/day]
RO Desalination	210	2.48
Hydro-pneumatic Energy Storage	325	2.26
Combined	535	4.74

The values shown in Table 6.7 include a safety factor to account for possible losses and also the overall efficiency of the solar pump controller. It can be seen that a minimum power of 535 [Watt] is required and that the daily energy production should be at least 4.74 [kWh/day]. When comparing the costs per [kWh] of energy of the donQi windmill and the Sundaya PV modules the choice to expand the system with PV modules is easily made. Currently the system consists of 8 Sunday LEC 1200 PV modules, this equals an installed capacity of roughly 740 [Watt] and can produce up to 3.68 [kWh/day]. Thus power requirements are met, but energy requirements are not. For this reason an additional 4 PV modules were installed, totaling to an installed capacity of roughly 1110 [Watt] which produces approximately 5.52 [kWh/day] on average. More details on the installed solar capacity will be discussed in section 7.2.2, next the additional investment costs will be discussed.

6.6. Additional Investment Costs

As mentioned before this is a follow project, one of the many advantages of taking part in a follow project is the reduced investment cost. Because the solar pump and controller, ERPI and pre-filter housings are already available the project budget is rather small. Based on the concept described earlier and the sizing calculations, an initial estimation of the required investment costs will be made. It should be noted that system evaluation (i.e. cost per unit of water produced, or energy required per unit water produced) are performed later on in this report. In the table below a list of the required system components can be found, the table also includes the components costs and the total investment costs required.

Table 6.8: List of required components and their costs

Component	Costs [Euro]
Hydro-pneumatic Storage Vessel	5980
Additional PV modules	560
Shallow Well	500
Oltremare Low3-4040 membrane	300
PVC pipes	200
Electrical Cables and Safety Sling	300
Total Investment Costs	€ 7440

This concludes the designing part of this thesis, first in section 7.1 a more detailed look at the plant layout, next in section 7.2 the actual components will be introduced. Followed by a detailed explanation of the experimental setup, i.e. the sensors, data logger and data analysis software used to evaluate the systems performance in section 7.3.

7. Experimental Setup

7.1. Test Site

The test site was an ex water treatment plant of PAM Jaya, situated at Muara Karang, North Jakarta. The site offered a good infrastructure in the sense that the desalination part of the installation could be safely stored inside an office. The exact plant layout and a detailed schematic of the desalination part are shown in Figure 7.1 and Figure 7.2 respectively.

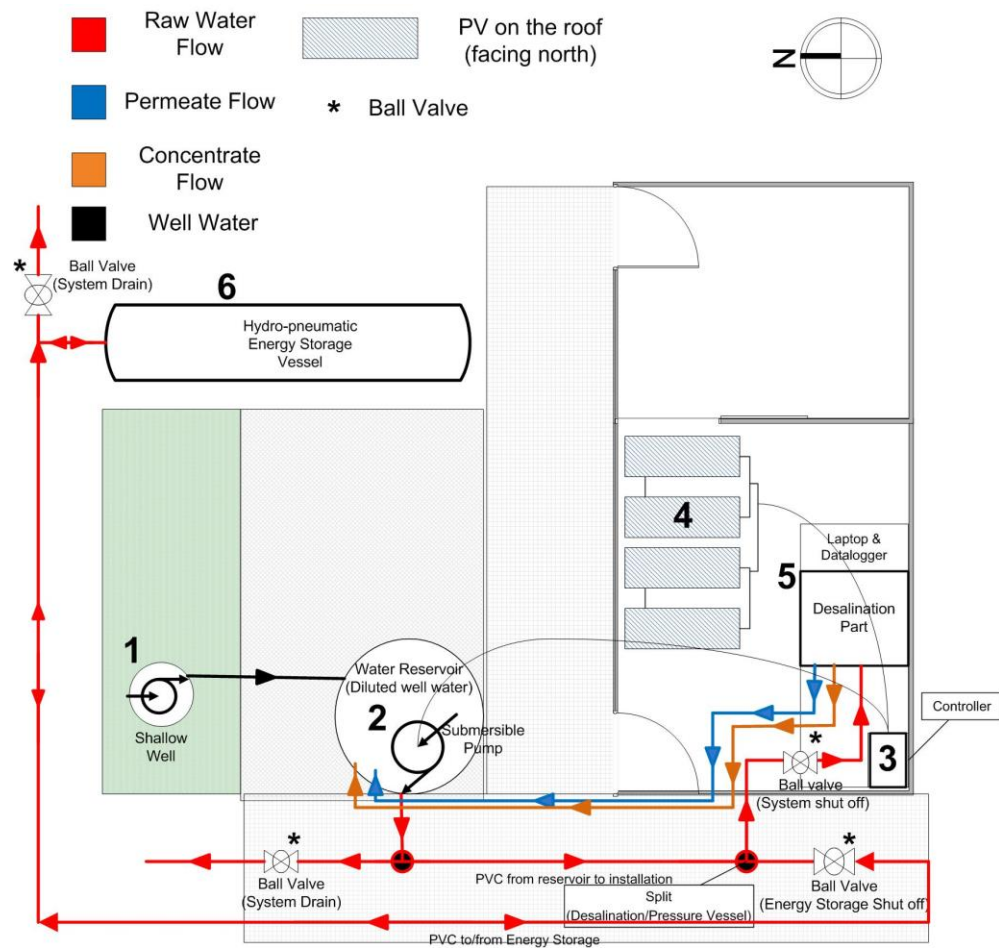


Figure 7.1: Top view of the plant layout at Muara Karang, North Jakarta

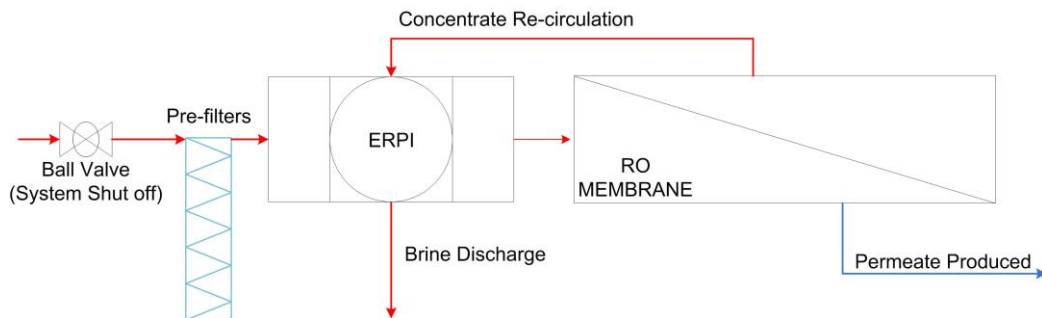


Figure 7.2: Detailed schematic of the desalination part

The key components of the pilot plant are number in Figure 7.1, the numbered items are:

1. Shallow Well
2. Feed Reservoir & Solar Pump
3. Solar Controller
4. PV Modules on the Roof
5. Desalination Part
6. Hydro- Pneumatic Energy Storage

Unfortunately there were some issues when setting up the pilot plant, issues that caused some minor deviations from the projected path. First of all, there was an unsuspected TDS increase of the shallow well water, secondly there were some delays acquiring the hydro-pneumatic vessel. When finally a second hand vessel was salvaged, there was a vessel failure. Mainly due to these reasons there were some minor changes in the concept, before going any further let's discuss the important components of the pilot plant.

7.2. System Components

In the following section the individual components will be discussed, supplemented by pictures and details of the setup.

7.2.1. Raw Water Supply

To serve as raw water input, a shallow well was designed and constructed for the pilot plant at Muara Karang. The well was dug to a depth of 30 meters and based on ground water surveys found from similar locations and also based on interviews with groundwater experts at PAM Jaya, it seemed that expecting a TDS of anywhere between 1,000 to 10,000[mg/l] was reasonable. Due to limited funds, no groundwater samples were retrieved prior to arrival in Jakarta and thus samples were taken (and analyzed by the lab of PAM Jaya) post drilling and post flushing of the well.



Figure 7.3: On the left the well during construction, and on the right the reservoir eventually used.

The first samples taken by PAM Jaya resulted in a TDS of 1,300 [mg/l]. This TDS was less than expected, however these samples were taken before proper flushing of the system. After proper flushing, the TDS of the well had risen to approximately 20,000 [mg/l]. This meant that the water inside the well could not be considered as brackish anymore, but should be considered as seawater (recall Table 4.1).

Unfortunately this meant that the well could not be used anymore as feed to the desalination plant. As a last resort two reservoirs reservoir totaling 9 cubic meter of storage capacity were installed, with inside a mixture of well water and fresh water. The storage vessel served as raw water to the desalination plant and also as collection of the permeate- and concentrate streams. I.e. the permeate and concentrate were re-circulated and recollected in the (feed) reservoir. The feed water had an TDS of about 6000 [ppm], the exact feed water TDs will be discussed presented and discussed later in this report.

7.2.2. PV Modules

After careful evaluation, it was decided not to expand the system with a wind turbine. Referring to the wind climate in North Jakarta (chapter 3.6) and the calculations performed in chapter 6, expansion of the current PV power input was preferred over the addition of a wind turbine. Previously there were a total of eight *Sundaya LEC-1200* PV modules installed, during this project a total of 12 modules were installed. The panels were placed on the roof directly above the desalination part of the plant. There weren't any trees to cause shading on the PV panels, west of the location there was however a higher structure. This structure caused shading during sunset and thus slightly affected PV power production during the last sun-hours of the day.



Figure 7.4: PV panels installed on the roof and their configuration.

A total of twelve *Sundaya LEC-1200* modules were installed, totaling a peak PV input of 1108 [Watt]. The installed PV capacity and the array configuration are mainly determined by the solar controller. As shown in section 7.2.3, the maximum PV input is limited to 1200 [Watt} and the maximum DC voltage is 200 [V_{DC}]. This resulted in the PV configuration shown in Figure 7.4, where it can be seen that it was opted to connect the PV modules in an array of 2 strings, of 6 modules each, connected in parallel. This configuration was chosen so that the maximum DC voltage of 200 [V_{DC}] would not be exceeded and since power losses are defined as:

$$P_{loss} = I^2 * R \tag{7.1}$$

Thus by having the string as large as possible, power losses are avoided. However what should be noted is that PV panels connected in series more easily affected by shading, as explained by Wang and Hsu (2011) shading is one of the major causes of mismatch in series connected panels. The authors explain

that shaded cells absorb electrical power generated by un-shaded cells, resulting in local hotspots where heat is dissipated. This results in a power output that is limited by the shaded cells. A more precise evaluation of the electrical losses will be discussed in chapter 8.

7.2.3. Solar Pump & Controller

The solar pump and controller converts the DC power input and controls the AC power output to the submersible pump. It is connected to the solar panels by a 10-meter electrical cable, while the cable to the pump has a length of 50 meters.

Solar Pump & Controller	
Manufacturer	Lorentz Germany
Model	PS1200 HR-14
Lift (+max 15%)	70 [m]
Max Flow Rate	2.7 [m ³ /h]
Max Efficiency	65 [%]
Solar Generator	350 – 1200 [Wp]
Max V _{oc}	200 [Volt DC]



Figure 7.5: Solar controller and Pump on the right and specifications on the left.

As a protection to avoid the pump running dry, a water level probe was installed slightly above the pump. Originally the pump was placed in a 30-meter shallow well, however due to an unanticipated high TDS a reservoir was used (as discussed earlier). This caused some issues when the PV power produced was at the system max. Partly due to the absence of head loss, at peak irradiation the pump had overheated several times, also at peak irradiation the pressure produced by the pump was close to 8 [bar]. This pressure caused a leak in one of the flow sensors, also due to an 8 bar input pressure the pressure after the ERPI exceeded 16 [bar]. This meant that several limits (sensors, membrane, tubing etc.) were being pushed, thus a ball valve was installed just behind the pump. This way a small head loss could be “simulated”, this seemed to solve the problem.

7.2.4. Pre-Filters & RO Membranes

7.2.4.1. Pre-Filters

Located inside the office directly after the “system shut-off ball-valve” are the two pre-filters. Both filters have 5 [μm] pores and are “wound-type” filters, this can be seen in Figure 7.6.



Figure 7.6: Pre-filters, system shut-off valve and inlet pressure gauge.

7.2.4.2. RO Membranes

Due to the issues regarding feed water and the absence of a pressure vessel, it was decided to start-up the installation using one of the old LOW1-2540 membranes. Even though the power input was scaled based on the presence of the hydro-pneumatic vessel and also on the larger feed flow requirements for the LOW3-4040 membranes, the choice was made to gather some initial data using the old membranes. The main reason was to preserve the new membranes in order to have brand new membrane when the hydro-pneumatic storage vessel was added to the system.



Figure 7.7: The white 2540 RO membrane is located in the front of the picture

As planned a single *Oltremare compact LOW3-4040* membrane was eventually installed. This membrane similarly to the 2540 membrane, is a spiral wound membrane and is located within a white pressure vessel. The feed to the membrane connects to the high-pressure outlet of the ERPI, while the concentrate of the membrane connects to the inlet of the ERPI. The permeate produced by the membrane was re-collected in the storage vessels discussed as earlier (brine discharged by ERPI also recollected). Unfortunately estimations were made based on the 4040 membranes, this meant that the system was over scaled when using the single 2540 membrane. A was placed behind the pump, as the pressure and consequently the flux were too large. To give an indication of the differences between the 2540 and the 4040 membranes, Table 7.1 is introduced. Here the relevant parameters are shown.

Table 7.1: Membrane parameters according to Sirio.

Membrane Type	Compact 4040-Low3	Compact 2540-Low1
Permeate flow [m ³ /day]	3.25	1.1
Feed flow [m ³ /day]	21.6	7.33
Membrane Area [m ²]	7.9	2.6
Flux [l/(m ² *h)]	17.1	17.6
Recovery Ratio [%]	15	15
Relative Feed Pressure [bar]	5.2	9.33
Relative Concentrate Pressure [bar]	5.1	9.23
Pressure pre-ERPI [bar]	3.5	-

7.2.5. ERPI

As discussed earlier, the ERPI re-uses the waste energy of the RO process, this reduces the energy requirements of the installation. At the front of Error! Reference source not found., the low-pressure inlet of the ERPI can be seen, this inlet is connected to the pre-filters. On the other side of the ERPI are the high-pressure outlet going to the membrane, and the high-pressure inlet connected to the concentrate stream of the membrane. Situated as highest on the ERPI is the discharge outlet, this is where the brine stream leaves the installation (usually discharged). In this case this stream is re-collected in the storage reservoir.

ERPI		
Manufacturer	Schenker	
Model	150-210 [l/hr]	
Recovery	14.67 [%]	
Feed Flow Design Capacity	16.7-23.31 [l/min], 1-1.40 [m ³ /h]	
Design Pressure	Input	9 [bar]
Design Pressure	Outlet	55 [bar]

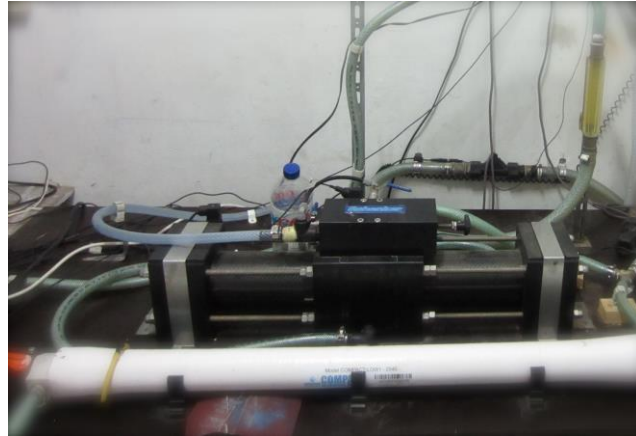


Figure 7.8: The ERPI on the right and specifications on the left.

7.2.6. Hydro-Pneumatic Storage Vessel

The hydro-pneumatic pressure vessel was bought via a vessel manufacturer in Bandung, Indonesia. Unfortunately due to all of the delays, the initial test run was performed without energy storage. During the process of finding the hydro-pneumatic storage vessel, it became clear that finding such a vessel was a great challenge (mainly due to the project budget). The vessel used in this project was a steel pressure vessel, with a total volume of 9 [m³]. This meant that the maximum water stored inside the vessel would be approximately 6 [m³]. The maximum designed working pressure of the vessel was 8 [bar], this pressure was chosen because the solar pump can physically not provide a higher pressure. In Table 7.2 and Figure 7.9 the specifications and a picture of the energy storage vessel can be found.

Table 7.2: Hydro-pneumatic Energy Storage Specifications

Hydro-pneumatic Energy Storage Vessel	
Manufacturer	PT. Celco Teknik Industri
Vessel Size [mm]	1200 *7500
Total Volume [m ³]	9
Designed Operating Pressure [bar]	8
Maximum Test Pressure [bar]	16
Material	Mild Steel



Figure 7.9: Hydro-pneumatic Storage Vessel

7.2.7. Tubing

The tubing of the system can be roughly divided into two sections, tubing outside of the office and tubing inside the office. All tubing before the pre-filters consists of 1" PVC piping. In general 4 [meter] sections of PVC are connected by means of male/female threaded sockets. T-connections were glued and all ball valves are PVC ball valves. The choice for socket connection was made in order to facilitate the removal of the installation upon completion of the project. Inside the office, or better said all tubing within the desalination part of the installation consists of ½" HDPE tubes. The tubes are interconnected by T-connections by means of nipples and clamps. These T-connections hold all of the sensors that are required to monitor the system parameters (pressure, temperature etc. etc.). Exceptions to the above-mentioned distinction are the concentrate- and permeate tubing. These are partly located inside the office and partly outside the office, and make use of ½" HDPE tubes.

7.3. Instrumentation

In order to monitor the systems behaviors a total of fifteen electrical sensors, five visual indicators and one datalogger are incorporated into the system. The visual indicators make ensure real time information regarding the systems without the need of any electricity. These visual indicators are also used to make ensure that the electrical sensors are functioning properly, and can also be used for (re-) calibrating some of the electrical sensors. The electrical sensors measure the respective parameters and provide an analog signal. These analogs signals are measured by the datalogger and are communicated to the datalogging computer. Using the *DasyLab* data acquisition software, all of these signals/measurements are recorded and used to perform operations/calculations. The information gathered from these sensors is eventually used to determine the systems performance. A detailed schematic of the integration of all the sensors and visual indicators into the system is displayed in Figure 7.10.

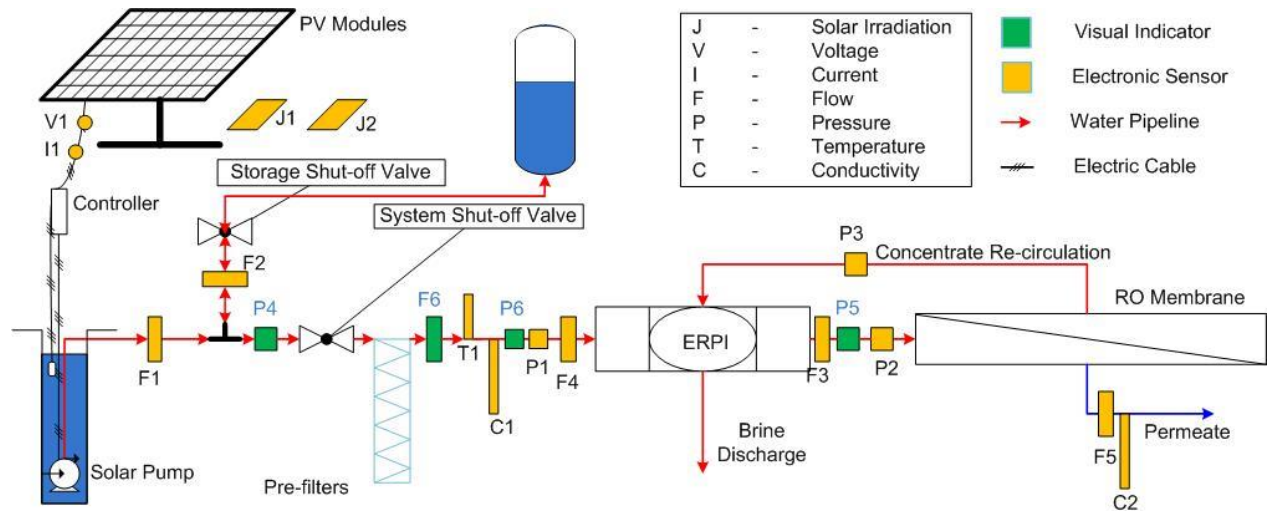


Figure 7.10: Sensors & visual indicators integrated into the system

It is of utmost importance that all sensors are properly calibrated, in the following section information regarding the calibration and accuracy of the sensors will be discussed.

7.3.1. Measurement Instrumentation & Datalogger

The specifications of the sensors shown in Figure 7.10, are shown below in Table 7.3. The table also shows the specifications for the datalogger used. Electricity from the grid was used to power the sensors, datalogger and datalogging computer. After installing all of the equipment and performing initial test runs, an issue quickly arose. Namely that the data acquisition would crash at seemingly random occurrences. It quickly became evident that electricity from the grid was not reliable and often went out for several minutes. Because these power outages never lasted for longer than fifteen minutes, an uninterrupted power supply (UPS) was added, connected to the UPS were the sensors and the datalogger.

Table 7.3: Sensors & Datalogger Specifications

	Measurement Device	Manufacturer	Type	Measurement Range	Accuracy
<i>Electronic Sensors</i>					
P1	Pressure Sensor	Druck	RS 313-4207	0 - 6 [bar]	2%
P2	Pressure Sensor	Druck	RS 313-4229	0 - 16 [bar]	2%
P3	Pressure Sensor	Druck	RS 313-4229	0 - 16 [bar]	2%
C1	Conductivity Sensor	Omega	CDTX1202-D	0.0 - 19.99 [mS/cm]	2%
C2	Conductivity Sensor	Omega	CDTX1203-D	0.0 - 1.99 [mS/cm]	2%
J1	Pyranometer	Kip & Zonen	CMP 3	0 - 2000 [W/m ²]	2-10 %
J2	Pyranometer	Kip & Zonen	SPLite 2	0 - 2000 [W/m ²]	2 - 10%
V1	Voltage Transducer	Camille Bauer	SINEAX TV 819	0-1000 [V]	0.2%
A1	Amp-Clamp	SANWA	CL33DC	0 - 30 [A]	2%
F1	Flowmeter	MOJO	MJ-HZ25DN	1 - 60 [l/min]	10%
F2	Flowmeter	Krohne Altoflux	SC80A5	60 - 80 [l/min]	1.5%
F3	Flowmeter	RS	RS 257-133	1.5 - 30 [l/min]	1.5%
F4	Flowmeter	RS	RS 257-133	1.5 - 30 [l/min]	1.5%
F5	Flowmeter	RS	RS 257-149	0.25 - 6.5 [l/min]	1%
T	Temperature Sensor	Endress+Hauser	Pt1000	200 - 250 [°C]	0.20%
<i>Visual Indicators</i>					
P4	Pressure Gauge	Wika	RS 110-826	0 - 10 [bar]	1.6%
P5	Pressure Gauge	-	-	0 - 16 [bar]	-
P6	Pressure Gauge	Wika	RS 110-826	0 - 16 [bar]	1.6%
F6	Flow Indicator	Parker	RS 441-4879	4 - 22 [l/min]	2%
	Dataogger	MCC Daq	USB-1616HS	± [Volt]	16 Bit

As mentioned earlier the data measured by the sensors was recorded and used for some elemental calculations. The *DasyLab* software and the worksheet are shortly discussed in the following section.

7.3.2. DasyLab Data acquisition Software

DasyLab was used to record all the sensor outputs, it's an easy to use software and enables real-time monitoring of systems, creation of complex applications with minimal programming, provides a complete library of elemental to complex computational functions and much more.

The data measured from the system was recorded at a frequency of 2 [Hz]. Several "saving modules" were programmed, modules saving the real time data, modules saving 5-second averages of the data and modules saving 30-second averages of the data. This was done in order to facilitate the data analysis at a later stage, reducing the data within *DasyLab* will reduce the computing time required by Matlab.

Besides these data related issues, *DasyLab* was also used in to create a built in function to set up a mass balance around the key "nodes" of the system, the key nodes over which the mass balances were setup are illustrate in Figure 7.11. The mass balances were setup under the assumption that there were no leakages in the system.

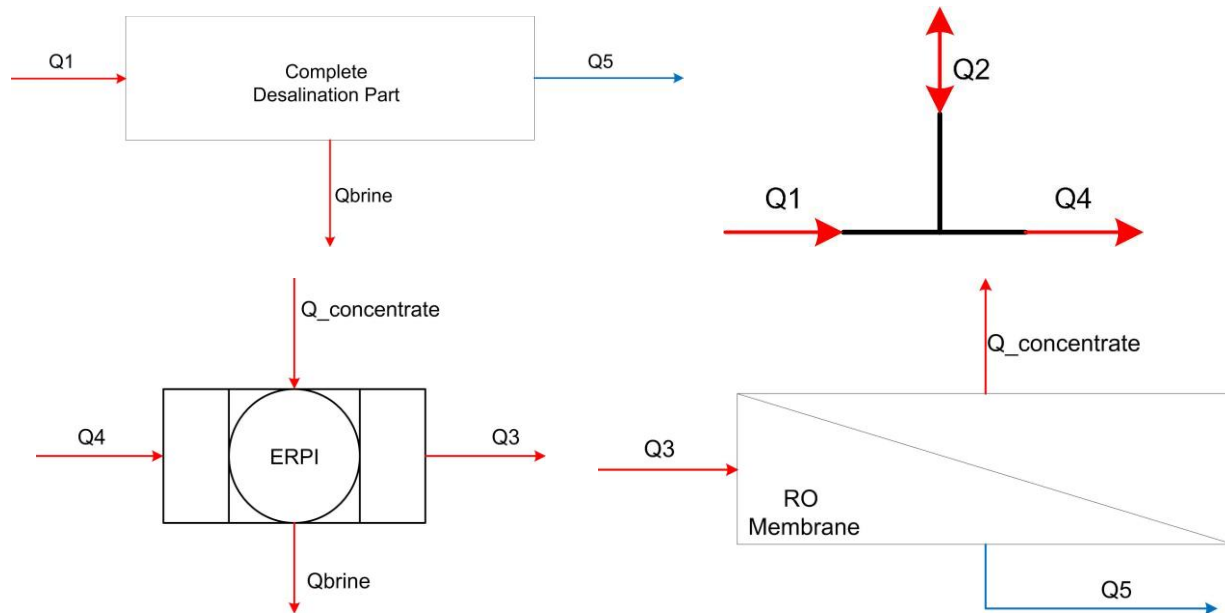


Figure 7.11: From top left corner to the bottom right corner: mass balance (MB) over the complete system, MB over T connection, MB over the ERPI, MB over the RO membrane.

Starting from the top left corner, ending at the bottom right corner are the nodes around the:

- Complete system
- T section, splitting the raw water into two flow: the flow to storage and flow to desalination part
- ERPI
- RO membrane (final part of system)

The names used for the flows are based (number) on the respective sensor measuring the flow, if there is no sensor measuring the flow a seemingly logical name was assigned to the flow. Note that the flow leaving the RO membrane is named $Q_{Conc.}$ (not Q_4), this is because flowmeter F_4 was not functioning. This meant that the concentrate flow leaving the RO membrane (entering the ERPI_ could not be monitored. As a result of this, there are now three flows/variables that are not independently measured. $Q_{permeate}$, $Q_{feed,ERPI}$ and $Q_{Conc.}$ are calculated by within DasyLab according to the following procedure. First, the mass balance over the complete system is given by:

$$Q_1 = Q_{brine} + Q_5 \quad (7.2)$$

Second, the mass balance over the T-section is given by:

$$Q_4 = Q_1 \pm Q_2 \quad (7.3)$$

It should be noted that the sign for Q_2 can have both positive and negative values, this is the only flow within the system that can flow in both directions. The mass balance over the ERPI is given by:

$$Q_4 + Q_{Conc.} = Q_3 + Q_{Brine} \quad (7.4)$$

And the mass balance over the RO membrane is given by:

$$Q_3 = Q_{conc.} + Q_5 \quad (7.5)$$

By substituting the equations above, the following three relationships were established, these relationships are valid as long as there are no leakages within the system.

$$Q_{brine} = Q_1 - Q_5 \quad (7.6)$$

$$Q_{conc.} = Q_3 - Q_5 \quad (7.7)$$

Using Eqs. (7.6)&(7.7), it was possible to monitor and record the respective flows and use these values to evaluate the systems performance. During the initial test run in December 2012 there was no energy storage, thus in this period $Q_2 = 0$. Before presenting the measured data, lets have a look at the expected system performance.

8. System Predictions

In this chapter the expected system behavior will be discussed. Based on information obtained from the specification sheets, from the literature and from the measurements performed by Vollebregt and Feenstra (2012) a pattern of expected behavior can be drawn. In the following sections the theory and assumptions used to draw this expectance pattern will be discussed.

8.1. Expected PV Performance

According to the manufacturers specifications the Sundaya LEC 1200 PV modules have a maximum efficiency of 17.3% at standard testing conditions. However, the maximum efficiency is not often used therefore the average efficiency of $\eta = 15\%$ is a more useful number. Unfortunately in practice PV modules do not operate under standard conditions, and efficiencies are often lower than specified. There are several factors that affect the PV module efficiency, shading & mismatch losses and temperature related losses are amongst the most important factors.

8.1.1. Shading Losses

It is well known and common knowledge that shaded PV modules produce less power. Whenever PV modules are shaded, less irradiance reaches the cell and thus less power is produced. One common phenomenon is dirt accumulation on top of the PV module. This type of dirt loss is practically unavoidable in autonomous systems. In climates such as Jakarta, where dust and pollution are common dirt losses can range from anywhere between 1-10%. For further estimation, 8% dirt losses will be assumed.

However, when discussing shading losses, this theory can be explored in a deeper sense. Shading of a small section of a PV module can have a surprisingly large effect on the output. Most PV modules consist of a large amount of smaller PV cells connected in series. Due to the series connection, the maximum current output is limited to the smallest current produced. Thus not only do the shaded cells produce less power, but also all of the other cells connected in series experience a reduced power output. This loss in power is typically dissipated as heat in the solar cells and in extreme cases can cause solar cell failure. As the PV modules were placed on top of the roof and no significant structures or trees were in the path of the sun, shading losses will be assumed to be minimal. Of course shading losses by clouds will be present, but this type of shading loss is not time depended and also not easily predicted. In the following section the affect of the cell temperature on the efficiency will be discussed.

8.1.2. PV Panel Temperature

The cell temperature affects PV module output, as the day progresses and solar irradiance increases its logical that the cell temperature increases. Also as indicated above, shading can also cause cell temperature increase. For this reason the cell temperature must be taken into account. According to Zeman (2010) the relationship between power output reduction and temperature increase is given by:

$$Power_{reduction} = 0.25\%/^{\circ}C \quad (8.1)$$

Using this information combined with the daily cell temperature profile the PV module efficiency pattern can be found for time along the day. This evaluation has been performed previously (Vollebregt

& Feenstra, 2012), however in practice the PV module efficiencies were found to differ significantly from this expected pattern. The actual hourly PV module efficiencies are shown below in Table 8.1.

Table 8.1: PV module efficiency for different times during the day(Vollebregt & Feenstra, 2012).

07:00	08:00	09:00	10:00	11:00	12:00	13:00	14:00	15:00	16:00	17:00	18:00
12.1%	11.8%	11.5%	11.2%	10.9%	10.8%	10.8%	10.9%	11.1%	11.3%	11.7%	11.9%

Assuming the PV module performance has not degraded in the time between measurements and assuming the additional Sundaya LEC-1200 Panels are of similar quality, the above-presented efficiencies will be used. These efficiencies have been empirically determined and include shading-, dirt- and temperature losses.

8.2. Solar Pump & Controller

8.2.1. Cable Losses

The power produced by the PV modules must be transferred to the controller and from the controller to the submersible pump. The power is transferred via 4 [mm²] copper cables. From the PV modules this is a two wire cables and from the controller to the pump the power is transferred via a three-phase electric cable. While traveling through the electric cables, there will be losses. The power losses inside copper cables can be calculated by using the equation Eq. (7.1):

$$P_{loss} = I^2 * R \quad (7.1)$$

Where R is given by:

$$R = l \frac{\rho}{A}$$

Where l is the length of the cable in meters, ρ is the electrical resistivity of the cable material (in this case copper) and A cross-sectional area of the cable. In this specific case, the electrical resistivity of copper is assumed to be $1.68 \cdot 10^{-8}$ [$\Omega \cdot m$] and the cross-sectional area is $4 \cdot 10^{-6}$ [m²]. The electrical cable from the PV modules to the controller has a length of 10 [m] and the cable from the controller to the pump is 50 [m] long. Thus the electricity travels through a total of 60[m] of copper wire. Note that a value for the current (I) is also required for the calculation. The current used for this calculation is the current at the PV module maximum power point, I_{mp} . Recall Table 6.5, where it can be seen that the I_{mp} for the PV modules used is 5.18 [A]. Now recall Figure 7.4 where the installed configuration is shown. Using elementary electrical engineering knowledge, a current at the maximum power point of 10.36 [A] is found. By filling in all this information into Eq. (7.1), a power loss of 27.05 [W] is found. A peak capacity of 1105 [W] is installed, this means that an estimated 2.5% power losses will occur due to the electric cabling.

8.2.2. Hydraulic Losses

As soon as water leaves the pump, it will experience hydraulic losses due to the piping system. There are several sources responsible for these hydraulic losses, a list of the most important losses is shown below:

- Losses due to the PVC surface roughness
- Losses due to bents and T-junctions.
- Losses inflicted by the measuring devices (flow-, pressure- and temperature monitoring devices)

Recall Eq. (6.1) first introduced in chapter 6.1:

$$W_{pump} = Q * \{(p_2 - p_1) + .5 * \rho * (v_2^2 - v_1^2) + \rho * g * (z_2 - z_1) + \rho * e_{fr}\} \quad (6.1)$$

This equation can be used to calculate the hydraulic pump power. Recall that the friction losses were neglected in the initial stages of this report. As previously mentioned, in practice friction losses will be present and thus in order to more accurately predict the system behavior these losses will now be further elaborated. The literature regarding the friction losses was mainly taken from Akker and Mudde (2008). Below the theory that enables the estimation of the friction losses can be seen:

$$e_{fr} = \sum_i \left(\frac{1}{2} * f * \frac{L}{d} * \langle v \rangle^2 \right)_i + \sum_j \left(\frac{1}{2} * K * \langle v \rangle^2 \right)_j \quad (8.2)$$

Where f is the friction factor and can be calculated by:

$$f = \begin{cases} \frac{64}{Re}, & Re < 2000 \\ 0.316 * Re^{-0.25}, & 4000 < Re < 10^5 \end{cases} \quad (8.3)$$

$$Re = \frac{\rho * v * L}{\mu}$$

Where μ is the viscosity and L is the pipe length in [m] and v is the velocity of the water in [m/s] and is calculated by:

$$v = Q/A = Q/0.25\pi * d^2 \quad (8.4)$$

Finally K is the dimensionless loss coefficient and can be found in data booklets such as Janssen and Warmoeskerken (2006). Below in Table 8.2 all of the inputs are summarized and their values and units are given.

Table 8.2: Relevant parameters for the friction loss calculation, their values and units.

Parameter Name	Symbol	Value	Unit
Density of Water	ρ	1000	Kg/m ³
Friction factor	f	$\begin{cases} \frac{64}{Re}, & Re < 2000 \\ 0.316 * Re^{-0.25}, & 4000 < Re < 10^5 \end{cases}$	-
Reynolds Number	Re	$Re = \frac{\rho * v * L}{\mu}$	-
Cross-sectional Surface area	$A = 0.25\pi * d^2$	$4.642 * 10^{-4}$	m ²
Water velocity	v	$Q/4.642 * 10^{-4}$	m/s

Volumetric Flow	Q	-	m^3/s
Dynamic Viscosity	μ	0.0009	$\text{Pa}\cdot\text{s}$
Bent loss coeff.	K_{bent}	1.3	-
T-junction loss coeff.	$K_{junction}$	1.0	-

8.2.3. Solar Pump & Controller Performance According to Manufacturer

Before combining all of this information and predicting the system behavior, the pump curves provided by the manufacturer are shown. Based in information from the specification sheet a maximum pump efficiency of 65%, can be expected. However, by filling in all of the system inputs, a more detailed efficiency, flow and head pattern can be drawn. An indication of the flows, pressures and efficiencies that can be expected by the solar pump can be seen in the figure below.

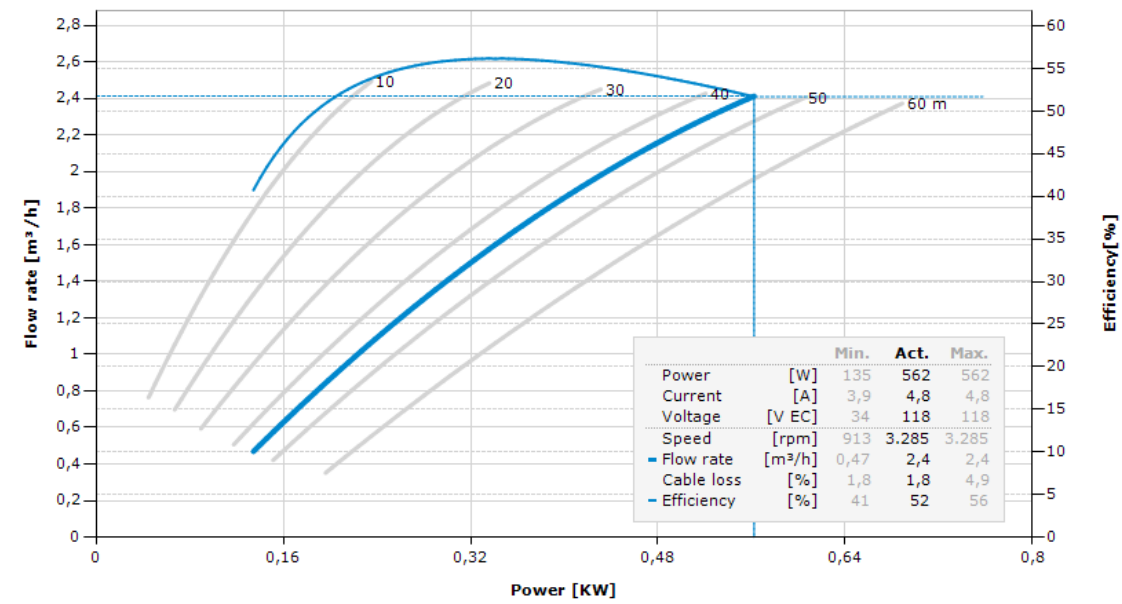


Figure 8.1: Pump Curves according to the manufacturer.

The pump performance is quite difficult to predict, even with all data available from the manufacturer. It can be seen that over the entire range of flows and pressures an efficiency of 41% - 56% can be expected. Typically solar pumps are used at a static head height (i.e. the pump will deliver a constant pressure), this was also the case in the previous project in Bali. However, due to the hydro-pneumatic energy storage the pump will be operating under variable conditions. The solar irradiance will vary along the day, and so will the delivered flow and required pressure. This makes for some interesting measurements and results. The next topic is the RO membrane and the energy recovery device (ERPI).

8.3. Membrane & Energy Recovery Device

The expected RO membrane and ERPI performance have already been previously discussed in this report. The RO membrane performance can be modeled using the Sirio software provided by Oltremare. The results of the modeling software have been presented before in Table 7.1.

Also the expected ERPI behavior has been discussed previously, recall **Error! Reference source not found.** where the required feed pressures going into the ERPI for several TDS values and flow rates is shown. What is interesting to evaluate later with the obtained results are the losses within the ERPI at the different input pressures and flow rates. Under supervision of Elemental Water Makers (ElementalWaterMakersB.V., 2012) an in depth experiment on the losses was performed by Snieder and Stubbe (2012). Thus the data obtained can be compared to these results.

8.4. Hydro-Pneumatic Energy Storage

As discussed in section 5.2.2 of this report, the concept of using a hydro-pneumatic tank as energy buffer in a PVRO system is unique and hasn't been attempted before. This makes the prediction of the behavior, especially the balance between the flows entering the desalination part of the system and the energy storage and the flow leaving the energy storage relatively hard. The pressure behavior inside the vessel is fairly straight forward, in the sense that starting from the pre-pressurized air pressure the pressure inside the vessel will increase as the day progresses. The air inside the hydro-pneumatic tank will be pre-pressurized to 2.5 [bar] and can reach a maximum pressure of 8 [bar] (maximum head delivered by the solar pump). The system behavior will be self-regulated, as the membrane will determine the corresponding flow to the water pressure at any given moment. The relationship between the volume of water stored inside the vessel and the pressure is a linear one given by Boyles Law (Wikipedia, 2013) (Recall (6.4)):

$$p_1 * V_1 = p_2 * V_2 \quad (6.4)$$

In order to prevent waterlogging (air dissolving into water) the theory suggests that the maximum amount of water inside the hydro-pneumatic tank should be approximately 2/3 of the total volume. With a starting pressure of 2.5 [bar] and a maximum pressure of 8[bar] the maximum water volume stored inside the tank should be 6.2 [m³]. This suggests that this requirement shall be met at all times. However, the exact relationship between air and water inside the tank is not known. Also the exact interaction between the media inside the vessel and the surrounding environment temperature is close to impossible to predict. And while in practice these phenomena will be present, they shall be neglected at this stage due to their complex nature. In the following chapter the measurement results of the setup in Jakarta will be presented.

9. Measurement Results

The results will be split up into three sections. First the data of the system without energy storage and the Low1-2540 membranes will be presented. Followed by the results of the originally designed system, i.e. the system with hydro-pneumatic energy storage and the Low3-4040 membrane and lastly a comparison between the key information/charts of the two configurations will be made. The data presented in this chapter was processed using Matlab.

9.1. Initial Test Period – Measurements Without Energy Storage

As mentioned earlier, the initial test period was performed sans hydro-pneumatic energy storage and with a Low1-2540 membrane instead of a Low3-4040 membrane. The results of this initial test period are presented in the sections to follow.

9.1.1. Sensor Issues & Calibration

After several months up setting up the pilot plant, there was still no hydro-pneumatic storage vessel available. Several test runs were performed, but due to the problem with the electricity from the grid no continuous measurements could be taken for a longer period. After installing the UPS, a test run of 1 week was logged. Prior to this test run, all of the sensors were re-calibrated. There were also some issues with sensors and the datalogger, which will be explained in this section.

9.1.1.1. Sensor and Datalogger Issues

As there was no hydro-pneumatic storage vessel, the ball valve regulating the flow to the storage vessel was shut. Flow meter *F2* was not used during this initial test period.

During one of the test runs, there was a major leakage at the high-pressure outlet of the ERPI. The tubing at this part of the system had detached itself, and there was no one at the site to shut off the system. Unfortunately there was no UPS installed yet and the system had crashed before the accident occurred. Originally there was approximately 4 [m³] of water in the feed reservoir, after the accident there was still approximately 2 [m³] left. Meaning that roughly 2[m³] was pumped and had leaked out of the system. After this accident the port of flowmeter *F1* and the current clamp *I1* recorded mainly noise. It was attempted to reset the datalogger, but with no success. Thus unfortunately flowmeter *F1* and the current clamp *I1* could not be used. The absence of flow meter *F1* had no consequence on the results. Since there was no flow to the storage vessel, *F1* and *F3* essentially were measuring the same flow. The absence of the current clamp however was very unfortunate, it was now no longer possible to measure the current delivered by solar cells. Meaning that the power produced by the PV modules could not be measured.

The two pyranometers worked perfectly during the day, recording irradiation values that were very similar. The *CMP 3* showed a slightly higher irradiance when compared to the *SP Lite2*, this can be explained by the different range in wavelength that can be measured by both the sensors. The *CMP 3* has a broader measuring range, this could explain the slight difference. During the night however, the *CMP* measured an irradiance of 200 [W/m²] on average, possible reason for this high value at night could be a presence of a large spot light illuminating the perimeter at night. However, the *SP Lite 2* did now show the same behavior at night. The average measured value of the two pyranometers was used

to evaluate the system, also solar data measured at night was discarded. Lastly, pressure sensor P1 was showing non-linear behavior. A recalibration could not solve this issue, so P3 (re-circulate pressure sensor) was moved and used as P1 (feed pressure sensor). The final calibration factors and adjustment factors are presented in the following section.

9.1.1.2. Sensor Calibration

All sensors were calibrated prior to the long test run, this test run was started on December 10th 2012 at 17:34 and was stopped on December 18th at 10:00. The final sensor calibration and correction factors used can be seen below in Table 9.1.

Table 9.1: Final Sensor Calibration and Adjustment

	Measurement Device	Unit	Calibration Factor	Final Adjustment
P1	Pressure Sensor	bar	$F(x)=2x - 3.7$	-
P2	Pressure Sensor	bar	$F(x)=1.995x - 3.84$	0.998
P3	Pressure Sensor	bar	-	*0
C1	Conductivity Sensor	mS/cm	$F(x)=5.24x - 5.4076$	Filtered and averaged
C2	Conductivity Sensor	mS/cm	$F(x)=0.8235x - 0.56$	Filtered and averaged
J1	Pyranometer	W/m ²	$F(x)=77760.498x$	Filtered and max set at [1200 W/m ²]
J2	Pyranometer	W/m ²	$F(x)=14430.01443x$	Filtered and max set at [1200 W/m ²]
V1	Voltage Transducer	Volt	$F(x)=100x$	-
A1	Ampere-Clamp	Ampere	-	0
F1	Flowmeter	l/min	$F(x)=12.5-25$	0
F2	Flowmeter	l/min	$F(x)=-19.109x + 124.11$	-
F3	Flowmeter	l/min	$F(x)=8.3333e-4x$	0.97
F4	Flowmeter	l/min	$F(x)=8.3333e-4x$	-
F5	Flowmeter	l/min	$F(x)= 2.1667e-4x$	1.01
T	Temperature Sensor	°C	$F(x)=57.5362x - 121.8188$	-

9.1.2. Daily Solar Pumped flow and Solar Radiation

Let's start by taking a look at the main driving force of the entire system, the solar radiation received. The solar pump is driven indirectly (via controller) by the solar radiation received (solar radiation=insolation), thus it seemed logical to pair these two parameters together. The solar radiation and the pumped volume during this initial one-week test run are displayed in Figure 9.1. From the measurements the following values were determined for the initial test run:

Table 9.2:Min, Max, Average and Standard Deviation values measured during test period 1.

	Average	Standard Deviation	Minimum	Maximum
Daily Solar Radiation [kWh/m²]	4.36	0.52	3.63	5.12
Daily Pumped Flow [Liter]	6096	411	5437	6670

As mentioned earlier, due to the absence of the energy storage vessel and due to the use of the Low1-2540 membranes, the system was over scaled and a valve had to be installed to create a pressure loss.

At full power the loss was approximately 2 [bar], a low power this pressure loss was less. The pressure loss could not be logged, thus the current relationship between the received solar radiation and pumped flow is not very useful.

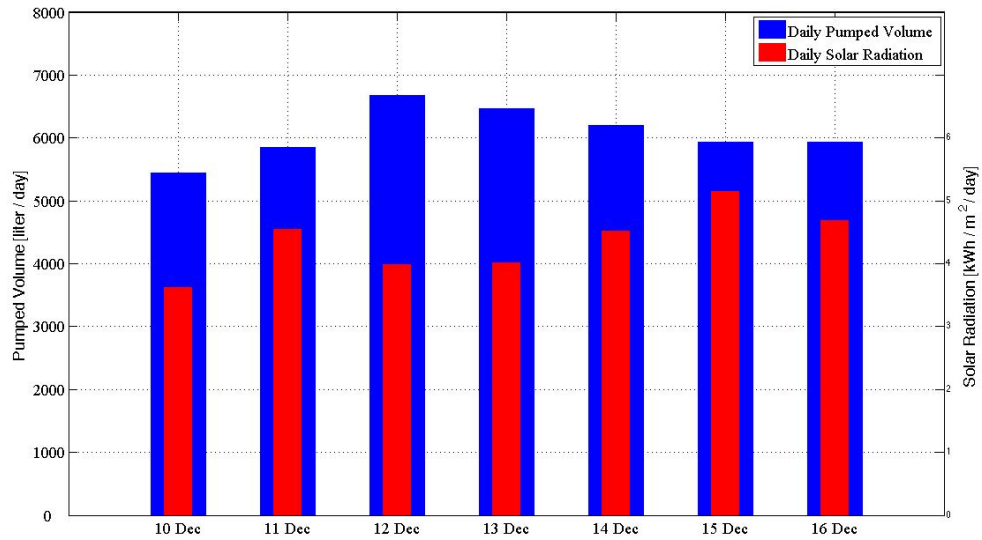


Figure 9.1: Daily solar radiation and daily pumped volume for initial test run.

The figure above is useful to give an indication of the amount of energy received and the amount of water pumped overall. However this chart does not provide a detailed look at the daily behavior of the system. For this reason the solar irradiance (power per surface area [W/m²]) and pumped flow shown in Figure 9.2. All of the data to follow in the data presented in this chapter will be 30-second average values, unless specified otherwise.

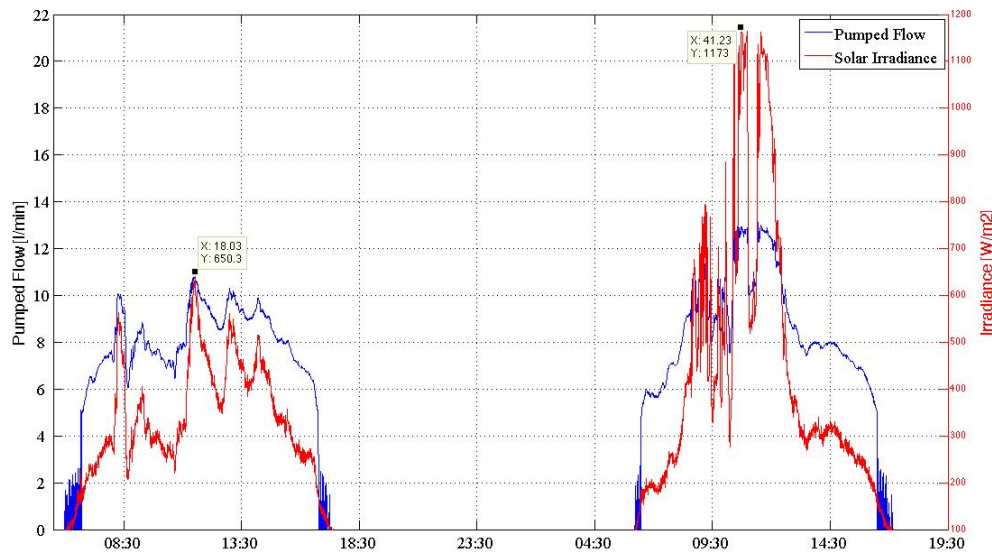


Figure 9.2: Solar Irradiance and pumped flow for 10 & 11 Dec (days 1 & 2 of test run).

From this plot it becomes clear that day 1 and day 2 of the test run experienced significantly different solar conditions. The maximum measured irradiance on 10 December was roughly 650 [W/m²], while the maximum measured irradiance on 11 December was 1173 [W/m²]. The month December is part of the rainy season and thus the solar conditions vary greatly from day to day, this is clearly illustrated in Figure 9.2.

It can be seen that the pump behavior directly follows the irradiance, the maximum measured pumped flow was roughly 13 [l/min]. This is significantly lowered when compared to the maximum flow rate of 40 [l/min] measured by Vollebregt and Feenstra (2012). A more detailed discussion of the results obtained can be found in chapter 10.

9.1.3. Desalination Part

In this section the results regarding the desalination part of the system can be found. In order to better understand the results given in this section, the systems working principles are shortly summarized in the following bullets:

- Raw (brackish) water is feed to the system
- Inlet pressure is intensified by the ERPI and fed to the membrane (brine also discharged by ERPI)
- The membrane produces a pure water stream (permeate) and a waste stream (concentrate)
- The concentrate (relatively high pressure) stream is re-circulated to the ERPI

9.1.3.1. Flows & Pressures

The pump directly determines the feed pressure. The feed pressured is the pressure that remains when after deducting the pressure losses (head, pipe, pre-filters, etc.) from the pressure delivered by the pump. The feed pressure and RO pressure produced by the ERPI (RO pressure) can be found in Figure 9.3. It can be seen that at a random point during day 2 of the test run, the feed pressure was 2.51 [bar] and that the ERPI intensified this pressure to 8.1[bar].

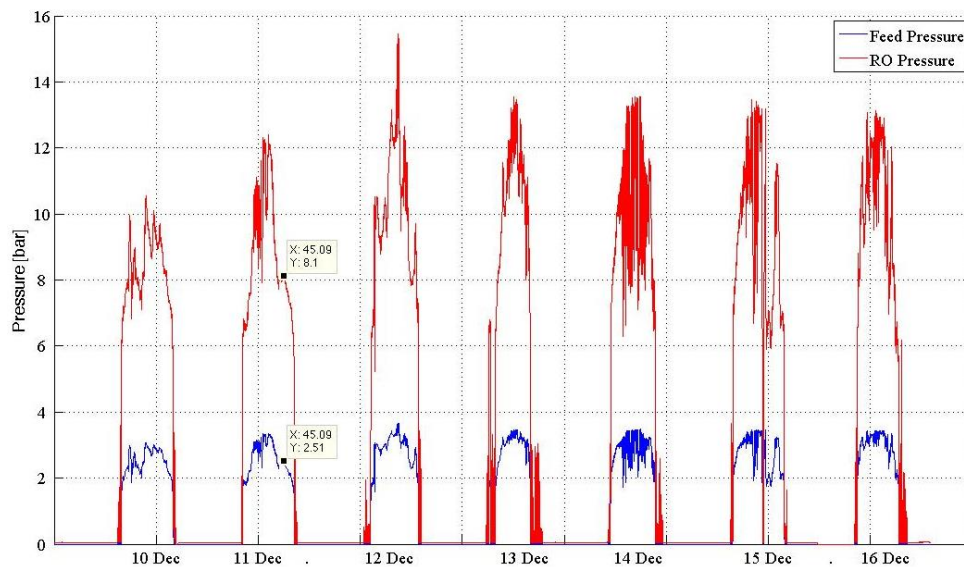


Figure 9.3: Feed and RO pressures measured during initial test run.

Figure 9.4 shows the feed pressure, RO pressure and feed flow measured on 10 December 2012. It can clearly be seen that all these values follow the same pattern, namely the solar irradiance. The figure also shows that the solar run time on 10 December was approximately 10 hours (pure run-time, excluding start-up time).

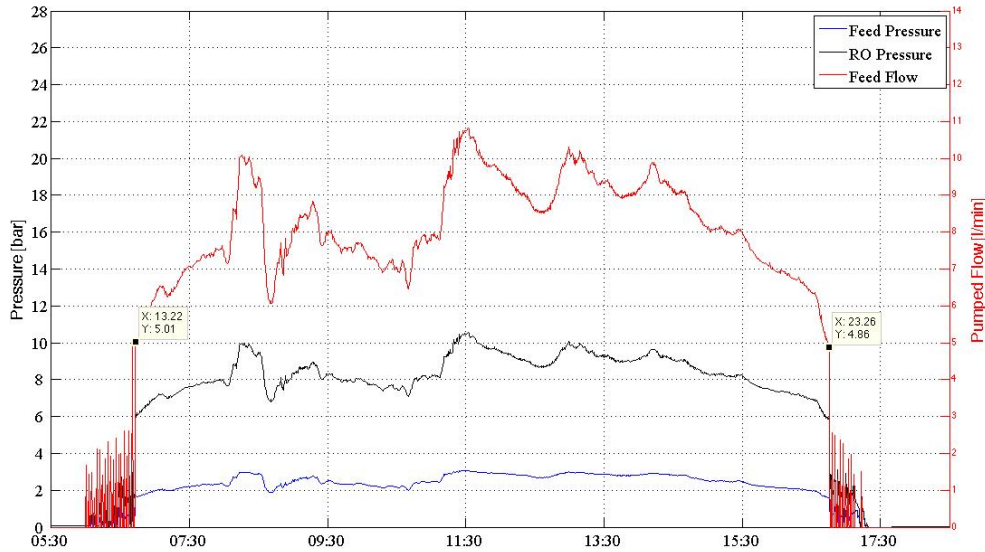


Figure 9.4: Feed pressure, RO pressure and feed flow on 10 December 2012.

Next in Figure 9.5 the feed pressure, RO pressure and feed flow for a 4-minute interval on December 10th is presented. The data used for this plot is the real time data recorded at a frequency of 2 [Hz].

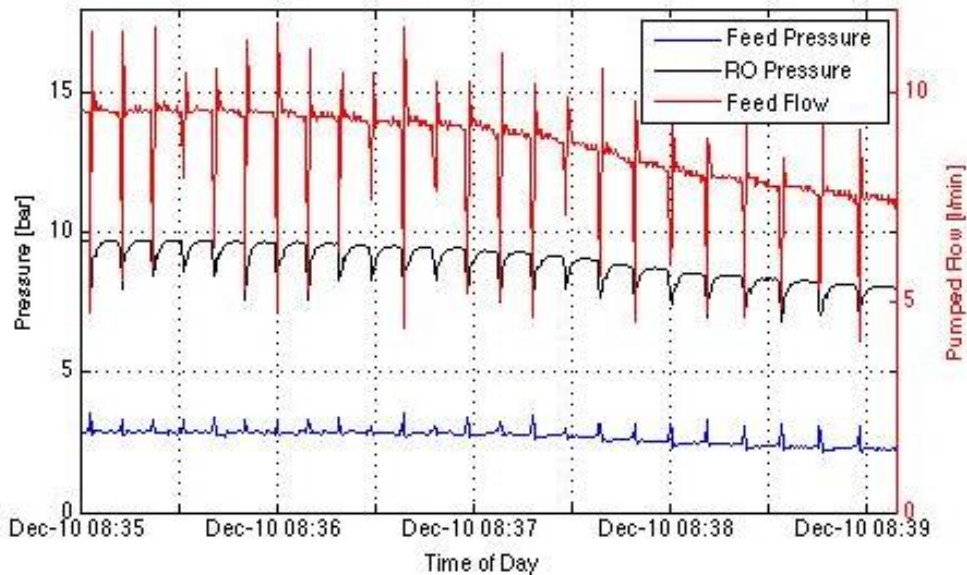


Figure 9.5: Feed pressure, RO pressure and feed flow during a 4-minute period on December 10th 2012.

The “noise” that can be seen in the figure above is caused by the reciprocating movement of the ERPI. Every time the piston inside the ERPI changes direction, a surge is created within the system. By looking

closely it can be seen that the ERPI causes roughly 6 pressure surges per minute, meaning that the traveling time from on en to the other is roughly 10 seconds. The next figure shows the relative flows within the system for December 10th.

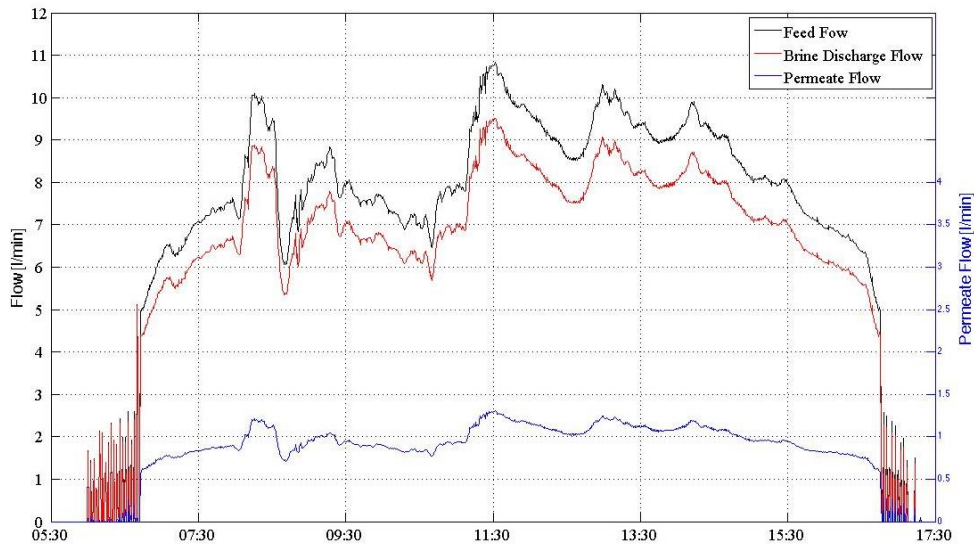


Figure 9.6: Feed flow, permeate flow and brine discharge flow for 10 December 2012.

Note that during start-up and shut-off of the system there is a lot of noise, this is caused by the system trying to restart itself. However the internal friction at this moment is too large (or power supplied is not enough). A more detailed look at the system start-up and shut-off behavior will be presented later on in this section.

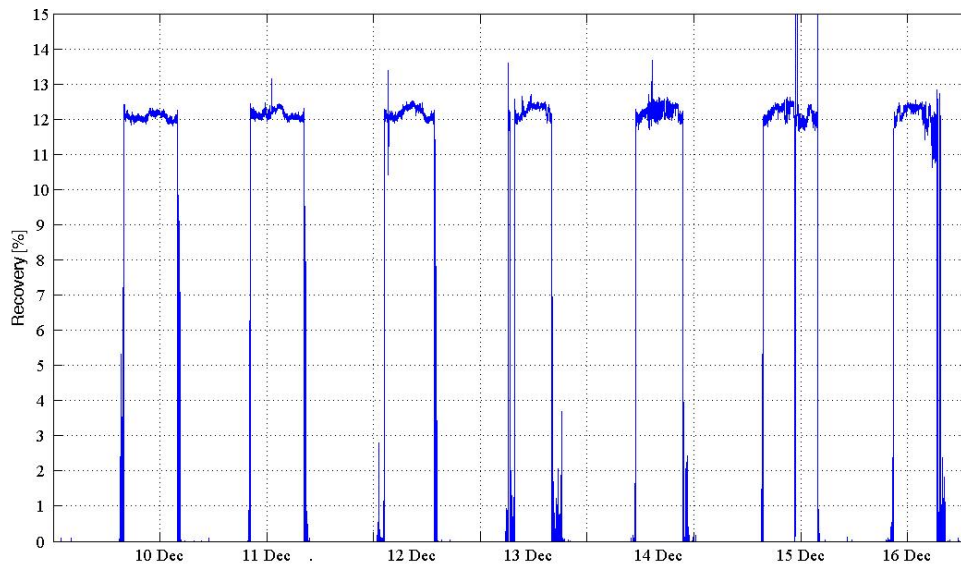


Figure 9.7: Recovery rates achieved during initial test-run.

Figure 9.7 shows the recovery rates for the initial test run performed in December 2012. It can be seen that once the system has started up, the average recovery rate achieved is 12.1 [%]. If the system start-up and shut-off are taken into account, the overall average recovery achieved during this initial test period was 10.2 [%].

9.1.3.2. Water Quality & Temperature

Water quality can easily be monitored by means of electrical conductivity (EC) measurements. EC meters were placed to record measure the feed conductivity and the permeate conductivity. Since the EC of these two flows is measured, the brine conductivity can easily be calculated by setting up an energy balance (if this is desired). The EC measurements are recorded in [S/cm] are converted to TDS values [mg/l] using the following equation (Walton, 1989):

$$TDS = K * EC \quad (9.1)$$

Where a value of 0.6 was used for K. The conversion to TDS was applied because TDS values are more common when discussing (RO) desalination plants. With the help of PAM Jaya, the EC sensors were re-calibrated one day prior to starting the test run. In Figure 9.8 the feed- and permeate TDS measured during the test period in December 2012 and also the recorded feed temperatures are displayed.

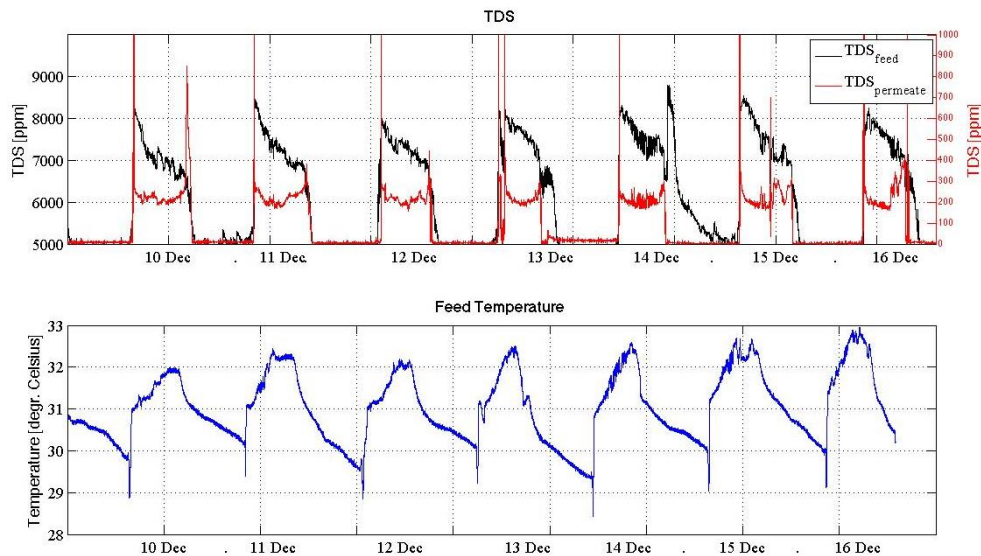


Figure 9.8: Feed and Permeate TDS on the top, and feed water temperature on the bottom.

From the top graph it can be seen that the Feed TDS shows a strange reducing behavior during the day. When the solar pump turns on the feed TDS is roughly 7500 [mg/l], after an entire day of pumping the feed TDS reduces 6000 [mg/l]. The bottom part of Figure 9.8 shows the feed water temperature measured during the test run in December 2012. It can be seen that the water in the tubing cools down at night and gradually increases during the day. It seems like the bottom and peak temperatures measured over night and during the day gradually increase as the week proceeds. It can be noted that the temperature and water quality behavior is repeated daily, a closer look at the permeate TDS and feed temperature can be found in Figure 9.9.

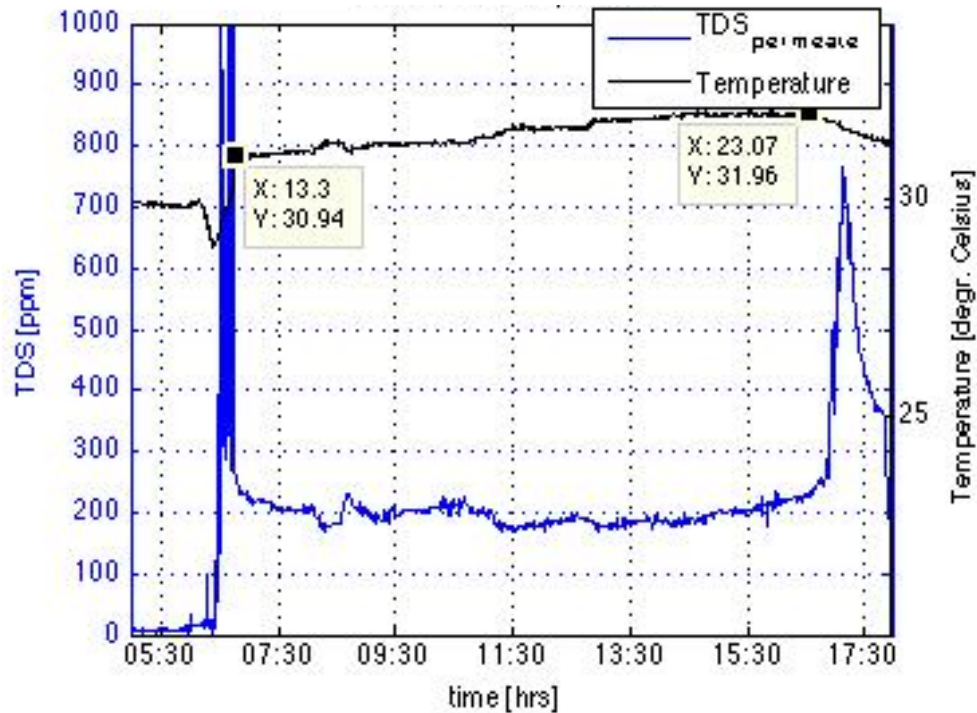


Figure 9.9: Permeate TDS and feed temperature for December 10th 20120.

Figure 9.9 illustrates that the temperature during the course of day 1 had increased by 1 [°C], according to the literature on average every increase of 1 [°C] causes an approximate EC (and thus TDS) increase of 2.2 [%] (Walton, 1989). This however does not pose as a problem for this project, the conductivity sensors used have a built in temperature compensation for a temperature range of 0 – 50 [°C]. The decrease of the feed water TDS can most likely be explained due to mixing of the water in the reservoir as the day proceeds. Two very steep permeate TDS increases can be observed during start-up and shutdown of the system, it can be seen that on both occasions the permeate TDS surpasses the earlier mentioned 600 [mg/l] requirement threshold.

9.1.4. Permeate Flux (Surface Load)

Figure 9.10 and Figure 9.11 show the permeate flux for the entire test period in December 2012 and a close-up of the permeate flux on 15 December 2012 respectively. With the help of the data cursors added on the plots, it can be seen that the maximum flux was measured on 12 December. The flux measured on that day was roughly 46.6 [l/h/m²], while the maximum flux measured on the day with the least solar radiation (10 December) was roughly 30.2 [l/h/m²]. In order to give a better look at the daily flux, the flux for 15 December 2012 is also shown. It can be seen that the maximum flux on 15 December was 39.2 [l/h/m²], and the flux at shutdown was 13.4 [l/h/m²]. It can also be seen that the irradiance received on 15 December varied strongly throughout the day.

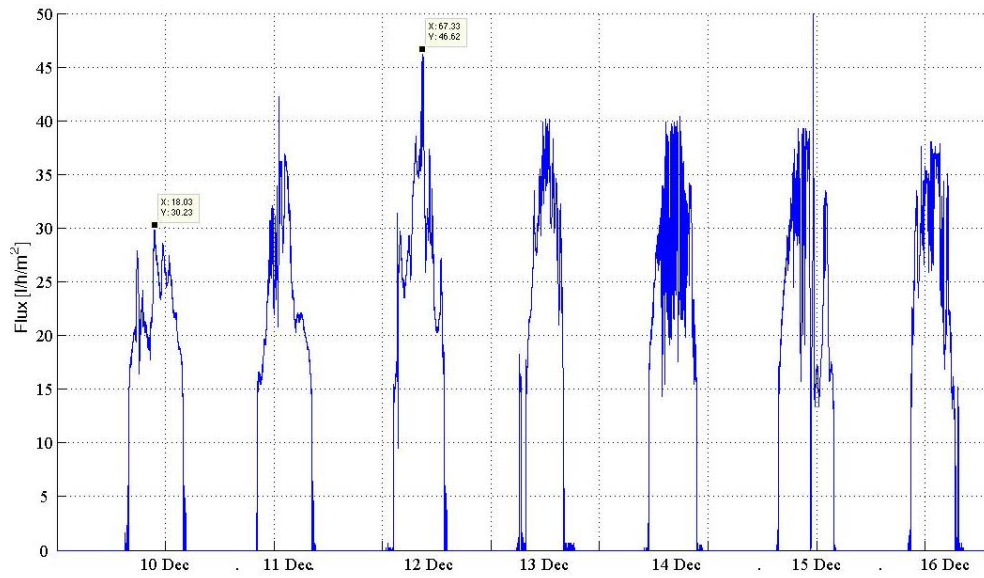


Figure 9.10: Flux during test period 1, 10-16 December 2012.

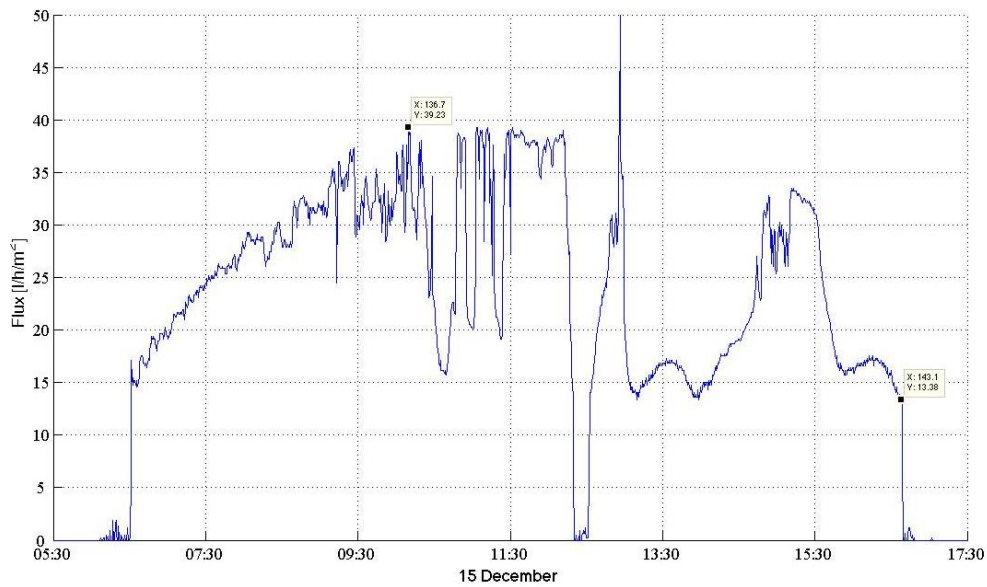


Figure 9.11: Flux on December 15th 2012.

9.1.5. System Start-up & Shut-off

When taking a closer look at the start-up and shutdown of the system, it can be seen that the start-up and shutdown does not occur smoothly. It can be seen that the start-up starts at approximately 6 am and the system shuts down around 4.30 pm. In this section a close up look will be taken at the shutdown characteristics of the system. Initially it was expected that the system would shut down at a working pressure of roughly around 1 [bar]. First lets have a look at the shutdown behavior of the system, the data of December 10th 2012 will be used as example.

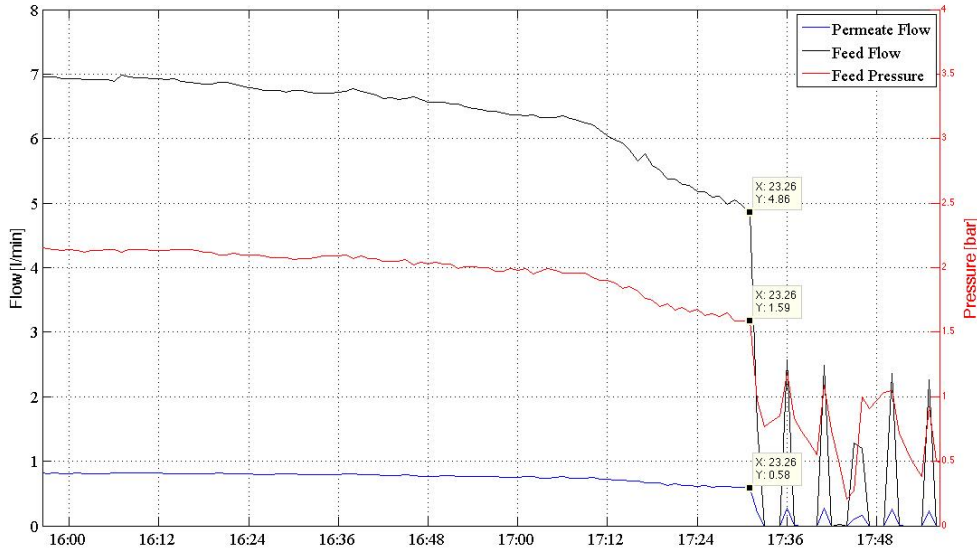


Figure 9.12: Feed flow, permeate flow and feed pressure during shut-down on December 10th 2012.

In Figure 9.12 it can be seen that the system shut down (permeate flow becomes zero) at a feed pressure of 1.59 [bar]. It can be noted that at this pressure both the feed flow and the permeate flow drop down to zero. It can also be seen that the system tries to start-up several times, however not enough pressure can be produced by the solar pump. This shutdown pressure is higher than expected, and can be explained by the fact that the solar pump is most likely encountering too much resistance to start-up (not enough power produced by PV modules). The fact that the solar pump tries to start-up several times indicates that there is still power produced by the PV modules. In Figure 9.13 the solar irradiance, feed pressure and the permeate TDS are plotted during the shutdown process of December 10th.



Figure 9.13: A closer look at the permeate TDS, Irradiance measured and feed pressure during shutdown.

It can be seen that at the time of the shutdown pressure (1.59 [bar]) the average irradiance measured by the pyranometers is 173.9 [Watt/m²]. Theoretically this means that the PV modules are still producing:

$$P_{PV} = 192.8 \text{ [Watt]}$$

This seems like a lot off power is dissipated, unfortunately the exact power produced by the PV modules could not be measured due to the faulty port on the datalogger. By integrating the irradiance during this shutdown period, the energy lost trying to star-up can be found. This simple calculation shows that the energy lost during this period is:

$$E_{lost} = 56.9 \text{ [Wh]}$$

Figure 9.13 also shows the increase of permeate TDS as the system is shutting down. This increase in permeate TDS is mainly determined by the lower feed- and RO pressure. It should be noted that the maximum permeate TDS measured during shutdown on December 10th was roughly 851 [ppm], this value exceeds the maximum TDs of 600 [mg/l] as advised by the WHO (2011).

9.1.6. Summary of the Results

The total and average results measured during the initial test run in December 2012 can be found below in Table 9.3. The average values presented below are measured during the actual running time of the system. The startup and shutdown values are not taken into account for the average values presented below

Table 9.3: Performance values of the system measured in the period of December 10th - December 16th.

Total insolation received	30.51 [kWh/m ²]
Total permeate water produced	4.37 [m ³]
Total Solar pumped volume	42.48 [m ³]
Average insolation per day	4.36 [kWh/m ²]
Average permeate water produced per day	618 liter
Average solar pumped volume per day	6.07 [m ³]
Average feed pressure	2.8 [bar]
Average RO pressure	9.6 [bar]
Average feed TDS	6670 [mg/l]
Average permeate TDS	200.8 [mg/l]
Average feed flow rate	9.5 [l/min]
Average recovery during operation	12.13 [%]
Average flux (Surface Load)	26.3 [l/h/m ²]
Average feed water temperature	31.8 [°C]
Average solar run time per day	10.16 [hours]
Percentage desalination run time	42.33 [%]

9.2. Second Test Period – Measurements Including Energy Storage

In this section the data with regard to the full system, including hydro-pneumatic energy storage and 4040 membrane can be found. Before presenting the data, the major issues with regard to the measuring equipment will be discussed.

9.2.1. Sensor Issues & Calibration

There was a small gap in between the first and second test period. During gap (period) the test site was affected by a major flood, most of the equipment was safely stowed away. With exception of flow sensor F1, this sensor had to be replaced. Prior to starting the second test period, a full sensor calibration was also performed again. Some noteworthy remarks are discussed below.

9.2.1.1. *Sensor and Datalogger issues*

Unfortunately the issues mentioned previously regarding the damaged ports on the datalogger could not be solved. This meant that the current clamp could not be connected, and thus current and power produced by the solar cells could not be monitored. The damage port also meant that the connection port of flowmeter F1 could not be used. Incidentally, it was also flowmeter F1 that had to be replaced due to the flood. It was opted to replace this sensor with a pulse-type sensor (as apposed to an analog output sensor). This meant that the extra counter port on the datalogger was used for measuring the solar pumped flow.

There were also some issues with flowmeter F2 (flow to/from storage). First of all, the (internal) resistors had to be replaced. This meant that this flowmeter was recalibrated and a different calibration factor was used. More on this can be found in Table 9.4. Also it appeared that this sensor was very sensitive to power peaks (as a result of the UPS having to switch on because of grid power outage). It happened on several occasions that the (internal) fuse was blown and needed replacing. On one occasion (day 2), the fuse was blown and caused a temporary/rapid increase in “flow to storage”. Subsequently the volume inside the vessel was also altered. The effects could easily be corrected within Matlab. This event can be seen in Figure 9.25, where at the end of day 3 (April 19th) the storage volume reaches zero due to a manual reset of the tank volume. The final calibration factors and adjustment factors are presented in the following section.

9.2.1.2. *Sensor Calibration*

The final calibration factors used can be found in Table 9.4. This final calibration was performed on April 16th 2013, one day before starting the log. The log was started on April 17th at 06:58 (in the morning). Prior to starting this log, the ERPI was also given a complete overhaul. This includes greasing the complete device and replacing the majority of the O-rings. The log was also started with fresh filter cartridges. The last noteworthy information is regarding to the pressure vessel and it’s capacity. The hydro-pneumatic pressure vessel had a capacity of 9000 [liter], which meant that approximately 5000-6000 [liter] of water could be stored inside the vessel. This was not enough to make it through the night, so manual interventions were required in order to prevent pressure loss inside the vessel (when the tank was empty). The interventions were performed by means of closing the ball valve between the pressure vessel and the installation.

Table 9.4: Final Sensor Calibrations and Adjustments used for test period 2.

	Measurement Device	Unit	Calibration Factor	Final Adjustment
P1	Pressure Sensor	bar	$F(x)=2x - 3.7$	-
P2	Pressure Sensor	bar	$F(x)=1.995x - 3.84$	0.998
C1	Conductivity Sensor	mS/cm	$F(x)=5.24x - 5.4076$	Filtered and averaged
C2	Conductivity Sensor	mS/cm	$F(x)=0.8235x - 0.56$	Filtered and averaged
J1	Pyranometer	W/m ²	$F(x)=77760.498x$	Filtered and maximum set at 1200 [W/m ²]
J2	Pyranometer	W/m ²	$F(x)=14430.01443x$	Filtered and maximum set at 1200 [W/m ²]
V1	Voltage Transducer	Volt	$F(x)=100x$	-
A1	Ampere-Clamp	Ampere	-	Not used
F1	Flowmeter	l/min	$F(x)=(2.172489e-2)*x$	1.04
F2	Flowmeter	l/min	$F(x)=-19.109x + 141.8$	-
F3	Flowmeter	l/min	$F(x)=(8.3333e-4)*x$	0.97
F4	Flowmeter	l/min	$F(x)=(8.3333e-4)*x$	-
F5	Flowmeter	l/min	$F(x)=(2.1667e-4)*x$	1.01
T	Temperature Sensor	°C	$F(x)=57.5362x - 121.8188$	-

9.2.2. Solar Pumped flow and Irradiance

Similar to the discussion on the results obtained during period 1, the first figure presented will be that of the solar radiation received during the test period and the total volume pumped. Essentially these two parameters are the driving force behind the entire system.

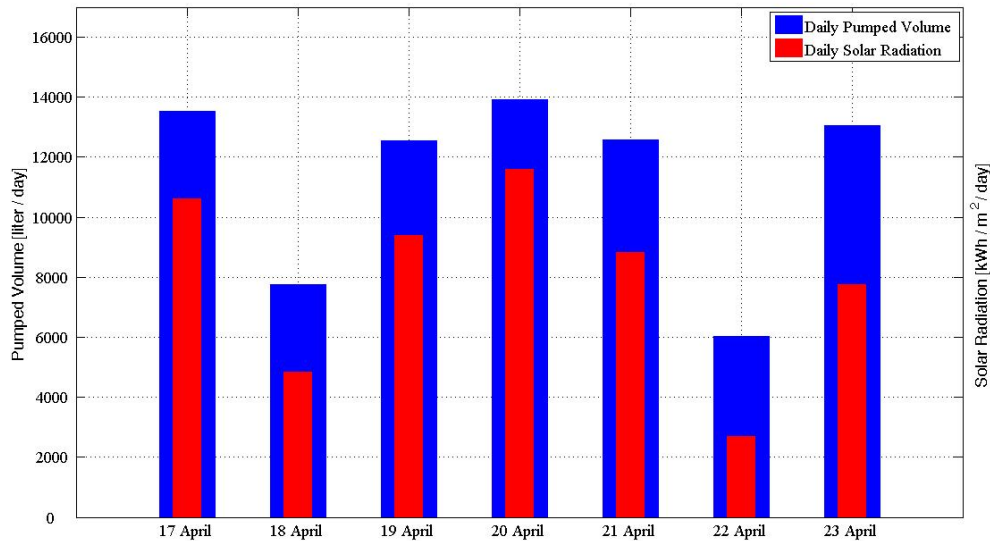


Figure 9.14: Daily solar radiation and pumped volume for second test period.

Figure 9.14 shows that the measured solar radiation and pumped volume for the week of April 17 through April 23. From the data shown in this figure the following key values were determined:

Table 9.5: Min, Max, Average and Standard Deviation for test period 2

	Average	Standard Deviation	Minimum	Maximum
Daily Solar Radiation [kWh/m ²]	4.22	1.68	1.43	6.14
Daily Pumped Flow [Liter]	11349	3122	6041	13929

While this information give insight in the amount of energy received, it does not show the detailed daily solar characteristics during this measuring period. Figure 9.15 shows the solar irradiance (power per surface area [W/m²]) measured by the pyranometers. The figure also shows the corresponding flow produced by the pump at this irradiance. The data presented in this figure and all of the other figures to follow in this section are based on 90 sec average values, unless specified otherwise.

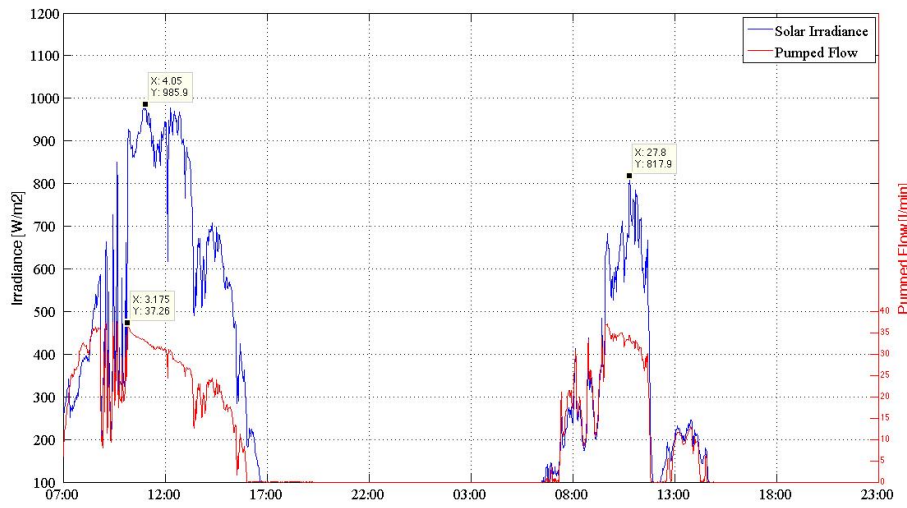


Figure 9.15: Solar irradiance and pumped flow for 17 & 18 April (Days 1 and 2 of test period).

Figure 9.15 shows the solar irradiance and pumped volume for two very distinctive days. From the plot it can be seen that the maximum irradiance measured on April 17th was 986[W/m²], while the maximum irradiance measured on April 18th was 818 [W/m²]. Similarly to the previous measuring period, it was still rainy season in Jakarta. From the figure it can even be seen that the pump shut-down for a short period right before 13:00. From the figure it can also be seen that the maximum flow rate measured during these days was 37.3 [l/min]. This flow rate is much higher then the maximum flow rate measured during the initial test period and is comparable to the maximum flow rate measured by Vollebregt and Feenstra (2012).

9.2.3. Desalination Part

In order to properly understand the plots presented below, recall the criteria explained in section 9.1.3.

9.2.3.1. Flows & Pressures

The pressure of the water leaving the solar the pump, is determined by the pressure inside the storage vessel. The pressure inside the storage vessel was not logged, however the pressure was logged prior to entering ERPI. Because of the close system, the pressure inside piping is identical to the pressure inside the storage vessel (if pressure losses within the piping system are neglected). As explained earlier, the

pressure entering the RO feed is intensified by the ERPI. The pressures pre- and post ERPI are presented below in Figure 9.16.

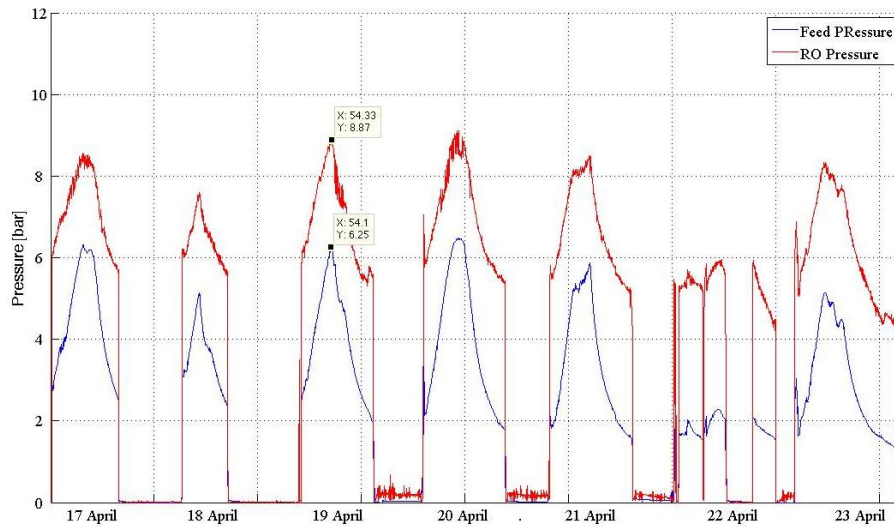


Figure 9.16: Feed- and RO pressure measured during the second test period.

In the figure it can be seen that everyday the pressure start at approximately 2 [bar] and increases until it reaches a maximum around noon (pressure vessel is full at this point). After reaching the maximum pressure, the pressure slowly decreases as the irradiance decreases and as the sun goes down. It can be seen that on April 22nd the measurements were interrupted. On this day, there were some meetings scheduled and coincidentally on this very little solar radiation was received. There was not enough energy storage for the system to run while the meetings were taking place. For this reason it was opted to close the valve to the energy storage and re-open this after the meeting had taken place, this can be identified by the abrupt pressure drop on April 22nd(and later pressure increase). This did not have any further consequences for the measurements. Once the valve was re-opened, the system restarted and the “solar run-time” was determined by subtracting the time (duration) of the stop.

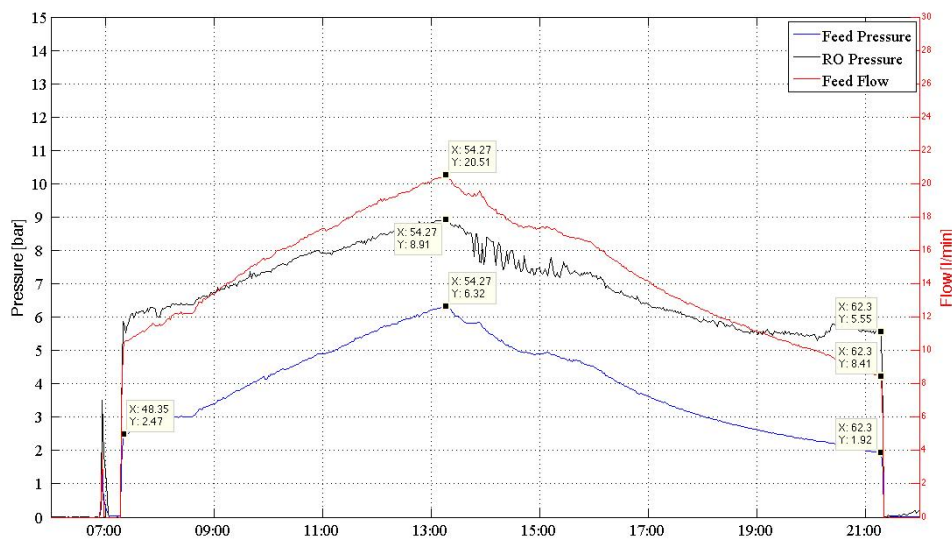


Figure 9.17: Feed pressure, RO pressure and solar pumped flow on April 19th.

Above in Figure 9.17 the Feed- and RO pressure and Feed flow for April 19th can be seen. Some data cursors were added in order to aid in identifying some important information. From the figure it can be seen that the system run-time on April 19th was just shy of 14 hours. The data cursors also show that at peak pressure the solar pump was delivering water at a pressure of 6.3 [bar] and that the feed flow (water entering RO) was 20.5 [l/min]. At this flow and pressure the ERPI intensified the water pressure to 8.9 [bar]. The system was manually shutdown at approximately 21:30 with the pressure inside the storage at 1.9 [bar]. Next in Figure 9.18 the feed- and RO pressure and feed flow are shown for a 5 min period on April 19th. For this plot, the real-time data measured at a frequency of 2 [Hz] was used.

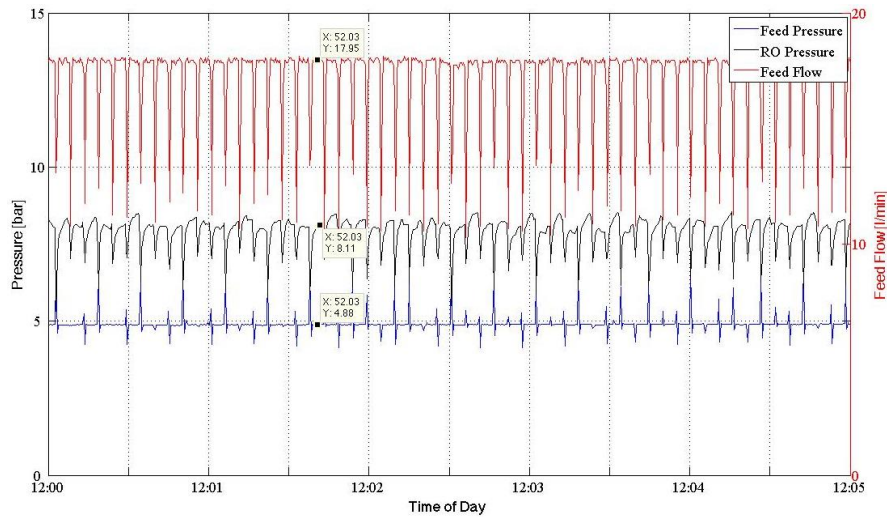


Figure 9.18: Feed- and RO pressure and feed flow during a 5 minute period on April 19th.

As performed earlier for test period 1, the close-up plot can be used to determine the piston traveling time. By analyzing Figure 9.18 closely, 6 pressure peaks can be counted within one minute. This results in a piston traveling time of roughly 9 seconds. This corresponds to the traveling time found earlier.

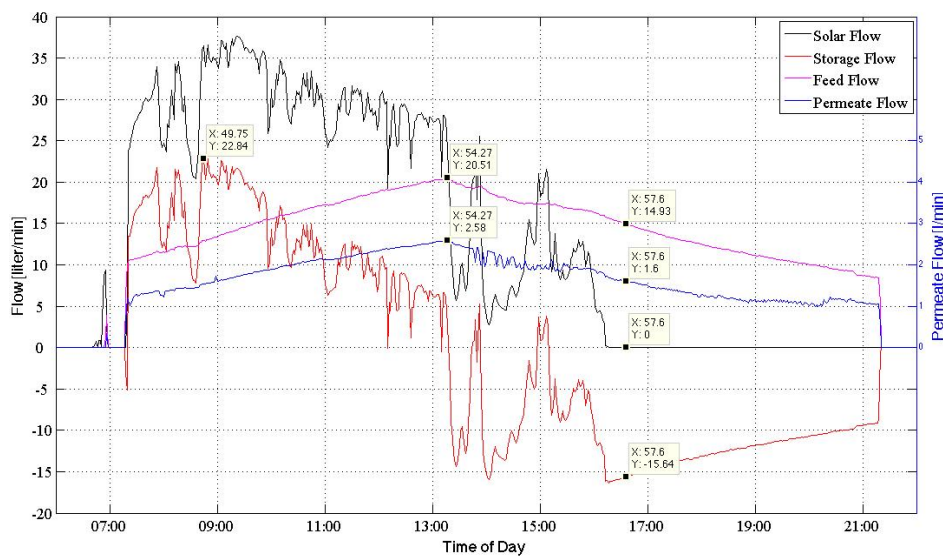


Figure 9.19: System flows on April 19th.

Figure 9.19 shows the system flows measured on April 19th. It can be seen that the solar flow and storage flow follow the solar irradiance pattern. The feed and permeate flow however cannot be compared to this pattern. As done earlier in several other plots, some data cursors were added to aid in discussion the flows presented in this plot. One of the noteworthy moments is the point at which the feed flow (and thus permeate flow) is at its maximum. It can be seen that at this point a feed flow of 20.5 [l/min] was measured, corresponding with this flow was a permeate flow of 2.6 [l/min]. Another noteworthy point, is the point at which the maximum storage flow was measured. A maximum storage flow of 22.8 [l/min] min was measured on April 19th.

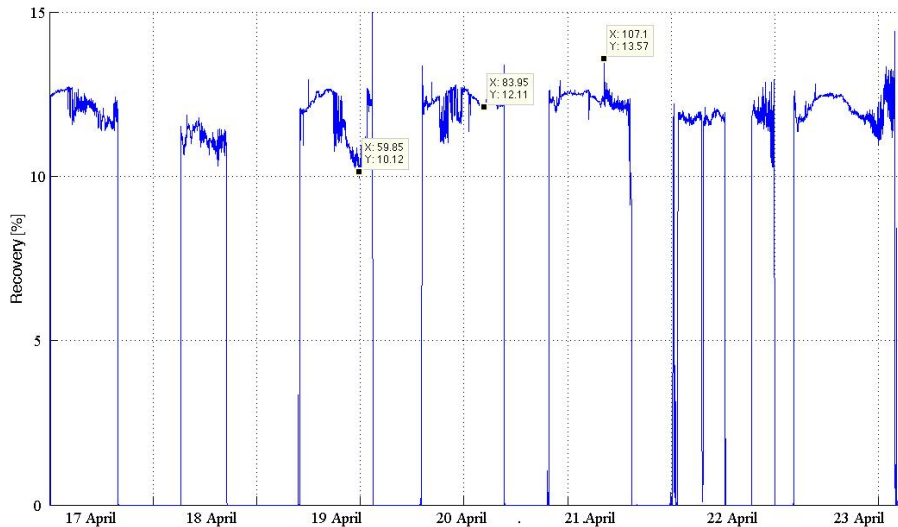


Figure 9.20: Recovery Rates achieved during second test period.

The recovery rates achieved during the second test period can be found above in Figure 9.20. The average recovery rate measured was 11.8 [%]. A couple of recovery rates are marked in the figure above, just to give an idea of the values measured.

9.2.3.2. Temperature & Conductivity

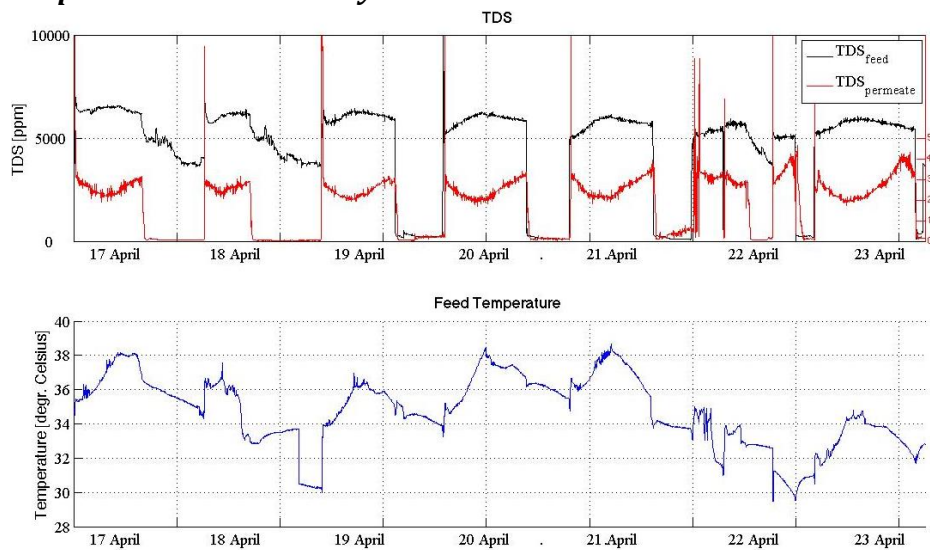


Figure 9.21: Feed- and permeate TDs at the top and feed water temperature at the bottom.

The feed- and permeate TDS and feed temperature can be seen above in Figure 9.21. The average feed TDS was 5754 [ppm], the average permeate TDS was 257 [ppm] and the average feed temperature measured was 35.2 [°C]. It can be seen however that on and after April 22nd the feed temperature dropped noticeably. A closer look at the permeate TDS and feed temperature for April 19th is shown below in Figure 9.22.

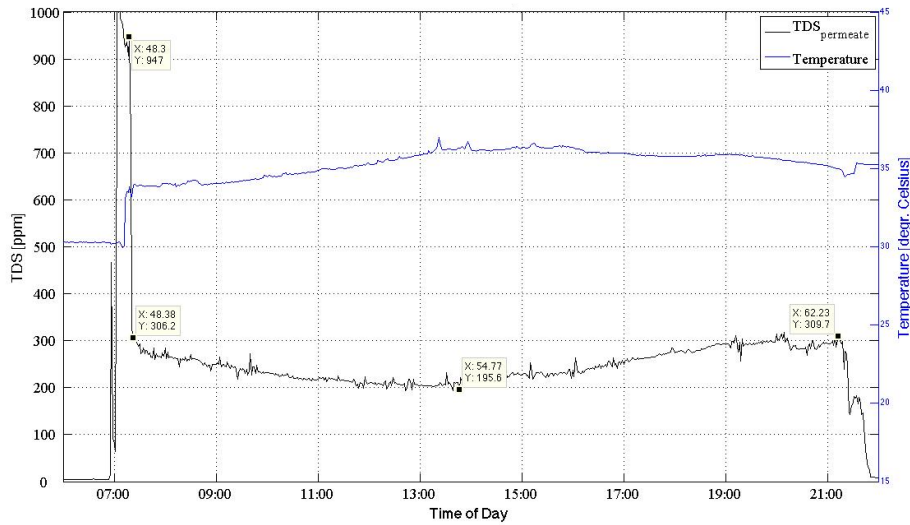


Figure 9.22: Permeate TDS and feed temperature on April 19th.

Three data cursors have been added to illustrate permeate TDS measured on April 19th. It can be seen that as the system starts-up in the morning the permeate TDS is slightly higher than 900 [ppm]. As soon as the system has started-up, a drinking water is produced with a TDS of 306 [ppm]. Around noon, when the pressure is at its peak, water with a TDS of 193 [ppm] is produced while just before the system shuts-down water with a TDS of 310 [ppm] is produced. With exemption of the TDS during start-up, the water produced during the entire day meets the WHO requirement of 600 [ppm] (WHO, 2011).

9.2.4. Permeate Flux (Surface Load)

Similarly to the results presented for test period 1 (system without energy storage), the permeate flux for test period 2 (system including energy storage) is now presented.

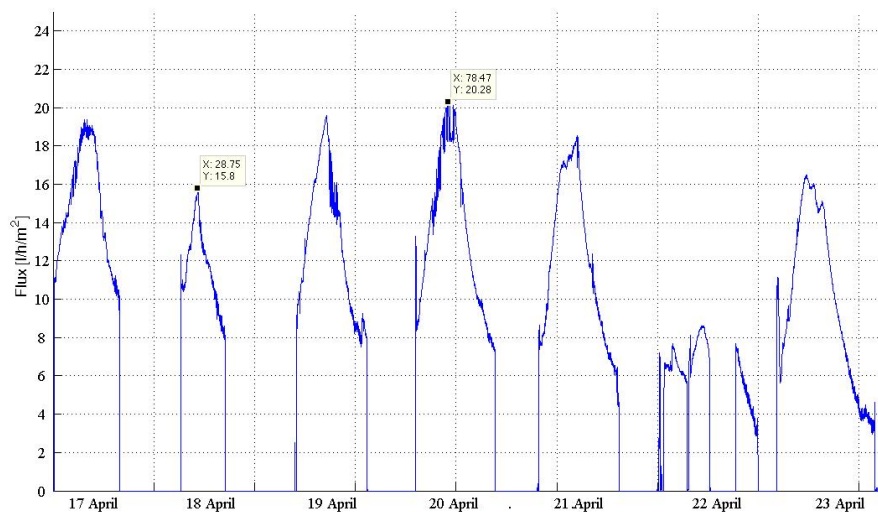


Figure 9.23: Flux for test period 2 (system including energy storage).

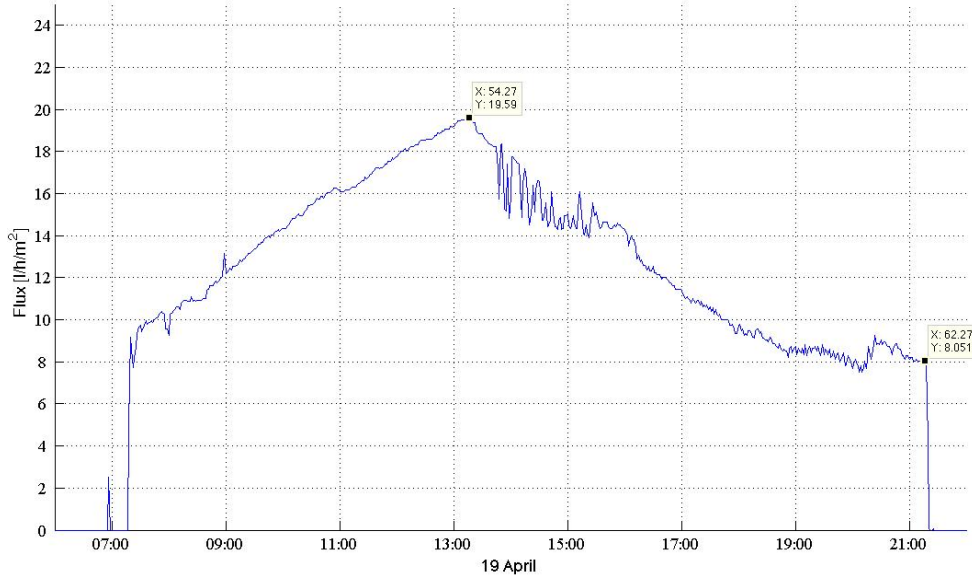


Figure 9.24: Flux on 19 April 2013

Figure 9.23 and Figure 9.24 show the flux measured during test period 2 and the flux on 19 April 2013. In the first figure it can be seen that the maximum flux measured for the system including the hydro-pneumatic energy storage vessel was 20.3 [l/h/m²]. It can also be seen that flux daily increases to about 12:00 at noon, where after the flux decreases again until the system comes to a halt. This is logical, as the pressure inside the vessel builds up in the morning and reduces soon after the irradiance reaches its peak levels. The flux is directly related to the pressure, thus this flux pattern is logical. A sample plot (close-up) of 19 April is also shown. The figure shows that the maximum flux measured on that day was 19.6 [l/h/m²] and that the flux was roughly 8 [l/h/m²] when the system shutdown. Next the results for the hydro-pneumatic storage vessel will be presented.

9.2.5. Energy Storage

In the following section the data regarding the energy storage (pressure vessel) will be presented.

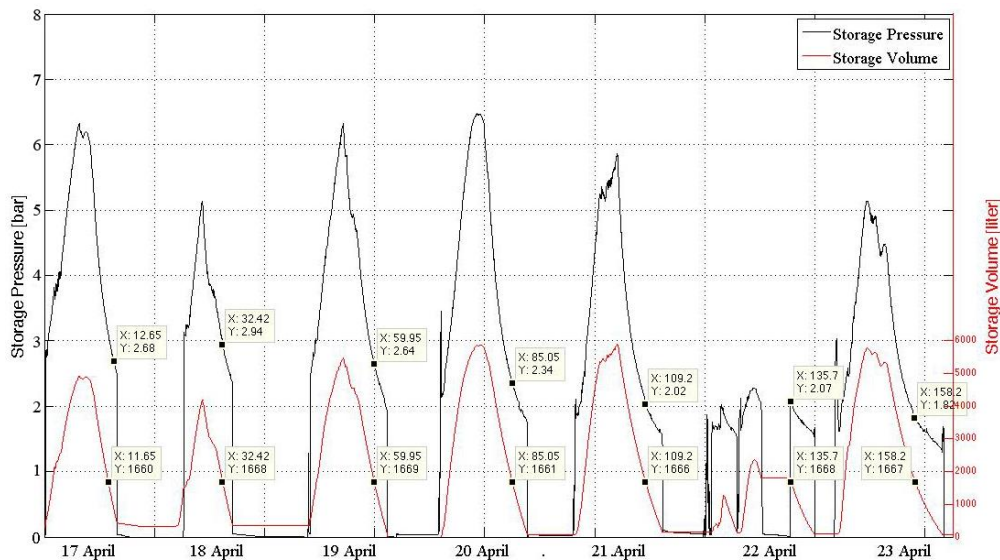


Figure 9.25: Storage pressures and volumes measured.

Figure 9.25 shows the storage volumes and pressures measured during test period 2. It can be seen that the pressure (and volume) starts a minimum everyday. As the day proceeds, the storage is filled and thus the pressure inside the vessel increases. As soon as the water volume approaches the design maximum (roughly 2/3 of the total vessel volume) the pressure inside the vessel decreases as water flows from the storage vessel into the desalination part of the system. During the entire test period, the air inside was only pressurized once (prior to starting the log). The air inside the storage vessel was pre-pressurized to 2.5 [bar]. Comparing the pressure at an arbitrary chosen volume inside the vessel can show the amount of pressures loss inside the storage vessel. The data markers shown in Figure 9.25 can be used to determine the pressure loss. Below in Table 9.6 the determined pressure loss is shown.

Table 9.6: Pressure Loss inside the Storage Vessel

Pressure Loss Info	Pressure at 1590 Liter	Pressure Change
Day 1	3.05	
Day 2	2.89	-0.16
Day 3	2.61	-0.28
Day 4	2.32	-0.29
Day 5	1.97	-0.35
Day 6	2.03	+0.06
Day 7	1.79	-0.24

It can be seen that a total of 1.26 [bar] was lost over the 7 days. In the next figure the storage pressure, volume and flows for April 19th can be found.



Figure 9.26: Storage pressure, volume and flow on April 19th.

It can be seen that at the start of day 3, the pressure inside the vessel is 2.47 [bar] with 535 [liter] of water inside the vessel. At its peak, the water volume inside the storage vessel is 5476 [liter] and pressurized to 6.32 [bar]. The system was stopped when the volume inside the storage vessel reached 104 [liter] at a pressure of 1.92 [bar]. The plot also shows the flow to/from the storage. It can be seen

that at the peak pressure the flow turn from positive to negative (i.e. water starts to flow out from the storage into the desalination part).

9.2.6. System Start-up & Shut-off

As the solar pump has automatically shutdown for several hours already when the system is stopped, there is no point in examining the shutdown behavior. As can be seen in all of the plots shown earlier, the system is quite stable during shutdown. The system start-up however will be shown below in Figure 9.27. For the plot below, the 30 sec average values were used.

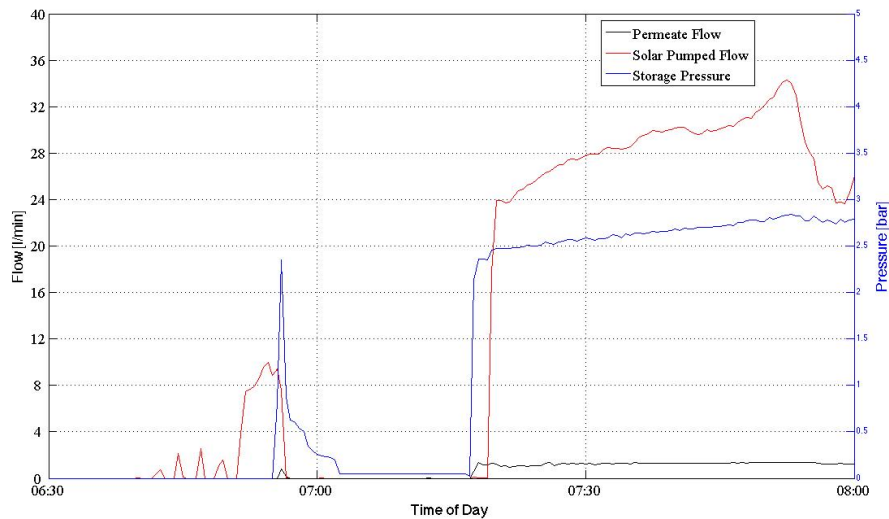


Figure 9.27: System start-up for April 19th.

It can be seen that in the morning the solar pump needs several attempts before it can start-up and start the daily production. By looking closely, it can be seen that between 6:30 and 7:00 AM, the solar pump needs 5 attempts before it can produce enough power and start the daily production.

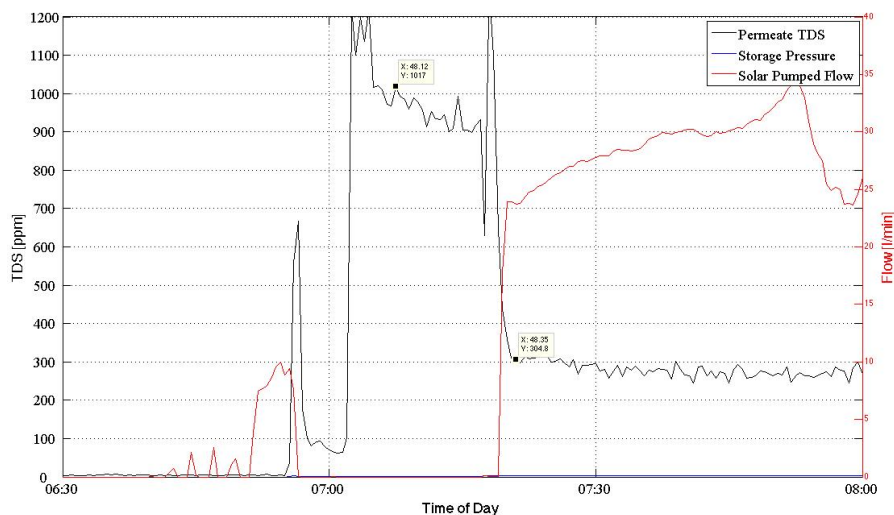


Figure 9.28: Permeate TDS during start-up on April 19th.

From Figure 9.28 it can be seen that during this start-up period the permeate passes the 1000 [ppm] mark. After system has full started-up (roughly 7:15 AM) the permeate TDS eventually decreases to the desired level.

9.2.7. Summary of the Results

Similarly to the results presented for the initial test period, a tabular summary of the key figures is presented below in Table 9.7.

Table 9.7: Performance values of the system measured during April 17th to April 23rd.

Total insolation received	29.52 [kWh/m ²]
Total permeate water produced	9.17 [m ³]
Total Solar pumped volume	79.44 [m ³]
Average insolation per day	4.22 [kWh/m ²]
Average permeate water produced per day	1310 liter
Average solar pumped volume per day	11.35 [m ³]
Average feed pressure	3.16 [bar]
Average RO pressure	6.0 [bar]
Average feed TDS	5754 [mg/l]
Average permeate TDS	257.3 [mg/l]
Average feed flow rate	11.7 [l/min]
Average recovery during operation	11.8 [%]
Average flux (Surface Load)	10.5 [l/h/m ²]
Average feed water temperature	35.2[°C]
Average daily run time	15.7 [hours]
Percentage desalination run time	65.3 [%]

In the following section, a comparison between the results measured for the two test configurations will be presented.

9.3. Comparison of the system Parameters

In this section of the report the results obtained for the two configurations (i.e. the configuration with 2540 membrane and no energy storage and the configuration with the 4040 membrane including energy storage).

9.3.1. Comparison of the Key Performance Values

First lets have a look at the comparison between the key performance aspects presented for both configurations. From Table 9.8 the following observations can be made:

- The solar climate (insolation received) was quite similar for the two test periods. The total insolation received during the second period was roughly 3% less when compared to the initial test period.
- The amount of water pumped and permeate produced is just about doubled. The permeate produced during the second test period was 110% more, when compared to the initial test period.
- The average feed pressure entering the ERPI was increased by approximately 13% (3.16 [bar] as opposed to 2.8 [bar]), while the pressure entering the RO membrane was significantly lower.
- The average feed TDs was lower during the second period, while the average permeate TDS was higher.

- The average feed flow rate measured during the second test period was roughly 23% higher than the feed flow measured during the initial test period.
- While the recovery rates achieved during both test periods are comparable, it should be noted that the average recovery rate during the second test period was slightly lower.
- The average feed water temperature during the second test period was significantly higher, a temperature difference of 3.4 [° C] can be noted.
- The percentage desalination time of the system increased from 42.3% to 65.3% for the system with energy storage when compared to the system without energy storage.

Table 9.8: Comparison of the key performance values

	Without Energy Storage	With Energy Storage
Total insolation received [kWh/m ²]	30.51	29.52
Total permeate water produced [m ³]	4.37	9.17
Total Solar pumped volume [m ³]	42.48	79.44
Average insolation per day [kWh/m ²]	4.36	4.22
Average permeate water produced per day [liter]	618	1310
Average solar pumped volume per day [m ³]	6.07	11.35
Average feed pressure [bar]	2.8	3.16
Average RO pressure [bar]	9.6	6.0
Average feed TDS [ppm]	6670	5754
Average permeate TDS [ppm]	201	257
Average feed flow rate [l/min]	9.5	11.7
Average recovery during operation [%]	12.13	11.8
Average flux (Surface Load) [l/h/m ²]	26.6	10.5
Average feed water temperature [°C]	31.8	35.2
Average run time per day [hours]	10.16	15.7
Percentage desalination run time [%]	42.3	65.3

9.3.2. Miscellaneous Noteworthy Comparisons

In this section some of the other noteworthy differences between the data of the two test periods will be presented. First of all, let's have a look at the flows measured for both periods.

9.3.2.1. Flows Measured

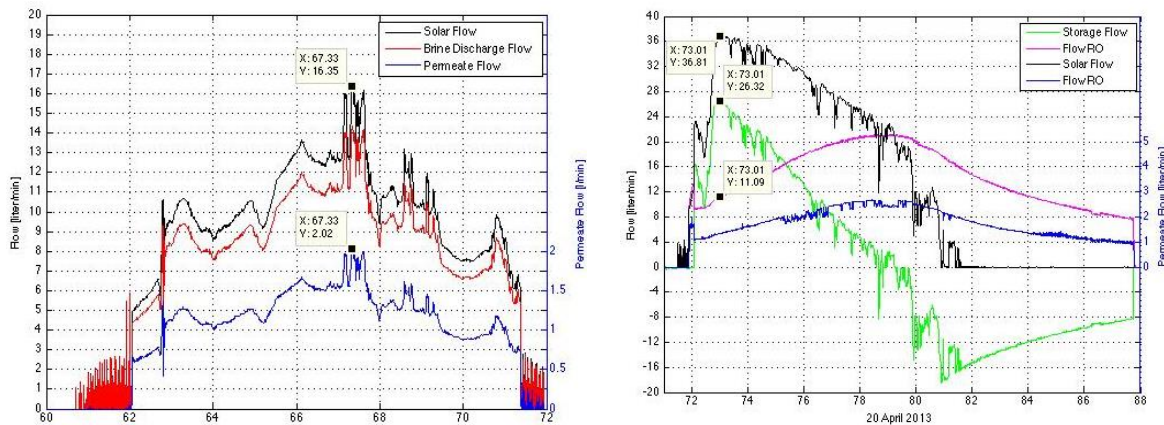


Figure 9.29: Flows for period 1 on the left and flows for period 2 on the right.

Above in Figure 9.29, the flows for the first period (no energy storage) and second period (including energy storage) can be seen. The data presented is from two arbitrary days and is plotted by using the 30-second average values. The figure is insightful because it shows the difference in flow patterns between the two configurations/periods. It can be seen that for period 1, all flows narrowly follow the solar radiation pattern, while for period 2 only the solar- and storage flow follow the solar radiation pattern while the permeate- and RO flow do not follow this pattern.

The figure also shows that that the maximum solar flow measured during period 2 is more than double the flow measured during period 1. Doubling of the solar flow can be explained by the circumstances under which the solar pump was delivering water to the system. During the first test period a single *Oltremare 2540* membrane was installed, this membrane has a much smaller membrane surface area compared to the *Oltremare 4040* membrane used in test period 2 (2.6 vs. 7.9 [m²]). This meant that at the higher feed flow rates (consequently higher fluxes) the pressure post ERPI exceeded 16 [bar] at peak power. The system was equipped with sensors with a maximum operating pressure of 16 [bar], so in order to prevent the pressure from exceeding this level a valve was installed to introduce a slight pressure loss. This meant that the pump was actually delivering water at a higher pressure than measured, and thus was operating in the upper regions of the H-Q curve resulting in a lower flow.

What can also be seen in Figure 9.29 is the difference in start-up and shutdown behavior between the two configurations. In period 1, the system required significantly more attempts to start-up in the morning and also during shutdown the solar pump would perform several attempts to start-up again. During period two the start-up and shutdown was much smoother, resulting in a more constant permeate TDS.

9.3.2.2. Recovery Rates Achieved

Below in Figure 9.30 the recovery rates for the two configurations/periods are shown. Similarly to the data above, the 30-second average values were used in these plots.

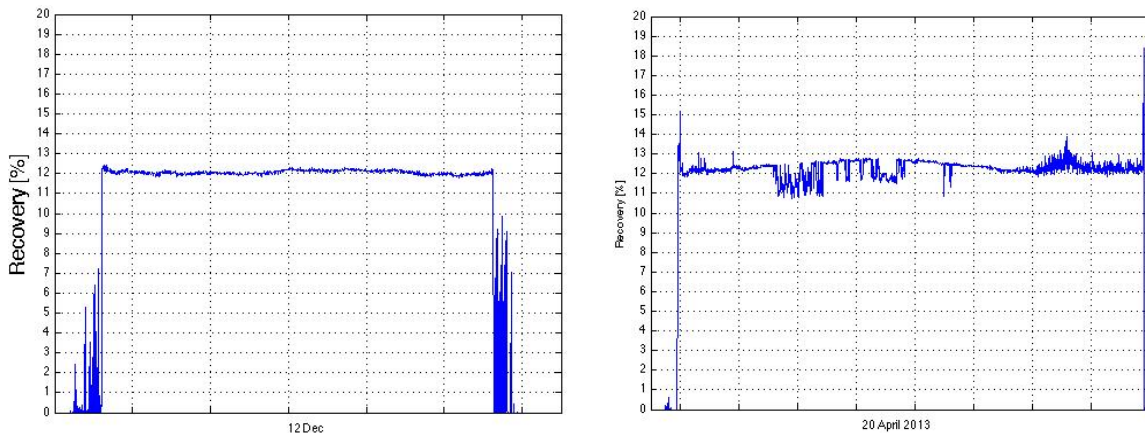


Figure 9.30: Recovery Rates for period 1 on the left and period 2 on the right.

Notice that that recovery rate for the configuration including energy storage shows significantly less constant behavior. With exception of the start-up and shutdown period, there is a lot more “noise” to be observed for the setup with energy storage. Next, let’s evaluate the pressure patterns and permeates TDS values measured for the two configurations.

9.3.2.3. Pressure Patterns and Permeate TDS

Below in Figure 9.31 the feed pressure and permeate TDS for the two configurations/periods can be seen. What makes the figure noteworthy is the different patterns shown. Both figure are plotted using the 30-second average values for two (the same as above) arbitrary days. Notice that both the pressure and the permeate TDs seem to follow the same solar radiation pattern as mentioned previously for the configuration without energy storage. The configuration with energy storage shows a completely different pattern. Notice that the pressure builds up as the day proceeds and when it reaches it's maximum (full energy storage), the pressure reduces until the system shuts down (storage vessel empty). Notice that the permeate follows this trend, but in reverse. At lower pressures the permeate TDS shows higher values and at peak pressure permeate water with lower TDS values are observed.

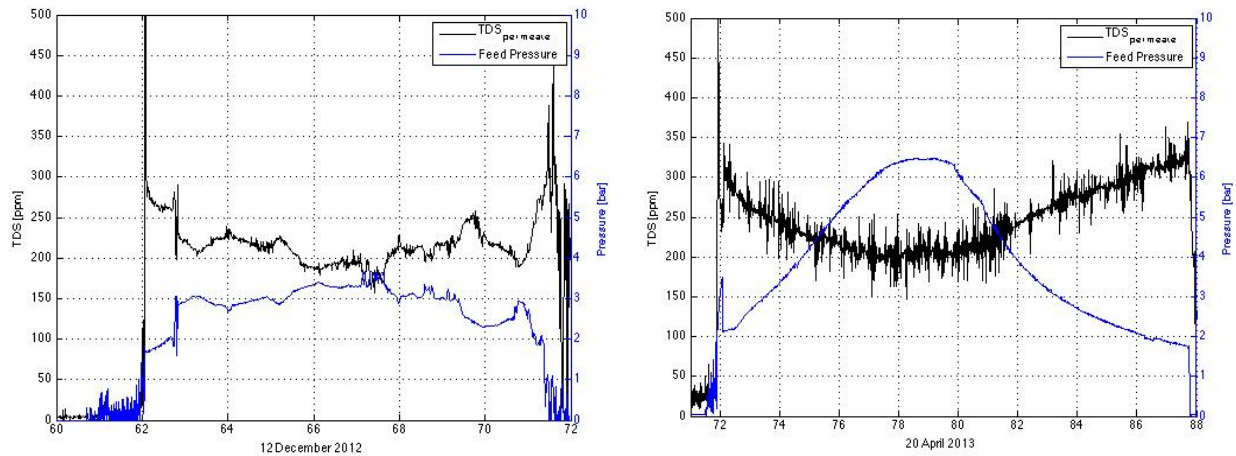


Figure 9.31: Feed pressure and permeate TDS for period 1 and period 2 (left and right respectively).

In the following chapter the results presented in this chapter will be discussed more thoroughly. The systems performance will be evaluated based on the expected behavior.

9.3.2.4. Permeate Flux (Surface Load)

The fluxes measured during the second period were almost half of those measured during the first period. This can be seen below in Figure 9.32.

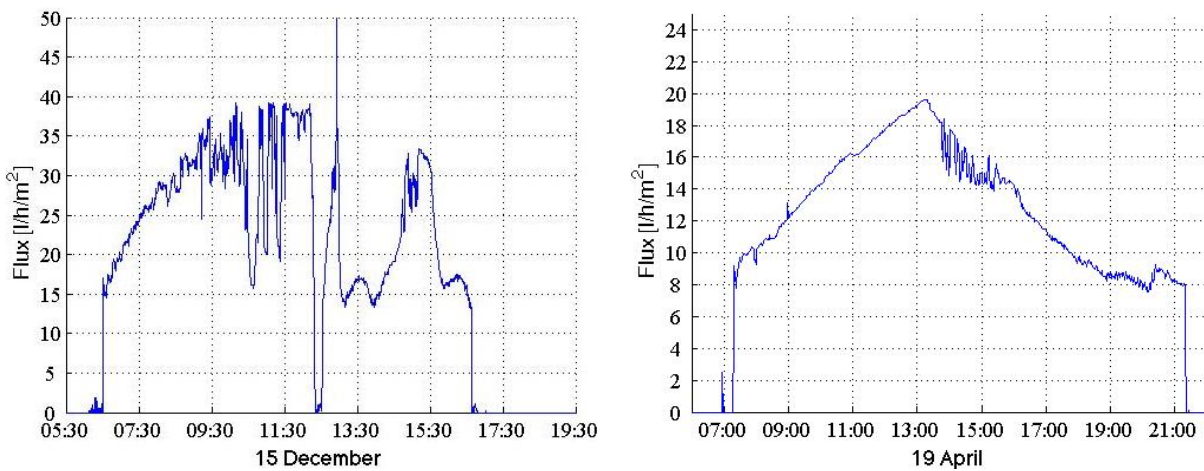


Figure 9.32: Permeate fluxes for two arbitrary days during test period 1 and test period 2 (left and right respectively).

What can be seen from the figure above is that the flux for the system including energy storage is less noisy. It can clearly be seen that it is significantly less influenced by the solar irradiance and hence the solar flow. This indicates that the energy storage successfully buffers energy throughout the day. However, the flux for the system with energy storage is significantly lower in comparison to the flux measured previously. A favorable flux is briefly experienced when the hydro-pneumatic tank is at its maximum storage capacity. A more detailed evaluation of the flux (mainly for the system including energy storage) can be found in section 10.4.3.

10. Discussion

Discussing the results and evaluating the performed and expected system performance is an important chapter. The first topic discussed in this chapter will be the measured daily irradiation and the irradiation used in initial estimation calculations.

10.1. Measured Solar Irradiation and Expected Solar Irradiation

Recall the solar data presented in chapter 3.6.2, based on the data measured an evaluation can be made to see whether the estimated daily solar radiation matches the measured solar radiation. The data presented earlier and the collected data during both test periods can be found below in Table 10.1.

Table 10.1: Average daily radiation according to literature and daily radiation measured.

	December	April
Rumbayan et. Al. [kWh/m ² /day]	4.76	4.95
NASA SSE [kWh/m²/day]	4.45	4.76
Measured [kWh/m²/day]	4.36	4.22

From the table above it can be seen that the measured radiation is slightly lower than the expected radiation. Since the NASA SSE data was used for initial performance calculations a comparison between the NASA SSE data and measured data will be made. For December it can be seen that the measured data was 0.09 [kWh/m²/day] less, while for April the measured data was 0.54 [kWh/m²/day] less. The lower daily irradiation measurements can be explained by the reasonably rainy month of April.

10.2. PV and Solar Pump Performance

As mentioned previously, the current produced by the PV modules could not be logged. This is very unfortunate, as an in depth analysis of the power produced by the PV module and the input to the solar pump/controller cannot be straightforwardly be performed. However, the PV power production (i.e. power and current) was logged previously in November 2012. This information was used to setup an evaluation scheme for the PV module performance. The solar pump/controller was evaluated using the actual power (measured) produced by the pump and comparing this to the expected pump performance and theoretically available solar energy/power. First, the PV module performance evaluation will be discussed.

10.2.1. PV Module Performance

Prior to the pipe failure in November 2012 it was possible to log both the voltage and current produced by the PV modules. Using this data a relation was setup for the correlation between the produced current, voltage and thus power at any given solar irradiation measured. The validity of the relation found for the produced voltage as function of the irradiation was checked with the measured voltage data measured in April 2013 and seemed acceptable. The theory behind this approach was that if the results of the equation matched the voltage pattern measured in April, that the relationship found for the current produced would also be valid. Hence the power output can be predicted using this information. After close evaluation, the equation explaining the correlation between the voltage and measured irradiance was found to be invalid, yielding 5 - 15% accuracy over the full irradiance range.

Fortunately the PV module performance was previously evaluated by Vollebregt and Feenstra (2012), assuming no degradation of the PV modules has taken place and that the additional modules (same brand, same model) have the same performance the solar pump and controller behavior will be evaluated using this relation between the irradiance and the power delivered by the PV modules.

10.2.2. Solar Pump & Controller Performance

Water is pumped at a certain flow and also under a certain pressure. As shown and discussed earlier, these two parameters were measured continuously and thus the pump performance can be evaluated using this information and the assumed PV power as described above. By using the equation below, the hydraulic power produced by the solar pump (including all the pipe losses prior to entering the ERPI) can be calculated as followed:

$$Power_{hydraulic} = p * Q \tag{10.1}$$

Where p is the pressure in [Pa] and Q is the flow of the water leaving the pump in [m^3/sec]. Using the 90-second average values and fitting a polynomial to the data generated the following chart.

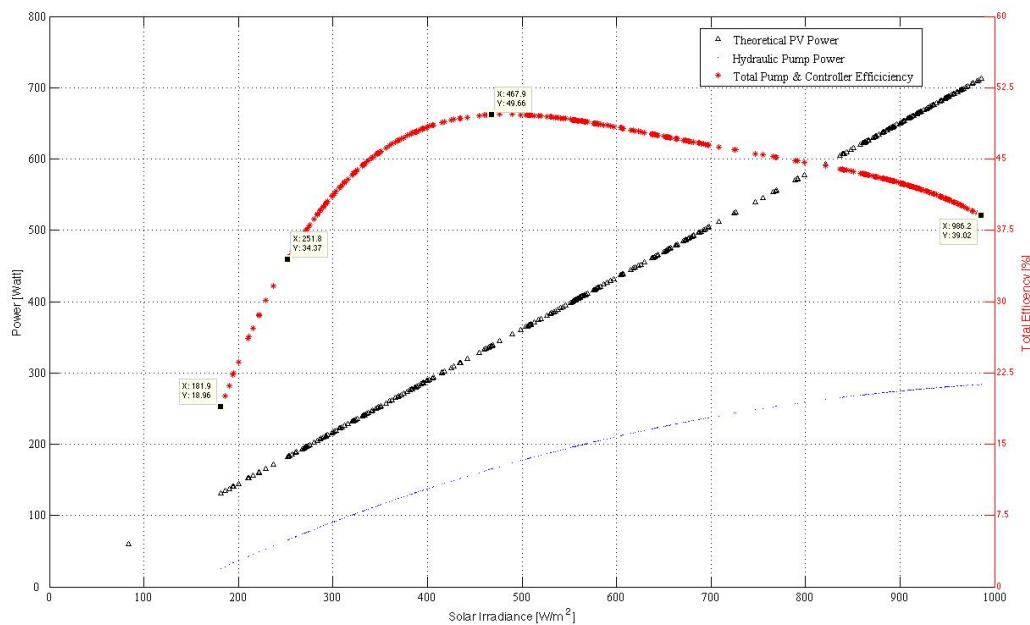


Figure 10.1: Total system efficiency, Hydraulic Power and Theoretical Power plotted versus the Solar Irradiance.

The figure above shows the total system efficiency, hydraulic power and theoretical power entering the solar controller. However, as indicated earlier the hydraulic power is measured just before entering the ERPI. Meaning that the hydraulic power is measured after all losses within the piping system have already occurred and also after all of the cable losses. The cable losses could not be evaluated due to the absence of the current clamp and the hydraulic losses could have been logged if pressure sensors were placed just at the pump exit. This means that the solar pump/controller efficiency cannot be thoroughly evaluated, however the efficiency shown above is still useful. This is the actual (total) efficiency of the complete system including all of the system losses (PV related losses, cable losses, pump & controller losses and hydraulic losses) up until entering the ERPI. It can be seen that at the lower irradiances the

total system efficiency is quite low (19%), while at higher irradiances the total system efficiency is approximately 39%. In optimum conditions, the total system efficiency reaches a maximum of 49.7%.

Using this information, one could calculate the losses and estimate the solar pump/controller efficiency. However, as the conclusion would be based on assumptions and as the pump/controller efficiency has already been previously evaluated, this has not been done. It can be noted however, that at first glance, it seems like the hydraulic power produce by the solar pump is lower then expected. The most probable causes and losses have already been previously discussed (hydraulic losses, cable losses, PV related losses). From the data it can be concluded that from an irradiance of approximately 250 [W/m²] and a PV power output of approximately 170 [W] the system shows an efficiency curve that is comparable to the expected performance shown in Figure 8.1. The maximum pump/controller efficiency was specified to be 56% while the overall maximum efficiency measured was 49.7%. This reduction in efficiency can be contributed to the hydraulic losses and cable losses.

While the information presented in this section is useful to evaluate the system behavior, it should be noted that a more thorough analysis of the solar pump/controller under these variable flow and pressure conditions would be useful in order to gain a better understanding of the system behavior. Previously the operating conditions were semi-stationary, resulting in “cleaner” data and easier to comprehend pump behavior curves. Due to the absence of some key sensors, some of these pump curves could not be generated. However, the insights gained into the behavior of the hydro-pneumatic tank are the most important and hence for the remainder of this report, the full focus shall be shifted to the desalination part of the system and the hydro-pneumatic energy storage device. A more elaborate discussion on possible improvements and useful additional test measurements will be presented in the final chapter of this report.

10.3. Desalination Part

10.3.1. RO Membrane Performance

The RO performance can be easily evaluated using the RO modeling software called SIRIO, developed by OLTREMARE (2013). In order to validate the 4040 membrane, the average values presented in Table 9.3 will be used. The SIRIO software requires an input for the feed water TDS, permeate flow rate, recovery rate, water temperature and the type of membrane used. Below in Table 10.2 the SIRIO values can be seen, next to the actual measured values.

Table 10.2: Expected and measured RO performance

	Sirio Values, Designed Capacity	SIRIO Values, Adjusted Capacity	Measured Values
Feed Pressure (RO pressure) [bar]	7	5.71	6.0
Feed flow rate [l/min]	15.0	11.7	11.7
Permeate Flux [l/m ² /h]	17.13	10.47	10.5
Permeate TDS [ppm]	167.7	251.7	257

From the table it becomes clear that the RO performed exactly as expected. For this part of the installation there were no unexpected observations made.

10.3.2. ERPI Performance

The ERPI performance can be compared to the data obtained previously by (Vollebregt & Feenstra, 2012). What can be discussed about the ERPI without looking at any charts is the stalling behavior reported by Vollebregt and Feenstra (2012). In their report the authors discussed the ERPI stalling on several occasions. During both test periods (configuration with energy storage and configuration without energy storage), it did not occur once that the ERPI had stalled. Possibly the higher and fluctuating operating pressures prevented the ERPI of stalling.

Below in Figure 10.2 the ERPI performance data are plotted. The feed and RO pressure data have been analyzed and averaged in order to find the friction losses within the ERPI. Below in Figure 10.2 the friction losses measured for the system in Jakarta has been plotted together with the friction losses measured in Bali (Vollebregt & Feenstra, 2012) and also with the theoretical friction losses.

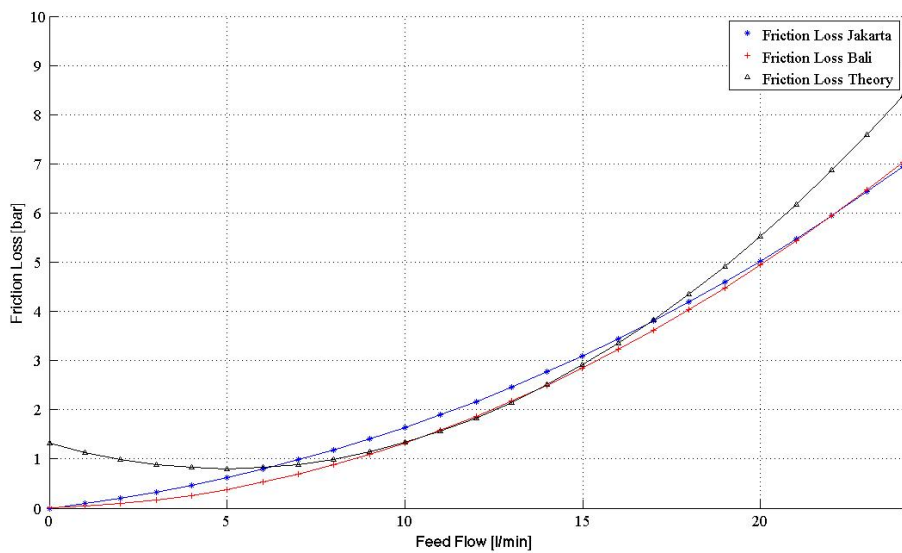


Figure 10.2: ERPI Friction Losses.

It can be seen that the friction losses measured in Jakarta are similar to those measured in Bali and also the theoretical values. The friction losses depicted in the figure above were determined using 90-second average values, the third degree polynomial describing the friction losses measured in Jakarta can be seen below:

$$\Delta P_{frictionlosses,measured} = 0.0001x^3 + 0.0068x^2 + 0.0911x - 0.0045$$

Where $\Delta P_{frictionlosses,measured}$ represents the friction losses in [bar] and x represents the feed flow rate in [l/min]. It can be seen that the outer regions (smaller and larger flows) of the data obtained in Jakarta show differences when compared to the previous data. If a polynomial of larger degree were to be used to fit the data, these differences could possibly be reduced. As the main focus of this project lies within the hydro-pneumatic energy storage, the ERPI performance was not evaluated further. In the following section the results regarding the hydro-pneumatic storage vessel (energy storage) will be elaborately discussed.

10.4. Hydro-Pneumatic Storage Pressure Performance

As mentioned above, the hydro-pneumatic energy storage was the big challenge during this project. It was not well known before the experiments were performed, how the vessel would influence the systems behavior. The basic principle is well known and understood. The vessel is filled with pre-pressurized air, as water enters the vessel the air is compressed and according to Boyles Law (Wikipedia, 2013) the relationship between volume and pressure inside the vessel can be described by:

$$p_1 * V_1 = p_2 * V_2 \quad (6.4)$$

However, during the design phase of this project there were several assumptions made that should be re-evaluated at this point. Recall the two assumptions made earlier in chapter 6.2:

- Air and water do not interact with each other within the pressure vessel.
- There is no (thermal) interaction between the air and water inside the pressure vessel and the surrounding environment.

These assumptions were made in order to make the initial estimation easier. However, in practice these assumptions are not valid. With the help of the data acquired, it will be shown to what extent these events took place during the second test period.

10.4.1. Interaction Between Water and Air Inside the Pressure Vessel

As explained in chapter 5.2.2, air will dissolve into water when the two media are in direct contact. The amount of air that dissolves into water increases as the pressures and also temperature goes up. Also the surface area of the contact between air and water influences the rate at which air dissolves into water.

Recall Figure 9.25 and Table 9.6, these two can be used to show that there was definitely some interaction between water and air inside the pressure vessel (air dissolving into water). The table is presented below again in order to aid in the explanation.

Table 10.3: Pressure Loss inside the Storage Vessel

Energy Storage, Pressure Loss Info	Pressure at 1590 Liter	Pressure Change [bar]
Day 1	3.05	
Day 2	2.89	-0.16
Day 3	2.61	-0.28
Day 4	2.32	-0.29
Day 5	1.97	-0.35
Day 6	2.03	+0.06
Day 7	1.79	-0.24

An arbitrary volume inside the pressure was chosen in order to illustrate the phenomenon of air dissolving in water. The principle behind this theory is that if the circumstances were ideal, and there was no interaction between the air and water inside the vessel. Then the pressure at the arbitrary

volume should be the equal when measured on the first day up until the last day. Of course when working with air under pressure, there are bound to be minor leakages in the system, but these should be negligible in comparison to the pressure loss due to the interaction described above. From the table it can be seen that the pressure was monitored when the water volume inside the pressure vessel was approximately 1590 [liter]. It can be seen that everyday the pressure dropped with exception of the measurement taken on April 22nd (day 6). A slight increase in pressure was measured, this is very unlikely and can be explained by the moment of the sample point. At the exact point of the sample, the system was idle. The valve between the energy storage and the system was shut, this means that the pressure inside the piping system was idle and this most likely explains the slight increase in pressure. Overall however, it can be seen that there was a total pressure loss of 1.26 [bar].

The fact that there was thermal interaction between the media inside the tank and the surrounding area can be explained by the temperature profile measured. First of all the average temperature of 35 [° C] is quite high. As already mentioned this is an increase of 3.4 [° C] when compared to the initial test period. The solar radiation received was similar for both period and during the second period the feed reservoir was doubled with respect to the first period. So the increase in temperature cannot be explained by the pump running at a higher rotational speed, but only by the presence of the energy storage. If we recall the temperature plot presented in Figure 9.21, it can be seen that the water temperature dropped quite significantly during the night of 21 April. This can be explained by very heavy rainfall during the night. It can also be seen that April 22nd was the least sunny day of test period two. From Figure 9.14 shows that a total of 1.43 [kWh/m²] of solar energy was received on April 22nd. This also explains why the water was not re-heated to like all of the other days. This shows that also the assumption of no thermal interaction between the medium inside the energy storage and the surrounding environment is not valid.

It should be noted that that hydro-pneumatic energy storage was placed vertically instead of horizontally. The main reason was the absence of funds to rent a crane to position the tank vertically. The fact that the tank was placed horizontally increased the effective surface area of the vessel facilitating the absorption of heat during the day. The horizontal placement also caused for the contact area inside the pressure vessel between the water and air to be significantly larger. If the tank was placed vertically, the pressure loss would most likely have been less due to the smaller contact area (between water and air) and less heat absorption.

10.4.2. Buffering Capacity

In this section the system's buffering capacity will be discussed. When discussing the buffering capacity, it is referred to the ability of the system to compensate for short periods of no sun. In other words, in moments of overpassing clouds and/or short periods of rainfall during the day the system should still produce drinking water at a constant rate and quality. Figure 10.3 shows the feed- & solar flow and solar irradiance in the top left section. A close up of the feed-, solar- and storage flows in the top right section, a close-up of the storage volume & pressure in the bottom section and a close-up of the feed flow and permeate TDS. 18 April was chosen as sample data, because this was one of the days with the least amount of solar energy received. On 18 April it can be seen that the pump shutdown shortly between 12:00 and 13:00 due to a rain shower. This is a perfect example of the systems buffering

capacity, it can be seen that even though the solar flow is zero that the storage flow takes over. During this period of the pump switching of and the energy storage taking over, the feed flow remains does not fluctuate. It can also be seen from the bottom section that also the pressure entering the system does not fluctuate. This “non-fluctuating” behavior ensures permeate production of constant quality.

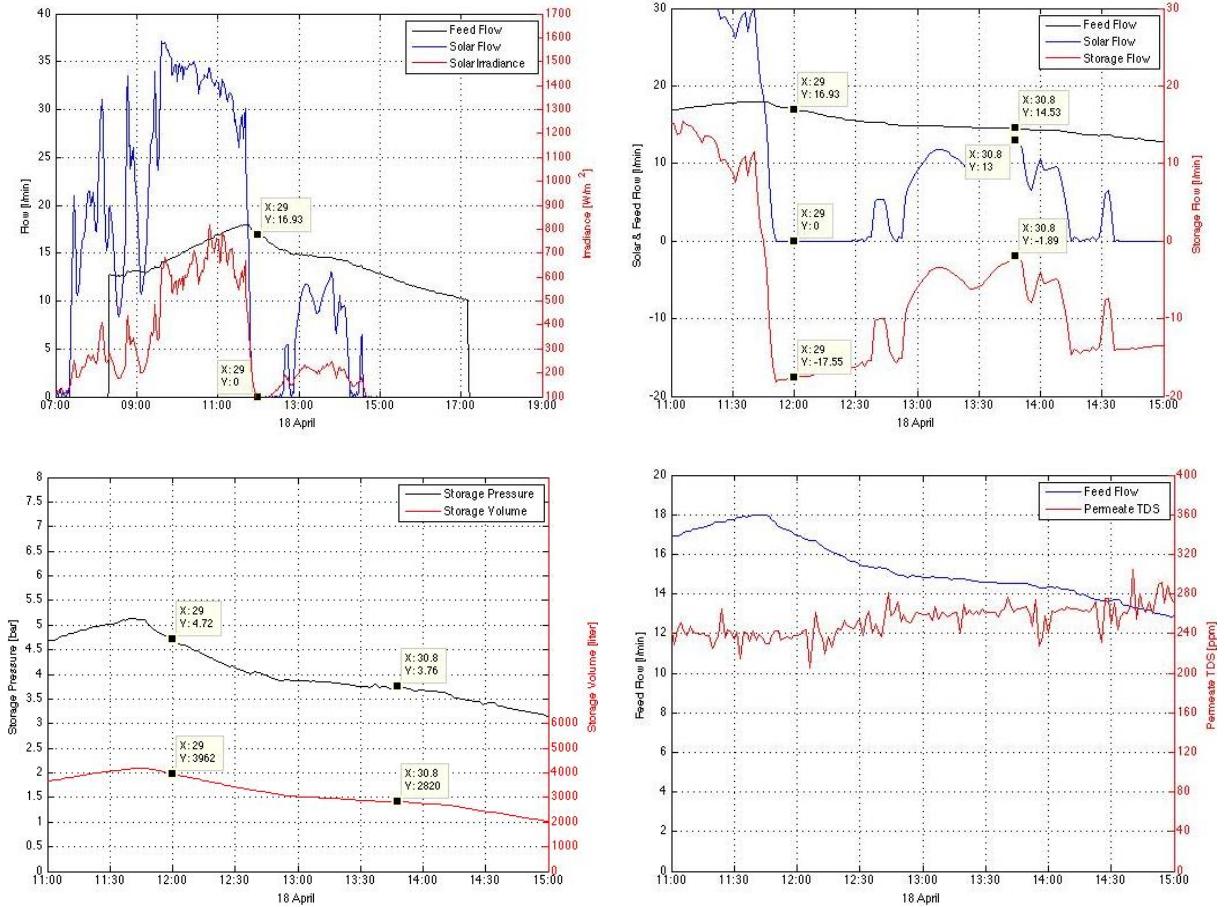


Figure 10.3: Illustrating the systems buffering capacity.

In the following section the permeate flux will be discussed.

10.4.3. Permeate Flux (Surface Load)

In this section a detailed discussion of the permeate flux, the influence that it has on the system behavior and which parameters could be adjusted in order to (positively) affect the flux. First of all let’s shorty introduce the permeate flux. It is also known as the surface load but often just referred to as the “flux” and is given in $[l/m^2 \cdot h]$. The symbol most commonly used is J_w and the flux is simply the permeate flow through one square meter of membrane surface area (van Dijk et al., 2009). This means that the higher the flux, the higher the permeate flow rate. However the flux is limited by fouling and concentration polarization. Typically an ideal flux of approximately $20 [l/m^2 \cdot h]$ is used, as the unwanted effects of fouling and concentration polarization increase at higher flux values.

As it can be seen from the data presented the flux measured during this research were not at levels at which these concerns arise. However, the flux measured for the configuration with energy storage was lower than expected. The most predominant parameter influencing the flux is the feed pressure. Increasing the feed pressure results in a higher flow rate required by the membrane and consequently a linear increase in the flux. Besides the pressure another parameter affecting the flux is the feed temperature, the theory suggests a flux increase of 3% per °C. However, the feed temperature also affects the water permeability, i.e. the less minerals are rejected and consequently (if the pressure is kept constant) permeate of lesser quality is produced. Hence the feed pressure is the most common parameter played with if a higher flux is required.

The average operating pressure for this system depended of the starting pressure inside the hydro-pneumatic tank. The solar pump determines the maximum operating pressure, it can deliver a maximum head of 80 [m] which can be translated to a pressure of 8 [bar]. The starting pressure inside the energy storage vessel was 2.85 [bar] and at the end of the week the starting pressure was 1.67 [bar], with the exception of 18 April the daily starting pressure gradually decreased as the week progressed. This daily starting pressure, average daily flux, average daily solar radiation received and the daily system runtime are shown below in Table 10.4.

Table 10.4: Daily starting pressure, average daily flux, average daily solar radiation, and daily runtime for period2.

	17 April	18 April	19 April	20 April	21 April	22 April	23 April
Starting Pressure [bar]	2.85	3.09	2.57	2.14	1.87	1.86	1.67
Average Daily Flux [$l/m^2 \cdot h$]	11.2	9.8	12.4	13	11.8	5.6	9.6
Average Daily Radiation [$kWh/m^2/day$]	5.62	2.46	4.98	6.14	4.68	1.43	4.11
Daily Runtime [hours]	17.11	10.52	14.63	16.28	16.29	14.96	19.99

After installing the energy storage the system runtime was increased from 42.3% to 65.3%. This is a significant increase. Naturally the system was designed to run continuously through the night, unfortunately obtaining a larger energy storage vessel proved to be to big of a challenge with regard to the project duration and project budget. However, the information acquired regarding this type of energy storage is extremely interesting, as no other research has previously used this type of system configuration.

Overall, it became clear that for a location such as Jakarta the energy storage is required to provide energy for a minimum 14 hours. This indicates that approximately double the current storage capacity is required for continuous operation (under similar conditions). However, from Table 10.4 it can be seen that on April 23rd the system ran just shy of 20 hours, while the average solar radiation received was not larger than usual. This indicates that the starting pressure inside the storage vessel can also influence the system runtime. Of course the lower operating pressures also affects the produced water quality and the flux. This shows that there is room for further research with regard to the influence of the starting pressure on the system runtime

It's difficult to draw conclusions from the information obtained, as the data collected is rather limited and none of the days show similar circumstances. However, one could suggest that by increasing the starting pressure inside the energy storage vessel the daily flux will most likely increase. A higher starting pressure suggests that the pump will work in upper sections of the H-Q curve, i.e. the pump will deliver a smaller flow. However, due to the higher pressure the flux will automatically increase. Finding the optimum starting pressure in the delicate balance of flux increase and sufficient energy being stored is the challenge for the future. Increasing the starting pressure by too much will result in a smaller window of operation, as the pump could possibly not meet the flow capacities required to feed both the desalination part and fill the energy storage simultaneously. Also by increasing the starting pressure, the available storage volume is reduced. In order to try to find the optimum parameters for the continuous operation of the installation as originally intended the data obtained has been used to adapt the system model. By playing with the hydro-pneumatic vessel volume and the initial pressure inside the vessel an attempt is made to find the optimum operating conditions. I.e. conditions where the flux is favorable, permeate quality is acceptable and the system is operated continuously. Some sample plots of the criteria described above can be seen below in Figure 10.4. Using the information from the plots it is shown what the possible influence could be if the start pressure inside the vessel were to be increased to 4.25 [bar].

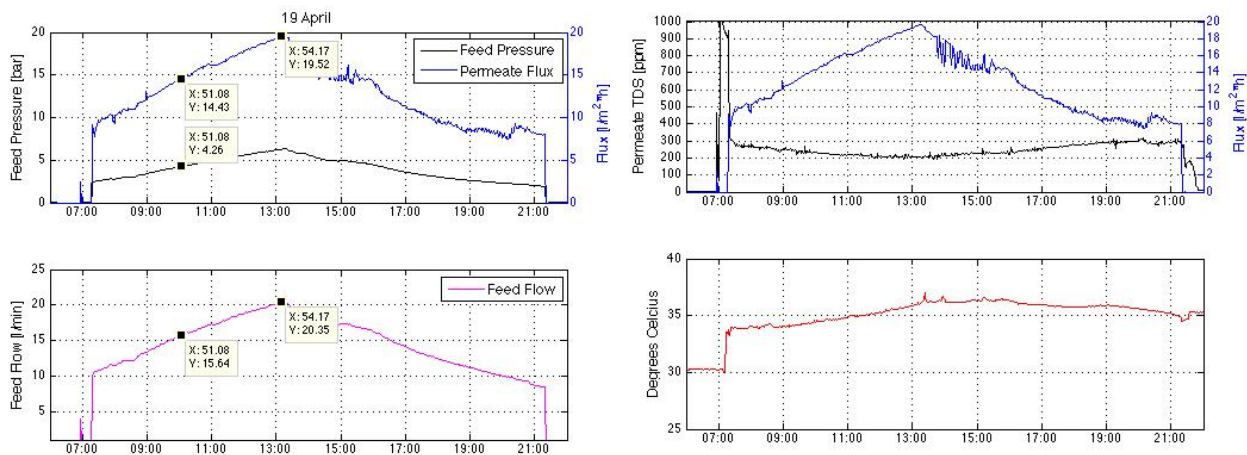


Figure 10.4: Sample plots to show the influence of initial pressure increase.

These plots are presented in order to aid as visual support in the sample calculation of the effect of increasing the starting pressure inside the hydro-pneumatic tank. Some data markers have been added, they illustrate the flux, flow and pressure at certain points during the day. Scaling up the system or adjusting some parameters can now be performed relatively easy, as the system is now better understood. Sample calculations were performed in order to illustrate the effect of increasing the initial pressure and the consequently required storage capacity to run the system continuously for 24 hours a day. Also the estimated resulting average flux is calculated, the results are shown in Table 10.5. Before advancing to the results of the sample calculations lets discuss the effect that the daily temperature increase has on the flux and the permeate TDS. Figure 10.4 confirms the theory discussed earlier that the permeate flux is predominately influenced by the feed pressure. It can also be seen that the

temperature increase on April 19th was roughly 2.7 [°C] barely has any influence on the permeate TDS. Thus it can be concluded that the temperature increase observed daily is not of great relevance.

Table 10.5: Some initial sample calculations to illustrate effect of increasing the starting pressure inside the vessel.

Start Pressure [bar]	Water Stored [liter]	Avg. Flow Rate [l/min]	Avg. Flux [l/m²*h]	Storage Multiplication factor for 24 hour production [-]
4	3857	17.7	16.7	3.85
3.5	4500	17.0	16.0	3.17
3	5143	16.3	15.2	2.66
2.5	5786	15.5	13.9	2.25
2.39	5927	15.2	14.4	2.15

The sample calculations show that increasing the initial pressure will also increase the permeate flux. However, as mentioned earlier, the available water storage capacity is also reduced. The art is to find the optimal conditions within this delicate equilibrium. This could be done by using the data presented and developing a model based on the acquired information. In the conclusion and recommendations section of this report, this topic will be addressed. Now that the results have been presented and thoroughly discussed, let's evaluate the system in terms of price per unit of drinking water produced and specific energy content.

11. System Evaluation

Now that the results have been discussed, the system evaluation can be performed. In this chapter an evaluation in terms of price per m³ of water and the specific energy content (SEC) will be performed, for the installed system and a configuration with a scaled-up energy storage vessel. Scaling up of the system will be performed using the actual data, as the data is more reliable in comparison to the sample calculations shown above. Also a normalized comparison will be made between the system with and without energy storage. To wrap up the chapter, the calculated drinking water prices will be compared to other RES-RO systems. It should be noted that VAT and transportation- and labor costs are not included in the following cost calculations. Also a RO life of 2 years is assumed (life should be longer in practice) and the pre-filter are assumed to have a life of 1 month. The depreciation times used for the calculations were either taken from the report of Vollebregt and Feenstra (2012) or estimated using information found in Moel, Verberk, and Dijk (2006).

11.1. System Without Energy Storage

11.1.1. Economical Evaluation

In this section the system will be evaluated based on the price per unit water produced. Typically PV-RO systems are evaluated by calculating the price per cubic meter of water produced (i.e. [€/m³]). The most popular and straightforward method of doing this is the “Equivalent Annual Cost” (EAC) method. In order to use this method, some basic requirements should be met. The equivalent annual costs method requires:

- A discount/interest rate **before** the analysis is started
- Estimate of the time period(s) involved

An interest rate of 3.75% was chosen, the interest rate is based on data collected on (MarketWatch, 2013). For the evaluation of the system, the system is assumed to hold no salvage value at the end of its life. The depreciation times (time period estimations) and system component costs can be found in Table 11.3. All of the figures filled in the table above are based on actual expenditures except for the annual operating costs for: chemicals, labor and maintenance & spare parts. It is difficult to obtain hard data for these three types of operating costs, hence the values used for the cost calculation are based on data found in (Al-Karaghoul, Renne, & Kazmerski, 2009; El-Ghonemy, 2013b). The papers discussed typical cost distribution of renewable powered RO systems, and according to the literature: the chemical, labor and maintenance costs account for 7%, 9% and 14% respectively of the capital costs.

The challenge however is to setup a fair basis in order to be able to perform a comparison between the different system configurations. This is required in order to present a fair comparison, because based on the results present in chapter 9.1 it can clearly be stated that the system was over-scaled and not performing optimally. The installed PV capacity was too large and thus reducing the installed PV capacity would reduce the capital costs and hence also the price per cubic meter of water produced. The optimized cost calculation for the system without energy storage (evaluated in test period 1) can be found below in Table 11.1.

Table 11.1: Costs for the System without Storage.

Item	Capital Costs [Euro]	Depreciation Time [Years]
PV Modules	587.5	25
PV Mounting System	22	25
Solar Pump & Controller	1750	10
Solar Pump Well Probe	75	10
ERPI	3200	10
Indication Sensors	300	10
Pre-filter Housing	50	20
Permeate Storage Vessel	624	10
30-Meter Shallow Well	468	50
PVC Tubing	110	40
PVC Connectors and Accessories	97	40
Electric Cabling and Safety Sling	234	10
Total Capital Costs	8713	
	Annual Operational Costs [Euro]	# Of Annual Replacements
RO Membranes	105	0.5
Filter Cartridges	120	24
Chemicals	71	-
Labor	79	-
Maintenance and Spare Parts	71	-
Total Annual Operational Costs	820	
	446	

The cost of the PV modules has been optimized/adjusted due to the lower capacity required (4 modules, totaling a capacity of just under 400 W_p). Also the amount of PVC tubing and required permeate storage vessel have been adjusted. The system costs presented above have been translated to yearly figures using the EAC method. The final results for the economic evaluation can be found in Table 11.2.

Table 11.2: Economic evaluation, system without energy storage.

Cost Calculation	
Equivalent Annual Costs	785 [€]
Annual Operational Costs	445 [€]
Total Annual Cost	1230 [€]
Yearly Produced Permeate	203 [m ³]
Price Per Cubic Meter of Water Produced	6.05 [€/m³]

The price calculated for the system without energy storage was 6.05 [€/m³]. This price is significantly higher than the price achieved by Vollebregt and Feenstra (2012). This already indicates that the lower the system capacity, the less cost attractive the system will be, especially when an energy recovery device is incorporated into the design. At these lower capacities, an energy recovery device weighs in significantly on the produced water price. Let's have a look at the SEC of the system described above.

11.1.2. Specific Energy Content

The SEC can be seen as the figure of merit for clean water production. It is defined as the amount of units of drinking water that can be produced for each unit of energy consumed. The most common unit used for the SEC is [kWh/m³] (Richards & Schäfer, 2010). Typically the SEC for BWRO can be divided in two categories, namely the SEC for systems without energy recovery and the SEC for systems including energy recovery. And while the SEC values found for solar driven BWRO varied significantly, the latest developments suggest that the SEC for systems without energy recovery range from 1.5 – 4 [kWh/m³] and for systems including energy recover the SEC typically ranges from 1-3 [kWh/m³] (Bilton, Wiesman, Arif, Zubair, & Dubowsky, 2011).

The SEC for the systems evaluated in this project were evaluated using the daily average solar radiation received and the average amount of permeate produced daily. Multiplying the daily solar radiation with the total PV surface area and the PV module efficiency, the theoretically available solar energy can be found. Dividing the average available energy by the average daily permeate produced yields the systems SEC.

For the system without energy storage a SEC of 1.82 [kWh/m³] was found for the desalination of feed water with an average TDS of 6670 [ppm]. When compared to the typical SEC values discussed above, the system's SEC is quite reasonable. In the following section the configuration with a 9 [m³] hydro-pneumatic energy storage vessel will be evaluated.

11.2. System with Hydro-pneumatic Energy Storage

11.2.1. Economical Evaluation

In a similar fashion as done for the previous system setup, a cost and SEC evaluation will be performed for the system without energy storage. The same EAC method described in the previous section was used to translated the Capital costs to EAC values and calculate the total annual costs. The capital and annual operational costs for the installed system with hydro-pneumatic energy storage can be found below in Table 11.3.

Table 11.3: Cost of the installed system.

Item	Capital Costs [Euro]	Depreciation Time [Years]
PV Modules	1762.5	25
PV Mounting System	43.39	25
Solar Pump & Controller	1750	10
Solar Pump Well Probe	75	10
ERPI	3200	10
Indication Sensors	300	10
Pre-filter Housing	50	20
Hydro-Pneumatic Storage Vessel	5980	25
Permeate Storage Vessel	624	10
30-Meter Shallow Well	468	50
PVC Tubing	110	40

PVC Connectors and Accessories	96.99	40
Electric Cabling and Safety Sling	234	10
Total Capital Costs	14693	
	Annual Operational Costs [Euro]	# Of Annual Replacements
RO Membranes	150	0.5
Filter Cartridges	120	24
Chemicals	89	-
Labor	115	-
Maintenance and Spare Parts	178	-
Total Annual Operational Costs	652	

Now that all of the contributing cost factors have been identified, the “equivalent annual cost” can be calculated. It should be noted that the calculations were performed, based on a 95% availability of the measured run-times. All of the key figures and the eventual price per cubic meter of produced water are presented in Table 11.4.

Table 11.4: Economic Evaluation Installed System (with storage).

Cost Calculation	
Equivalent Annual Costs	1273 [€]
Annual Operational Costs	652 [€]
Total Annual Cost	1925 [€]
Yearly Produced Permeate	455 [m ³]
Price Per Cubic Meter of Water Produced	4.23 [€/m³]

For the installed and evaluated system a price of 4.23 [€/m³] was found, this price does not include the VAT, transportation costs and installation costs. These factors will not be further discussed in this evaluation. In order to give an idea of the cost distribution of the system Figure 11.1 is presented below, the figure presents the cost distribution of the installed system.

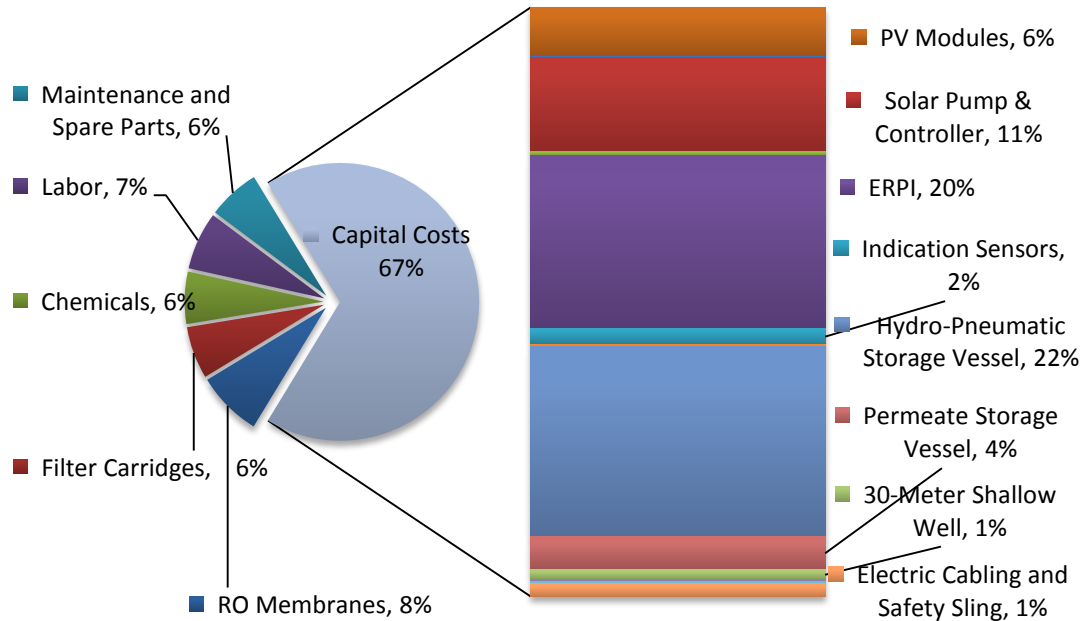


Figure 11.1: Cost Distribution of the installed system.

Even though the costs per system are very depended of the location, the local solar climate and the feed water quality amongst things it is nice to evaluate the system cost distribution. Al-Karaghoul et al. (2009) presented some data on the typical cost distribution for RO systems, the information can be found in Table 11.5. When comparing the cost distribution of the system installed in Jakarta and the data shown in Table 11.5, it can be said that the figures are fairly similar. For the Jakarta system with energy storage the capital costs accounted for 67% of the total costs and the operational costs accounted for 33% of the total cost (according to the literature 30-90% and 10-30% respectively). It can also be seen that for conventional RO systems the RO membrane costs account for 14% to the total costs, while in the Jakarta system the membrane costs account for 8% of the total costs. Let's have a look at the SEC for the installed system (with energy storage).

Table 11.5: Cost distribution for conventional- and renewable powered RO systems.

Conventional RO Systems	Percentage of Total Costs [%]
Capital Costs	31
Energy Costs	26
Maintenance & Repair Costs	14
Membrane Replacement Costs	13
Labor Costs	9
Chemical Costs	7
Renewable Powered RO System	
Capital Costs	30 - 90
Operational Costs	10 – 30
Energy Costs	0 - 10

11.2.2. Specific Energy Content

Similarly as done for the previous system, the SEC of the configuration as installed and tested was evaluated. A SEC of 2.50 [kWh/m³] was found for feed water with an average TDS of 5754 [ppm], this value is slightly higher when compared to the SEC found for the previous configuration. The higher SEC can be explained by the amount of PV modules installed. The system as installed and evaluated did not make full use of the installed PV capacity, as the energy storage was not sufficient to produce water all through the night. The system could be optimized in terms of available energy storage capacity, this would most likely reduce the price of the water produced and also reduce the SEC. An evaluation of the system with optimized energy storage capacity will be discussed in the following section.

11.3. System with Scaled-up Hydro-pneumatic Energy Storage

As discussed earlier in this report, the system was originally designed for continuous operation. In other words the system was designed to run 24 hours a day. Unfortunately it was not possible to find a hydro-pneumatic storage vessel with the required capacity. However, useful information was gathered and can be used to predict the systems behavior and also estimate the required capacity for continuous operation. In the following section the economical evaluation for the system with the required storage capacity for continuous operation will be performed.

11.3.1. Economical Evaluation

In order to perform the economical evaluation, the information from Table 9.8 can be used. Based on the average daily produced permeate and the average daily runtime, the required additional storage capacity can be estimated. The average required additional runtime is calculated as followed:

$$T_{required,average} = 24 - T_{runtime,average} = 24 - 25.6 = 8.4 \text{ [hours]}$$

Now using the average feed flow rate, the estimated additionally required storage capacity is calculated to be:

$$V_{required,average} = Q_{feed,average} * T_{required,average} \approx 5900 \text{ [m}^3\text{]}$$

The storage capacity described above is the actual water storage required. Based on data obtained, it can be said that for the required storage capacity the current capacity should be doubled. For this cost evaluation simply the price of two identical hydro-pneumatic energy storage vessels will be used. In practice a larger vessel or some other creative solution should be able to yield in lower capital costs for the hydro-pneumatic energy storage vessel. It should also be evaluated whether the pump can deliver the required amount of water to fill the energy storage vessel daily. Based on previous energy calculations and also on the average pressure obtained from the measurements in Jakarta and using the average pressure and daily solar flow observed by Vollebregt and Feenstra (2012), the configuration with 12 Sundaya PV modules and the Lorentz PS1200-HR14 should meet the daily pumping requirements. The capital and annual operational costs, followed by the EAC and total annual costs can be found below in Table 11.6 and Table 11.7 respectively.

Table 11.6: Capital and operational costs for the system with adjusted energy storage capacity.

Item	Capital Costs [Euro]	Depreciation Time [Years]
PV Modules	1762.5	25
PV Mounting System	43.39	25
Solar Pump & Controller	1750	10
Solar Pump Well Probe	75	10
ERPI	3200	10
Indication Sensors	300	10
Pre-filter Housing	50	20
Hydro-Pneumatic Storage Vessel	11960	25
Permeate Storage Vessel	624	10
30-Meter Shallow Well	468	50
PVC Tubing	110	40
PVC Connectors and Accessories	96.99	40
Electric Cabling and Safety Sling	234	10
Total Capital Costs	20673	
	Annual Operational Costs [Euro]	# Of Annual Replacements
RO Membranes	150	0.5
Filter Cartridges	120	24
Chemicals	115	-
Labor	148	-
Maintenance and Spare Parts	230	-
Total Annual Operational Costs	764	

Table 11.7: EAC and total annual costs for the system with adjusted energy storage capacity.

Cost Calculation	
Equivalent Annual Costs	1646 [€]
Annual Operational Costs	764 [€]
Total Annual Cost	2409 [€]
Yearly Produced Permeate	695 [m ³]
Price Per Cubic Meter of Water Produced	3.47 [€/m³]

It can be seen that for the system with adjusted energy storage capacity the capital costs have increased to 20673 [€] and the produced water price reduces to 3.47 [€/m³] of permeate produced. Before continuing to the conclusion and recommendations, let's have a look at the SEC for the system with adjusted energy storage capacity.

11.3.2. Specific Energy Content

The cost evaluation shows that the price of the water produced has reduced for the system with optimized energy storage capacity. This indicates that also the SEC will be reduced for this optimized configuration. Similarly to the evaluations performed for the previous two configurations, the SEC was evaluated for this optimized system. The evaluation yielded a SEC of 1.64 [kWh/m³]. This is the lowest

SEC of the three systems evaluated in this report. Also when compared to other SEC's found for typical BWRO configurations (discussed previously), this value could be considered as competitive.

Before continuing to the conclusions and recommendations, a tabular summary of the cost and SEC evaluations performed in this report.

11.4. Summary of System Evaluation

Below in Table 11.8 a tabular summary of the economical and SEC evaluation can be found.

Table 11.8: Tabular summary of the economical and SEC evaluation for the configurations evaluated in this report..

	Configuration without energy storage	Configuration with 9 [m³] hydro-pneumatic energy storage	Configuration with optimized energy storage
Water Cost [€/m ³]	6,05	4,23	3,47
SEC [kWh/m ³]	1,82	2,5	1,64

It can be seen that the configuration without energy storage produces water at a relatively high cost per cubic meter when compared to all of the other configurations. This is in part due to the solar pump and controller that aren't optimal for the capacity of the system. However, as mentioned in the economical evaluation all PS1200 Lorentz solar pumps (different capacities and heads) cost equal. The main factors contributing to the high costs are the cost of the ERPI and also the produced permeate per day. The results show that an energy storage device significantly increases the daily capacity and the benefits strongly outweigh the additional required investment costs. It should also be noted that the addition of the energy storage will most likely positively affect the membrane life and thus also the yearly operational and maintenance costs.

When comparing the system installed and evaluated in Jakarta to the optimized system with increased energy storage capacity, it can be seen that both the cost of the produced water and the SEC are reduced. This shows that even though the investment costs for the hydro-pneumatic energy storage vessel are large, the benefits of the additional storage are significant. It should also be noted that it should be possible to find a cheaper solution for the hydro-pneumatic storage vessel. Especially in countries such as Indonesia, where labor is cheap and regulations are less intense. However, when working with water and/or air under pressure, one should always exercise utmost caution and safety should not be neglected.

Now that all of the results have been presented and discussed, and that the different configurations have been evaluated, let's move on to the final part of this report. In the final chapter, conclusions will be drawn and possible improvements and recommendations will be discussed.

12. Conclusions & Recommendations

In the conclusions it will be evaluated whether the objectives mentioned in the introduction were met. Further more, the experienced gained will be used to setup a list of recommendations and possible improvements for future project in this field of work.

12.1. Conclusions

The objective set at the start of this project was to design, implement and evaluate a BWRO pilot plant powered solely by renewables. The intention was for the pilot to be continuously operated by means of a battery-free energy storage solution. The collected data was to be used in order to evaluate the system behavior and it's feasibility.

After addressing the global fresh water scarcity and the saltwater intrusion in north Jakarta's aquifers, several renewable powered RO solutions were described. Using the knowledge gained from the literature research and the results obtained previously in Bali, the new system concept was worked out. The previous pressurized water storage concept proved to be difficult to implement in Jakarta during this project. A novel energy storage concept where storage of pressurized feed water in a hydro-pneumatic storage vessel was chosen. The wind climate in Jakarta was judged to be unfavorable and thus PV modules were chosen as renewable energy source. The energy requirements were evaluated and the system scale-up calculations determined the required additional equipment and investment.

The pilot plant was then setup in North Jakarta and two separate evaluation periods were completed. The first consisted of a system with energy recovery and no energy storage, while during the second period the originally designed system with hydro-pneumatic energy storage was evaluated. Such a BWRO system with hydro-pneumatic energy storage hasn't been previously developed and thus detailed predictions of the system proved to be a challenge.

After completion of the second test period, the data was analyzed back in Delft and the system behavior and key system components were thoroughly analyzed. The data obtained was compared to the predicted behavior and some components were compared to data obtained of projects closely related to this one.

In conclusion the concept of using a hydro-pneumatic storage vessel for upstream feed water storage as opposed to downstream drinking water storage proved to be a viable solution. A tabular summary of the results obtained is shown once again in Table 12.1.

Table 12.1: Tabular summary of the achieved results.

System Parameters	
Average permeate water produced per day [liter]	1310
Average feed pressure [bar]	3.16
Average RO pressure [bar]	6.0
Average permeate TDS [ppm]	257
Average recovery [%]	11.8
Average flux (Surface Load) [l/h/m ²]	10.5

Average run time per day [hours]	15.7
Water costs for installed system [€/m ³]	4.23
SEC for installed system [kWh/m ³]	2.50
Water costs for optimized system [€/m ³]	3.47
SEC for installed optimized [kWh/m ³]	1.64

Unfortunately it was not possible to obtain the required storage capacity for 24 hour a day water production. However, the buffering capacity proved to meet the requirements for continuous semi-constant production of drinking water of acceptable quality. The balance between water entering the desalination part of the system and water going towards the storage proved to be completely self-regulating. The water costs and specific energy content for both the installed system and optimized system proved to be competitive to other solutions previously evaluated and documented.

As discussed previously, one of the main improvement points is the permeate flux. With the knowledge and experience obtained during this project, system behavior can now be more easily predicted and estimations regarding the relative flows and the permeate flux can now be more easily made. The initial starting pressure inside the energy storage vessel provides the designer the freedom to find and choose a personal preference between the permeate flux, quality of the water produced and desired storage capacity.

It can be concluded that hydro-pneumatic energy storage has proven to be a viable and feasible solution for energy storage in small-scale renewable driven RO desalination. The main barrier for successful implementation of this concept into future designs, is the capital cost related to the energy storage vessel. However, with its minimal space requirements (compared to the previous concept), the design has broad implementation possibilities. In comparison to battery systems, the design is simple and requires minimal knowledge and relatively low operational costs.

12.2. Recommendations

12.2.1. Possible System Improvements

There are several additions or improvements that could be made to the system. When compared to the pressurized water storage of Vollebregt and Feenstra (2012), the start-up of this design has an extra barrier. Namely pre-pressurizing the air inside the hydro-pneumatic storage vessel. A useful addition to this design would be a solar compressor (and pressure intensifier). Lorentz, the same manufacturer of the solar pump and controller also sells solar compressors and controller. Addition of a solar compressor and controller would ensure that the system runs on 100% renewable energy. The addition of this component would also ensure that the starting pressure would be re-adjusted everyday and thus the daily operating conditions would be kept constant.

The next two improvements are also related to the energy storage device. The addition of a pressure controlled shut-of valve to prevent the loss of pre-pressurized air (should the hydro-pneumatic energy storage vessel run empty) is highly advised. Also adding a separator inside the energy storage vessel would be useful. This would prevent the interaction between air and water inside the storage vessel and thus reduce pressure losses.

Similar advice as provided by Vollebregt and Feenstra (2012), the development of a brackish water energy recovery device would greatly reduce pressure losses and could significantly increase the recovery, consequently lowering the SEC.

12.2.2. Wind Energy as additional Energy Buffer

The local climate mainly determines the renewable energy source of choice. Implementation of this design in an environment with a favorable wind climate would be very interesting. The combination of PV modules and solar energy already complement each other nicely as they serve as a type of energy buffer. Combining these two energy sources with hydro-pneumatic energy storage concept, could yield in a system with smaller required energy storage capacity.

12.2.3. Developing a Model

As mentioned several times already, this concept is quite the first of its kind. This means that there is little knowledge available on the system behavior. Calculations and estimation during this project were made using data sheets, Matlab and Excel and simulation software explaining the pump and RO performance. A software/model designed especially for this application would attract more attention to this concept. The use of the acquired data in order to develop a model could prove very useful in optimization of the system and finding the optimal pressure, flux and storage capacity.

12.2.4. Scale-up Possibilities

At the moment this concept shows limited scale-up possibilities. The energy storage is relatively expensive and requires double the volume of the required water storage volume. Cheaper vessel solution should be possible, especially in developing countries such as Indonesia where regulations are less strict. Solutions such as construction of pressure vessels using large diameter steel or PVC pipes and storing these underground are interesting options. Further research into manufacturing of cheaper storage vessels would greatly improve the chance of success of this concept.

As previously mentioned, the development of a cheaper energy recovery device designed especially for brackish water desalination purposes should be at the top of the priority list for brackish water desalination development goals. The current energy recovery device shows major losses at lower operating pressure and higher flow rates, and is one of the major cost contributors. The ERPI recovery rate should also be increased, typically recovery rates of 20-30% can be observed in BWRO systems with energy recovery.

12.2.5. Seawater Desalination

Lastly let's discuss the application of this concept for seawater desalination. It should be easily possible to apply this concept to seawater desalination. Hydro-pneumatic pressure vessels are typically rated for operation anywhere between 8-16 [bar], this pressure is sufficient for the ERPI to intensify and deliver working pressures for seawater desalination. Logically a larger installed PV- and pump capacity would be required. Adding a booster pump could also be a possible solution.

References

- . *AED Design Requirements: Hydropneumatic Tanks*. (2009). Afghanistan: Afghanistan Engineer District.
- Akker, H. v. d., & Mudde, R. (2008). *Fysische Transportverschijnselen* (Vol. 3). Delft: VSSD.
- Al-Karaghoul, A., Renne, D., & Kazmerski, L. L. (2009). Solar and wind opportunities for water desalination in the Arab regions. *Renewable and Sustainable Energy Reviews*, 13(9), 2397-2407. doi: <http://dx.doi.org/10.1016/j.rser.2008.05.007>
- Al-Kharabsheh, S. (2006). An innovative reverse osmosis desalination system using hydrostatic pressure. *Desalination*, 196(1-3), 210-214. doi: 10.1016/j.desal.2005.11.023
- Al-Qahtani, H. (1996). Feasibility of utilizing solar energy to power reverse osmosis domestic unit to desalinate water in the state of Bahrain. *Renewable Energy*, 8(1-4), 500-504. doi: [http://dx.doi.org/10.1016/0960-1481\(96\)88907-5](http://dx.doi.org/10.1016/0960-1481(96)88907-5)
- Alghoul, M. A., Poovanaesvaran, P., Sopian, K., & Sulaiman, M. Y. (2009). Review of brackish water reverse osmosis (BWRO) system designs. *Renewable and Sustainable Energy Reviews*, 13(9), 2661-2667. doi: 10.1016/j.rser.2009.03.013
- Bakker, K. (2007). Trickle Down? Private sector participation and the pro-poor water supply debate in Jakarta, Indonesia. *Geoforum*, 38(5), 855-868. doi: 10.1016/j.geoforum.2005.11.011
- Bakker, K., Kooy, M., Shofiani, N. E., & Martijn, E.-J. (2008). Governance Failure: Rethinking the Institutional Dimensions of Urban Water Supply to Poor Households. *World Development*, 36(10), 1891-1915. doi: 10.1016/j.worlddev.2007.09.015
- Bilton, A. M., Wiesman, R., Arif, A. F. M., Zubair, S. M., & Dubowsky, S. (2011). On the feasibility of community-scale photovoltaic-powered reverse osmosis desalination systems for remote locations. *Renewable Energy*, 36(12), 3246-3256. doi: <http://dx.doi.org/10.1016/j.renene.2011.03.040>
- Brennan, E. M., & Richardson, H. W. (1989). Asian megacity characteristics, problems, and policies. *International Regional Science Review*, 12(2), 117-129.
- Cheah, S. (2004). *Photovoltaic reverse osmosis desalination system*.
- de Carvalho, P. C. M., Riffel, D. B., Freire, C., & Montenegro, F. F. D. (2004). The Brazilian experience with a photovoltaic powered reverse osmosis plant. *Progress in Photovoltaics: Research and Applications*, 12(5), 373-385. doi: 10.1002/pip.543
- Delinom, R. M., Assegaf, A., Abidin, H. Z., Taniguchi, M., Suherman, D., Lubis, R. F., & Yulianto, E. (2009). The contribution of human activities to subsurface environment degradation in Greater Jakarta Area, Indonesia. *Science of The Total Environment*, 407(9), 3129-3141. doi: 10.1016/j.scitotenv.2008.10.003
- El-ghonemy, A. M. K. (2013a). Waste energy recovery in seawater reverse osmosis desalination plants. Part 1: Review. *Renewable and Sustainable Energy Reviews*, 18(0), 6-22. doi: <http://dx.doi.org/10.1016/j.rser.2012.09.022>
- El-Ghonemy, A. M. K. (2013b). "Water desalination systems powered by renewable energy sources, Review": [Renewable and Sustainable Energy Rev. 16 (2012) 1537-1556]. *Renewable and Sustainable Energy Reviews*, 24(0), 629. doi: <http://dx.doi.org/10.1016/j.rser.2013.03.072>
- El-Manharawy, S., & Hafez, A. (2001). Water type and guidelines for RO system design. *Desalination*, 139(1-3), 97-113. doi: [http://dx.doi.org/10.1016/S0011-9164\(01\)00298-3](http://dx.doi.org/10.1016/S0011-9164(01)00298-3)
- ElementalWaterMakersB.V. (2012) Retrieved March 15th 2013, from <http://www.elementalwatermakers.com/>
- Eltawil, M. A., Zhengming, Z., & Yuan, L. (2009). A review of renewable energy technologies integrated with desalination systems. *Renewable and Sustainable Energy Reviews*, 13(9), 2245-2262. doi: <http://dx.doi.org/10.1016/j.rser.2009.06.011>

- Generaal, C. (2011). *Wind Driven Reverse Osmosis Desalination for Small Scale Stand-Alone Applications: Evaluation of system configurations and selection of an optimal configuration for Somaliland by means of a SIMULINK model*. (MSc. in Aerospace Engineering Master of Science), TU Delft, Delft.
- GKEREDAKI, E. (2011). *AUTONOMOUS PHOTOVOLTAIC-POWERED REVERSE OSMOSIS FOR REMOTE COASTAL AREAS*. (Master Master's), TU Delft, Delft.
- Gude, V. G., Nirmalakhandan, N., & Deng, S. (2010). Renewable and sustainable approaches for desalination. *Renewable and Sustainable Energy Reviews*, 14(9), 2641-2654. doi: 10.1016/j.rser.2010.06.008
- Habali, S. M., & Saleh, I. A. (1994). Design of stand-alone brackish water desalination wind energy system for Jordan. *Solar Energy*, 52(6), 525-532. doi: [http://dx.doi.org/10.1016/0038-092X\(94\)90660-2](http://dx.doi.org/10.1016/0038-092X(94)90660-2)
- Heijman, S. G. J., Rabinovitch, E., Bos, F., Olthof, N., & van Dijk, J. C. (2009). Sustainable seawater desalination: Stand-alone small scale windmill and reverse osmosis system. *Desalination*, 248(1-3), 114-117. doi: <http://dx.doi.org/10.1016/j.desal.2008.05.045>
- Herold, D., & Neskakis, A. (2001). A small PV-driven reverse osmosis desalination plant on the island of Gran Canaria. *Desalination*, 137(1-3), 285-292. doi: [http://dx.doi.org/10.1016/S0011-9164\(01\)00230-2](http://dx.doi.org/10.1016/S0011-9164(01)00230-2)
- . *Hydropneumatic Pressure Systems*. (2005) *Technical Information Bulletin* (Vol. 101). Indianapolis, USA: Peerless Pump Company.
- . *Hydropneumatic Tank Control Systems*. (2011). Washington: Washington Dept of Health.
- Janssen, L. P. B. M., & Warmoeskerken, M. M. C. G. (2006). *Transport Phenomena Data Companion* (3rd ed.). Delft: VSSD.
- Jones, J. A. A. (2010). *Water Sustainability: A Global Perspective*. London, United Kingdom: Hodder Education.
- Kurniasih, H. (2008). Water Not For All: The Consequences of Water Privatisation in Jakarta, Indonesia.
- Lattemann, S., Kennedy, M. D., Schippers, J. C., & Amy, G. (2010). Chapter 2 Global Desalination Situation. In C. E. Isabel & I. S. Andrea (Eds.), *Sustainability Science and Engineering* (Vol. Volume 2, pp. 7-39): Elsevier.
- Liu, C. C. K., Jae-Woo, P., Migita, R., & Gang, Q. (2002). Experiments of a prototype wind-driven reverse osmosis desalination system with feedback control. *Desalination*, 150(3), 277-287. doi: [http://dx.doi.org/10.1016/S0011-9164\(02\)00984-0](http://dx.doi.org/10.1016/S0011-9164(02)00984-0)
- Manwell, J., McGowan, J., & Rogers, A. (2009). *Wind Energy Explained: Theory, Design and Application*: John Wiley & Sons.
- MarketWatch. (2013) Retrieved June 8th, 2013, from <http://www.marketwatch.com/tools/pftools/>
- McIntosh, A. (2003). Asian Water Supplies: Reaching the urban poor., from http://www.adb.org/Documents/books/asian_water_supplies/asian_water_supplies.pdf
- McKenna, E., McManus, M., Cooper, S., & Thomson, M. (2013). Economic and environmental impact of lead-acid batteries in grid-connected domestic PV systems. *Applied Energy*, 104(0), 239-249. doi: <http://dx.doi.org/10.1016/j.apenergy.2012.11.016>
- Meerganz von Medeazza, G. (2004). Water desalination as a long-term sustainable solution to alleviate global freshwater scarcity? A North-South approach. *Desalination*, 169(3), 287-301. doi: 10.1016/j.desa1.2004.04.001
- Mezher, T., Fath, H., Abbas, Z., & Khaled, A. (2011). Techno-economic assessment and environmental impacts of desalination technologies. *Desalination*, 266(1-3), 263-273. doi: <http://dx.doi.org/10.1016/j.desal.2010.08.035>
- Miranda, M. S., & Infield, D. (2003). A wind-powered seawater reverse-osmosis system without batteries. *Desalination*, 153(1-3), 9-16. doi: [http://dx.doi.org/10.1016/S0011-9164\(02\)01088-3](http://dx.doi.org/10.1016/S0011-9164(02)01088-3)

- Misdan, N., Lau, W. J., & Ismail, A. F. (2012). Seawater Reverse Osmosis (SWRO) desalination by thin-film composite membrane—Current development, challenges and future prospects. *Desalination*, 287(0), 228-237. doi: <http://dx.doi.org/10.1016/j.desal.2011.11.001>
- Moel, P. d., Verberk, J., & Dijk, J. v. (2006). *Drinking Water: Principles and Practices*. Singapore: World Scientific Publishing Co. Pte. Ltd.
- Mohamed, E. S., & Papadakis, G. (2004). Design, simulation and economic analysis of a stand-alone reverse osmosis desalination unit powered by wind turbines and photovoltaics. *Desalination*, 164(1), 87-97. doi: [http://dx.doi.org/10.1016/S0011-9164\(04\)00159-6](http://dx.doi.org/10.1016/S0011-9164(04)00159-6)
- Mohamed, E. S., Papadakis, G., Mathioulakis, E., & Belessiotis, V. (2008). A direct coupled photovoltaic seawater reverse osmosis desalination system toward battery based systems — a technical and economical experimental comparative study. *Desalination*, 221(1–3), 17-22. doi: <http://dx.doi.org/10.1016/j.desal.2007.01.065>
- Moran, M. J., & Shapiro, H. N. (2006). *Fundamentals of Engineering Thermodynamics* (5th ed.). England: John Wiley & Sons Inc.
- Moreno, F., & Pinilla, A. (2005). Preliminary experimental study of a small reverse osmosis wind-powered desalination plant. *Desalination*, 171(3), 257-265. doi: <http://dx.doi.org/10.1016/j.desal.2004.06.191>
- OLTREMARE. (2013). OLTREMARE LIQUID SEPERATION Retrieved February 17th, 2013, from <http://www.oltremaremembrane.com/>
- Onodera, S.-i., Saito, M., Sawano, M., Hosono, T., Taniguchi, M., Shimada, J., . . . Delinom, R. (2009). Erratum to “Effects of intensive urbanization on the intrusion of shallow groundwater into deep groundwater: Examples from Bangkok and Jakarta”. *Science of The Total Environment*, 407(9), 3209-3217. doi: 10.1016/j.scitotenv.2009.01.049
- Pandolph, J. E. (Unknown). Hydropneumatic Tanks. In T. C. Inc. (Ed.). Florida.
- . Pump Cycles Program. (2009). *Hydro-pneumatic Tank Pump Cycle Cpntrl* Retrieved March 12, 2012, from http://www.kypipe.com/pump_cycles_overview
- . *Renewable Energy Potential*. (2006). Amsterdam: Energy Recipes Retrieved from <http://www.energyrecipes.org/>.
- Richards, B. S., & Schäfer, A. I. (2003). Photovoltaic-powered desalination system for remote Australian communities. *Renewable Energy*, 28(13), 2013-2022. doi: 10.1016/s0960-1481(03)00081-8
- Richards, B. S., & Schäfer, A. I. (2010). Renewable Energy Powered Water Treatment Systems, Chapter 12. In C. E. Isabel & I. S. Andrea (Eds.), *Sustainability Science and Engineering* (Vol. Volume 2, pp. 353-373): Elsevier.
- Riffel, D. B., & Carvalho, P. C. M. (2009). Small-scale photovoltaic-powered reverse osmosis plant without batteries: Design and simulation. *Desalination*, 247(1–3), 378-389. doi: 10.1016/j.desal.2008.07.019
- Rijsberman, F. R. (2006). Water scarcity: Fact or fiction? *Agricultural Water Management*, 80(1–3), 5-22. doi: 10.1016/j.agwat.2005.07.001
- Robinson, R., Ho, G., & Mathew, K. (1992). Development of a reliable low-cost reverse osmosis desalination unit for remote communities. *Desalination*, 86(1), 9-26. doi: [http://dx.doi.org/10.1016/0011-9164\(92\)80020-A](http://dx.doi.org/10.1016/0011-9164(92)80020-A)
- Rumbayan, M., Abudureyimu, A., & Nagasaka, K. (2012). Mapping of solar energy potential in Indonesia using artificial neural network and geographical information system. *Renewable and Sustainable Energy Reviews*, 16(3), 1437-1449. doi: <http://dx.doi.org/10.1016/j.rser.2011.11.024>
- Schenker. Retrieved February 19th, 2013, from <http://www.schenker.it/en/home.php>
- Sharmila, N., Jalihal, P., Swamy, A. K., & Ravindran, M. (2004). Wave powered desalination system. *Energy*, 29(11), 1659-1672. doi: <http://dx.doi.org/10.1016/j.energy.2004.03.099>

- Snieder, & Stubbe. (2012). Reverse Osmosis Desalination with Energy Recovery Device for Brackish Water: TU Delft.
- Spyrou, I. D., & Anagnostopoulos, J. S. (2010). Design study of a stand-alone desalination system powered by renewable energy sources and a pumped storage unit. *Desalination*, 257(1–3), 137-149. doi: 10.1016/j.desal.2010.02.033
- SSE. (2013). Surface metrology and Solar Energy Retrieved 12 November, 2012, from <http://eosweb.larc.nasa.gov/cgi-bin/sse/>
- Steinberg, F. (2007). Jakarta: Environmental problems and sustainability. *Habitat International*, 31(3–4), 354-365. doi: 10.1016/j.habitatint.2007.06.002
- Susandi, A. (2008). POTENTIAL AREA FOR SOLAR ENERGY GENERATOR AND ITS BENEFIT TO CLEAN DEVELOPMENT MECHANISM (CDM) IN INDONESIA. In I. T. Bandung (Ed.). Indonesia.
- Thomson, M. (2003). *Reverse-Osmosis Desalination of Seawater Powered by Photovoltaics Without Batteries*. (Doctoral), Loughborough University.
- Thomson, M., & Infield, D. (2003). A photovoltaic-powered seawater reverse-osmosis system without batteries. *Desalination*, 153(1–3), 1-8. doi: [http://dx.doi.org/10.1016/S0011-9164\(03\)80004-8](http://dx.doi.org/10.1016/S0011-9164(03)80004-8)
- Thomson, M., Miranda, M. S., & Infield, D. (2003). A small-scale seawater reverse-osmosis system with excellent energy efficiency over a wide operating range. *Desalination*, 153(1–3), 229-236. doi: [http://dx.doi.org/10.1016/S0011-9164\(02\)01141-4](http://dx.doi.org/10.1016/S0011-9164(02)01141-4)
- Thye, J. (2010). *Desalination: Can it be greenhouse gas free and cost competitive*. Yale.
- Tzen, E., Theofiloyianakos, D., & Kologios, Z. (2008). Autonomous reverse osmosis units driven by RE sources experiences and lessons learned. *Desalination*, 221(1–3), 29-36. doi: <http://dx.doi.org/10.1016/j.desal.2007.02.048>
- van der Kooij, D., Veenendaal, H. R., & Scheffer, W. J. H. (2005). Biofilm formation and multiplication of Legionella in a model warm water system with pipes of copper, stainless steel and cross-linked polyethylene. *Water Research*, 39(13), 2789-2798. doi: 10.1016/j.watres.2005.04.075
- van Dijk, J. C., Verberk, J. Q. J. C., Heijman, S. G. J., Rietveld, L. C., de Ridder, D., Grefte, A., & Andeweg, P. (2009). *Drinking Water Treatment*. Delft: Sanitary Engineering Department, TU Delft.
- Vollebregt, S., & Feenstra, R. (2012). *The Design, Implementation and Evaluation of a Renewable Driven Desalination System*. (Master of Science), TU Delft, Delft.
- Walton, N. R. G. (1989). Electrical Conductivity and Total Dissolved Solids—What is Their Precise Relationship? *Desalination*, 72(3), 275-292. doi: [http://dx.doi.org/10.1016/0011-9164\(89\)80012-8](http://dx.doi.org/10.1016/0011-9164(89)80012-8)
- Wang, Y.-J., & Hsu, P.-C. (2011). An investigation on partial shading of PV modules with different connection configurations of PV cells. *Energy*, 36(5), 3069-3078. doi: <http://dx.doi.org/10.1016/j.energy.2011.02.052>
- . Water Safe bc. (2006). *Hydropneumatic Tanks* Retrieved march 5th, 2012, from <http://www.watersafebc.ca/infoforoperators/waterdistributionsystems/waterstorage/hydropneumatictanks/default.aspx>
- WHO. (2011). *Guidelines for Drinking-water Quality* (4th ed.): World Health Organization.
- Wikipedia. (2012) Retrieved February 5th, 2012, from <http://en.wikipedia.org/wiki/Jakarta>
- Wikipedia. (2013). Boyle's Law Retrieved January 20th, 2013, from http://en.wikipedia.org/wiki/Boyle's_law
- Zeman, M. (2010). *Solar Cells*. Delft: Delft University of Technology.

Appendices

Appendix A – Groundwater Samples throughout Jakarta

Table 1 – Major element nitrate-N, nitrite-N, and Phosphate content in shallow groundwater (unconfined aquifer) samples in Greater Jakarta Area.

Sample site	pH	Ca ²⁺ (mg/l)	Mg ²⁺ (mg/l)	K ⁺ (mg/l)	Na ⁺ (mg/l)	HCO ₃ ⁻ (mg/l)	Cl (mg/l)	SO ₄ ²⁻ (mg/l)	N-NO ₃ (mg/l)	N-NO ₂ (mg/l)	PO ₄ ³⁻ (mg/l)
South Jakarta											
SJ 1	6.96	1.20	0.39	0.08	1.83	2.03	0.85	0.32	134	0.54	1.1
SJ 2	5.50	0.33	0.77	0.03	0.09	0.25	0.81	0.18	1.14	0.00	0.5
SJ 3	6.47	1.34	0.79	0.03	0.70	1.27	0.94	0.25	568	0.00	0.6
SJ 4	6.19	0.53	0.79	0.04	0.87	1.16	1.04	0.22	1.28	0.00	1.7
SJ 5	7.61	4.36	1.59	0.21	2.26	6.86	1.37	0.75	0.94	0.15	1.7
SJ 6	4.87	0.67	0.57	0.03	1.04	0.58	1.13	0.36	668	0.02	0.1
SJ 7	6.96	1.07	1.06	0.05	0.48	1.54	0.52	0.50	0.20	0.04	0.2
SJ 8	6.58	1.07	1.06	0.05	1.28	1.16	1.70	0.49	3.84	0.05	0.0
SJ 9	6.96	2.55	0.53	0.03	0.97	1.58	1.42	0.63	972*	0.02	0.0
SJ 10	7.76	1.34	0.92	0.09	1.39	2.47	0.94	0.54	0.28	0.03	0.8
East Jakarta											
EJ 1	7.70	1.20	0.79	0.12	1.35	2.800	0.47	0.13	0.08	0.02	1.0
EJ 2	5.95	1.20	1.46	0.05	0.97	1.56	1.32	0.08	0.18	0.00	1.0
EJ 3	5.75	0.94	1.59	0.05	2.53	0.87	3.07	0.47	15.16*	0.08	1.1
EJ 4	4.79	0.40	0.26	0.38	1.39	0.48	0.94	0.24	6.72	0.00	0.6
EJ 5	5.60	0.53	0.98	0.26	0.87	0.49	1.23	0.38	6.26	0.01	0.4
EJ 6	7.00	3.09	0.53	0.14	2.01	3.56	0.94	0.39	2.46	0.03	0.8
West Jakarta											
WJ 1	7.13	4.16	1.33	0.08	2.61	5.08	0.62	1.27	9.72*	0.30	1.1
WJ 2	6.58	1.93	3.74	0.76	13.57	6.59	5.89	6.35	0.23	0.01	0.6
WJ 3	5.94	0.42	0.74	0.13	3.39	1.36	1.97	1.29	0.09	0.01	0.6
WJ 4	6.51	1.43	1.38	0.79	9.13	4.78	2.25	4.07	0.35	0.00	0.2
WJ 5	7.20	4.46	6.39	0.92	36.15	13.53	24.43	8.41	1.43	0.54	0.1
WJ 6	6.29	18.72	10.42	0.35	19.14	3.36	37.04	8.08	0.28	0.01	0.59
WJ 7	6.58	1.12	1.12	0.56	9.35	2.91	4.97	4.48	19.23*	0.01	0.6
WJ 8	6.89	6.43	6.68	0.84	5.96	9.04	2.54	5.86	12.57*	0.00	0.3
WJ 9	7.22	3.81	6.97	0.68	22.61	14.23	14.36	3.82	1.02	0.14	1.5
Central Jakarta											
CJ 1	7.37	2.28	1.46	0.08	1.74	3.59	0.32	1.27	2.08	0.06	1.1
CJ 2	7.58	5.11	2.26	1.03	4.47	10.17	1.27	0.56	1.60	0.90	0.06
CJ 3	7.19	1.36	1.16	0.18	3.36	3.36	0.52	1.77	14.00*	0.00	0.60
CJ 4	7.01	2.37	3.42	0.28	7.30	9.37	4.76	0.14	16.30*	0.00	0.30
CJ 5	6.86	5.15	2.59	0.64	5.46	6.85	4.42	1.64	12.03*	0.00	0.2
CJ 6	7.00	2.75	0.45	0.28	2.70	2.10	1.13	2.35	3.00	0.00	0.5
CJ 7	7.63	1.08	3.15	0.89	29.58	11.64	19.11	2.59	1.89	0.00	0.0
CJ 8	7.36	3.14	2.44	0.38	8.09	5.09	5.12	2.02	18.40*	0.00	0.6
North Jakarta											
NJ 1	7.40	2.25	3.45	0.40	16.44	12.47	7.15	1.42	1.27	0.24	0.3
NJ 2	4.04	2.86	3.84	0.52	5.05	11.91	0.76	0.29	1.98	0.00	0.1
NJ 3	6.91	4.72	2.85	1.23	21.53	14.38	11.37	2.28	1.43	0.07	0.1
NJ 4	8.01	0.44	0.26	0.19	12.41	8.86	1.79	0.38	12.50*	0.00	0.2
NJ 5	7.05	4.31	2.21	0.52	4.02	7.69	1.92	0.28	11.45 8	0.00	0.2
NJ 6	6.86	5.85	1.89	0.64	7.97	7.57	6.95	1.01	1.79	0.24	0.2
NJ 7	6.83	5.67	5.98	0.64	6.96	10.59	4.15	2.78	2.35	0.00	0.4
NJ 8	7.07	2.37	1.98	0.25	6.79	7.94	2.73	0.45	2.02	0.00	0.1
NJ 9	6.94	2.43	3.32	0.56	8.27	8.32	4.70	1.58	2.81	0.00	0.1

Note: * marks are for high nitrate contents samples which were taken from dense populated area. All samples were taken from shallow groundwater (unconfined aquifers).

Appendix B – Average Data

December 2012

Day	Daily Pumped Volume [l]	Permeate Produced [l]	Daily Solar Radiation [kWh/m ²]	Solar Run-time [hours]	Daily Run-time [hours]	Average Flow to RO [l/min]	Average Recovery [%]	Flux [l/h/m ²]
1 //10 Dec	5437	587	3.625	10.42	10.42	8.15	12.1	22.40
2//11 Dec	5848	632	4.54	10.03	10.03	8.68	12.1	24.06
3// 12 Dec	6670	680	3.98	10.88	10.88	10.05	12.2	27.93
4// 13 Dec	6460	549	4.02	10.28	10.28	10.61	12.2	29.67
5// 14 Dec	6198	632	4.52	9	9	9.88	12.2	27.49
6// 15 Dec	5934	659	5.15	10.4	10.4	9.02	12	24.97
7// 16 Dec	5936	588	4.69	10.1	10.1	10.00	12.1	27.67
Total	42483	4327	30.525	71.11	71.11			
Average	6069	618.14	4.36	10.16	10.16	9.48	12.13	26.31
Standard Deviation	411.28	45.71	0.51	0.58	0.58	0.88	0.08	2.56
Minimum	5437	549	3.625	9	9	8.15	12	22.40
Maximum	6670	680	5.15	10.88	10.88	10.61	12.2	29.67

April 2013

Day	Daily Pumped Volume [l]	Permeate Produced [l]	Daily Solar Radiation [kWh/m ²]	Volume to Storage [l]	Solar Run-time [hours]	Daily Run-time [hours]	Average Flow to RO [l/min]	Average Recovery [%]	Flux [l/h/m ²]
1// 17 April	13531	1521	5.62	4629	9.14	17.11	12.2	12.1	11.21
2// 18 April	7745	819	2.56	3859	7.9	10.52	11.8	10.9	9.77
3// 19 April	12559	1439	4.98	5127	9.49	14.63	14.1	11.6	12.42
4// 20 April	13929	1685	6.14	5880	10.17	16.28	14.2	12.1	13.05
5// 21 April	12568	1515	4.68	5839	8.24	16.29	12.6	12.3	11.77

6// 22 April	6041	680	1.43	3362	9.92	14.96	6.3	11.7	5.60
7// 23 April	13068	1511	4.11	5690	9.73	19.99	10.5	12	9.57
Total	79441	9170	29.52	34386	64.59	109.78			
Average	11348.71	1310.00	4.22	4912.29	9.23	15.68	11.67	11.81	10.47
Standard Deviation	3122.13	392.04	1.68	1003.27	0.86	2.88	2.70	0.47	0.10
Minimum	6041	680	1.43	3362	7.9	10.52	6.3	10.9	5.22
Maximum	13929	1685	6.14	5880	10.17	19.99	14.2	12.3	13.27

Hydraulic Pump Power @ 500 [W/m2]

Time1	Time2	Irr1	Irr2	Irr500	TimeX	Flow1	Flow2	Press 1	Press2	timeX	Flow X	PressX	Hydraulic Power [W]
97.70	97.72	470.80	535.50	500.00	97.71	37.22	38.42	2.32	2.36	97.71	37.76	2.34	147.15
97.72	97.75	535.30	498.40	500.00	97.75	38.42	37.53	2.36	2.36	97.75	37.57	2.36	147.77
97.83	97.85	374.80	504.60	500.00	97.85	32.55	37.63	2.34	2.41	97.85	37.45	2.41	150.27
97.90	97.95	575.10	381.60	500.00	97.92	38.36	31.33	2.45	2.40	97.92	35.63	2.43	144.34
97.97	98.00	335.30	524.60	500.00	98.00	29.89	37.26	2.40	2.50	98.00	36.30	2.49	150.47
98.00	98.03	524.60	482.70	500.00	98.02	37.26	36.34	2.50	2.51	98.02	36.72	2.51	153.36
98.17	98.20	491.10	652.70	500.00	98.17	35.14	38.68	2.58	2.64	98.17	35.33	2.58	152.13
100.98	101.00	572.94	496.54	500.00	101.00	23.82	19.70	5.24	5.24	101.00	19.89	5.24	173.68
101.15	101.18	490.27	543.69	500.00	101.15	19.71	23.34	5.18	5.21	101.15	20.37	5.19	176.06
101.33	101.35	494.68	547.80	500.00	101.33	19.87	22.29	5.27	5.27	101.33	20.11	5.27	176.65
101.38	101.43	657.69	448.07	500.00	101.41	26.44	16.36	5.28	5.30	101.41	18.86	5.30	166.42
101.93	101.95	403.14	586.11	500.00	101.94	14.52	25.76	5.13	5.18	101.94	20.47	5.16	175.92
102.33	102.35	505.70	369.58	500.00	102.33	17.60	9.78	5.43	5.38	102.33	17.27	5.43	156.26
102.55	102.58	657.76	447.04	500.00	102.57	23.23	15.22	5.42	5.40	102.57	17.23	5.41	155.24
102.58	102.60	447.00	600.00	500.00	102.58	15.22	23.51	5.40	5.41	102.58	18.09	5.40	162.93
102.70	102.73	582.49	460.50	500.00	102.72	22.84	15.56	5.46	5.43	102.72	17.92	5.44	162.44
103.03	103.05	443.86	634.52	500.00	103.03	14.34	24.21	5.40	5.43	103.03	17.25	5.41	155.47
103.20	103.23	441.60	608.30	500.00	103.21	14.60	22.90	5.48	5.50	103.21	17.51	5.49	160.11
103.35	103.38	695.00	485.00	500.00	103.37	26.12	16.12	5.63	5.60	103.37	16.83	5.60	157.18
103.40	103.43	461.00	627.00	500.00	103.41	14.98	23.83	5.59	5.60	103.41	17.06	5.59	159.00
103.50	103.53	654.00	435.00	500.00	103.52	24.27	13.03	5.65	5.62	103.52	16.37	5.63	153.54
103.55	103.58	470.00	661.00	500.00	103.55	16.51	25.24	5.61	5.64	103.55	17.88	5.61	167.33
103.60	103.63	459.00	583.50	500.00	103.61	14.72	22.19	5.61	5.62	103.61	17.18	5.61	160.73

104.05	104.08	519.00	474.00	500.00	104.06	16.47	14.00	5.84	5.82	104.06	15.43	5.83	149.94
104.08	104.10	474.00	617.50	500.00	104.08	14.00	21.76	5.82	5.82	104.08	15.41	5.82	149.44
104.13	104.15	650.80	492.40	500.00	104.15	23.22	14.63	5.84	5.82	104.15	15.04	5.82	145.93

Appendix C – Cost Calculations

Item	Capital Costs [Euro]	Depreciation Time [Years]	EAC, Installed System	EAC, No storage	EAC, Optimized Storage
PV Modules	1762.5	25	109.86	36.62	109.86
PV Mounting System	43.3914	25	2.70	1.35	2.70
Solar Pump & Controller	1750	10	213.08	213.08	213.08
Soler Pump Well Probe	75	10	9.13	9.13	9.13
ERPI	3200	10	389.64	389.64	389.64
Indication Sensors	300	10	36.53	36.53	36.53
Pre-filter Housing	50	20	3.60	3.60	3.60
Hydro-Pneumatic Storage Vessel	5980	25	372.74	0.00	745.49
Permeate Storage Vessel	624	10	75.98	37.99	75.98
30-Meter Shallow Well	468	50	20.86	20.86	20.86
PVC Tubing	109.16	40	5.31	2.66	5.31
PVC Connectors and Accessories	96.99	40	4.72	4.72	4.72
Electric Cabling and Safety Sling	233.84	10	28.47	28.47	28.47
Total Capital Costs	14692.8816		1272.63	784.65	1645.37
	# of Annual Replacements	Operational Costs - Installed System [Euro]	Operational Costs - No Storage	Operational Costs - Optimized	
RO Membranes	0.5	150.00	105.00	150.00	
Filter Cartridges	24	120.00	120.00	120.00	
Chemicals		89.08	70.62	115.18	
Labor		114.54	78.46	148.08	
Maintenance and Spare Parts		178.17	70.62	230.35	
Annual Operational Costs		651.79	444.70	763.61	
Total Annual Costs		1924.42	1229.35	2408.98	
Annual Permeate Produced [m³]		454.55	214.44	694.84	
Price Per cubic meter		4.23	5.73	3.47	

